الجمهورية الجزائرية الديمقراطية الشعبية

People's Democratic Republic of Algeria

وزارة التعليم العالي والبحث العلمي

Ministry of Higher Education and Scientific Research

جامعة زيان عاشور بالجلفة

ZIANE Achour University of DJELFA

كلية العلوم والتكنولوجيا

Faculty of Sciences and Technology

Department: Electrical Engineering

Order N°:...../2020

Defense authorization N°: 146/2020

DOCTORAL THESIS

Presented by:

RABIAI Attia

With a view to obtaining the doctoral diploma in 3rd Cycle Doctoral (D-LMD)

Branch: Automatic Applied

Specialty: Maintenance in Industrial Instrumentation

Topic

H-Bridge Multi-level Inverter Model Predictive Control Based For Reliability Enhancement

Supported on: 25 / 06 /2020, before the jury composed of:

Last name and first name	Grade	Institution of affiliation	Designation
Mr. Ahmed HAFAIFA	Professor	ZIANE Achour University of DJELFA	President
Mr. Abdellah KOUZOU	Professor	ZIANE Achour University of DJELFA	Supervisor
Mr. Noureddin HANINI	MCA	YAHIA Fares University of MEDEA	Examiner
Mr. Salam ABUDURA	Professor	YAHIA Fares University of MEDEA	Examiner
Mr.Ameur Miloud KADDOURI	MCA	ZIANE Achour University of DJELFA	Examiner

بِسْمِ اللَّهِ الرَّحْمَٰنِ الرَّحِيمِ

الحمد لله ربّ العالمين

والصّلاة والسّلام على أشرف المرسلين سيّدنا ونبيّنا

محمّد النّبيء الكريم وعلى آله وصحابته أجمعين

قال الله تعالى:« وَقُل رَبِّ زِدْنِي عِلْماً »

« سورة طه، الآية 114»

بسم الله الرّحمان الرّحيم والصّلاة والسّلام على أشرف المرسلين سيّدنا ونبيّنا محمّد وعلى آله وصحابته أجمعين، وبعد:

قال تعالى: «فَاذْكُرُونِي أَذْكُرْكُمْ واشْكُرواْ لِي ولاَ تَكْفُرُونِ» «سورة البقرة، الآية 102»

قال تعالى: «وإِذْ تَأَذَّنَ رَبُّكُمْ لَإِنْ شَكَرْتُمْ لَأَزِيدَنَّكُمْ ولَإِنْ كَفَرْتُمْ إِنَّ عَذَابِي لَشَدِيدٌ» «سورة إبراهيم، الآية 7»

قال تعالى: «يَا أَيُّهَا النَّاسُ اذْكُرُوا نِعْمَتَ اللَّهِ عَلَيْكُمْ هَلْ مِنْ خَالِقٍ غَيْرُ اللَّهِ يَرْزُقُكُم مِّنَ السَّمَاءِ وَالْأَرْضِ لَا إِلَٰهَ إِلَّا هُوَ فَأَنَّىٰ تُؤْفَكُونَ» «سورة فاطر، الآية 3»

بادئ البدء وفي المقام الأوّل اشكر الله سبحانه تعالى وأقول الحمد لله الذي هدانا لهذا وما كنّا لنهتدي لولا ان هدانا الله، فله الحمد وحده وله الشّكر وحده على انّه وفّقني لإنجاز هذه الأطروحة ومنحني القوّة والصّبر والعزيمة، فلك الحمد يا الله حمدا كثيرا طيّبا مباركا فيه حمدا يليق بجلال وجهك وعظيم سلطانك.

قال رسول الله صلّى الله عليه وسلّم: « لا يَشْكُرُ اللهَ مَن لا يَشْكُرُ النّاسَ » حديث صحيح

اتوجّه بخالص الشّكر والامتنان والتّقدير للسيّد المحترم الأستاذ الدكتور: قوزو عبد الله المشرف على أطروحة الدكتوراه وذلك نضير تعبه وجهوده الكبيرة وصبره معي طوال مشواري لإنجاز هذه الأطروحة، وكذا على نصائحه المفيدة وتوجيهاته القيّمة.

وأخصّ بالشّكر الجزيل وجميل العرفان السيّد المحترم الموقّر الأستاذ الدكتور: حفيفة أحمد، عميد كلّية العلوم والتكنولوجيا، مدير مخبر الأتمتة التّطبيقية والتّشخيص الصّناعي بجامعة الشّهيد زيّان عاشور بالجلفة، على تشريفه لي بترأسه للجنة مناقشة الدكتوراه من جهة ومن جهة أخرى على دعمه ومساندته لي بكل الوسائل المّادية والمعنوية.

كما أشكره أيضاً على ان أتاح لي انجاز هذا العمل المقدّم في هذه الاطروحة بمخبر الأتمته التّطبيقية والتّشخيص الصّناعي بكليّة العلوم والتكنولوجيا بجامعة الشّهيد زيّان عاشور بالجلفة.

أخص أيضا بالشّكر الجزيل وببالغ الثّناء لجنة التّكوين في الدكتوراه شعبة الأتمته التّطبيقية وعلى رأسها السيد المحترم الأستاذ الدكتور: حفيفه أحمد، على أنها اتاحت لنا الفرصة للتكوين في الدكتوراه ويسرت لنا الأمور لكي ننجز هذه الأطروحة في أحسن الظّروف.

كما اتقدّم بجميل الشّكر والعرفان لأعضاء لجنة المناقشة، كل من السّادة: الأستاذ حنيني نور الدين، الأستاذ الدكتور ابو دورة سلام الأستاذين بكلّية التكنولوجيا بجامعة الشّهيد يحي فارس بالمدية والدكتور قدوري عامر ميلود الأستاذ بكلّية العلوم والتكنولوجيا بجامعة الشّهيد زيّان عاشور بالجلفة، على تكرّمهم وتشريفهم لي بقبولهم مناقشة أطروحتي للدّكتوراه وعلى تصويباتهم وملاحظاتهم.

أشكر والدايّ اللّذين كانا دائمًا دعما مهما جدًّا لي. شكرا جزيلا لكلّ العائلة ولكلّ الأصدقاء والأحباب ولكلّ من اهتم لأمرنا لإنجاز هذه الأطروحة.

كما أتقدم بخالص الشّكر للأخ والصّديق والزّميل بن عطيه عبد العزيز، رئيس مصلحة الوسائل العامة بمديرية جامعة الشّهيد زيّان عاشور بالجلفة على مساندته الماديّة والمعنوية.

أشكر كذلك السّيدة المحترمة الأستاذة: عمراوي مارية، نائب رئيس الجامعة للتّكوين العالي فيما بعد التّدرج، التّأهيل الجامعي والبحث العلمي على مرافقتها ومساندتها المعنوية.

كما أتقدم بالشكر الجزيل للسيدين المحترمين، السيد بن مسعود الطاهر والسيد روبيح عبد القادر الأستاذين بكلّية العلوم والتكنولوجيا بجامعة الشّهيد زيّان عاشور بالجلفة على مرافقتها ومساندتها المعنوية و المادية.

كما أشكر الأصدقاء والزملاء بنيابة مديرية الجامعة للتّكوين العالي فيما بعد التّدرج، التّأهيل الجامعي والبحث العلمي على دعمهم لي وتشجيعهم المتواصل خاصة كل من السادة: حلباوي الحاج عمر، يونسي حافظ، رقيات العيد، نعاس عبد الله.

وفي الأخير أودّ ان اعرب عن خالص شكري و امتناني لكلّ أولئك الذين ساعدوني من قريب او من بعيد و لم اذكر أسماءهم على انجاز هذه الأطروحة.

والله الموفّق و المستعان و عليه التّكلان و لا حول و لا قوة إلا بالله العلي العظيم و الحمد لله ربّ العالمين و صلّى الله و سلّم و بارك على سيّدنا و نبيّنا محمّد وعلى آله و صحبه أجمعين.

ربيــع عطيــه

عين الإبل في:15 مارس 2020

أهـــدي ثمـرة عمـلي المتواضــع هــذا الـى:

والديّ الكريمين اللّذين ربّياني وسهرا عليّ لأجل ان أكون كما انا عليه اليوم جزاهما الله عنّي خير الجزاء، قال الله تعالى: « وَوَصَّيْنَا الْإِنْسَانَ بِوَالِدَيْهِ حَمَلَتْهُ أُمُّهُ وَهْنًا عَلَىٰ وَهْنٍ وَفِصَالُهُ فِي عَامَيْنِ أَنِ اشْكُرْ لِي وَلِوَالِدَيْكَ إِلَيَّ الْمَصِيرُ » «لقمان، الآية 14»

الى روح أمي العزيزة الغالية رحمها الله

الى جمع افراد عائلتي.

الى جميع الأصــدقاء كلّ باسمه.

الى جميع الزّملاء بجامعة الشّهيد زيّان عاشور بالجلفة.

الى كلّ من ساعدني من قريب او من بعيد على انجاز هذه الأطروحة.

ربيـــــع عطيـــه

عيـن الإبـل في: 20 جـــــوان 2019

ملخّـــص

تمّ اقتراح نموذج خوارزميّة تحكّم تنبّؤيّة لمحوّلات الطّاقة الكهربائيّة نظرًا لديناميكيّتها الجيّدة، أدائها العّالي، قدرة تتبّعها الآنيّة الدّقيقة وتحديدها مجموعة المدخلات لتوافقيّات التّبديل الممكنة لعاكس الاستطاعة. في الوقت الحاضر، أصبحت خوارزميّة التّحكم التّنبؤيّة محل جذب واهتمام للباحثين، وراجع ذلك بفضل تقدّم، تطوّر وكذا سرعة المعالجات الدّقيقة الحديثة والتّقنيات الحاليّة المتاحة.

تستخدم خوارزميّة التّحكم التنبؤيّة نموذجًا زمنيّا متجزّئا لمعادلات النّظام المدروس من أجل التّنبؤ بالقيم المستقبليّة للجهد والتيّار الكهربائيّين من خلال معادلات حمل المحرّك التّحريضي المتمثّل في المقاومة والوشيعة من أجل جميع متّجهات الجهد الممكنة المتولّدة عن عاكس(ممّوج) الاستطاعة. متّجه الجهد الذي يقلّل من معادلة الكلفة هو الذي يتّم اختياره.

يتّم استخدام معادلة الكلفة لتقيّيم متّجهات الجهد في عيّنة الوقت الموالية إستباقيّا واختيار أقلّهم خطأً. يتم تحديد متّجه الجهد الأمثل المقابل لمتّجه إشارة التيّار المرجعي ويتمّ تطبيق حالة التبديل الموافقة لهذا المتّجه على المحوّل خلال عيّنة الوقت الموالية. إن النّتائج توضّح أن نموذج خوارزميّة التّحكم التّنبؤيّة فعّال للغاية ويتميّز بأداء ديناميكي أفضل للنّظام المقترح.

الكلمات المفتاحيّة: خوارزميّة تحكم تنبؤي، تعديل عرض النّبضة الشّعاعي، عاكس(ممّوج) نصف قنطرة متعدّد المستويات، التشوّه التوافقيّ الكلّي، مصدر جهد مستمر، حالات التّبديل.

Abstract

Predictive control algorithm model (MPC) has been proposed for power electronic converter systems, because of its good dynamic, its high performance, its accurate current tracking capability and the finite set of inputs possible switching combinations. Nowadays, predictive control algorithm model (MPC) is attracting the attention of researchers due to the development, the speed, the advances in modern microprocessors, and present technologies available.

The predictive control algorithm uses a discrete-time model of the system by use the equations of the load of induction motor to predict the future values of the load current and voltage for all possible voltage vectors generated by the inverter. The voltage vector, which minimizes by a cost function, is selected.

The cost function is used to evaluate all the voltage vectors at the next sampling time. An optimal voltage vector is selected and its corresponding switching state is applied to the converter during the next sampling sequence. Finally, the results show that the predictive control algorithm model (MPC) very effectively, and better dynamic performance of the proposed system.

Keywords: Predictive control algorithm model (MPC) , Space vector pulse width modulation (SVPWM), Cascaded H-bridge multilevel inverter (CHBI), Total harmonic distortion (THD), DC voltage source, switching states.

Résumé

Un modèle d'algorithme de commande prédictif a été proposé pour les convertisseurs d'électroniques de puissance, en raison de sa bonne dynamique, de sa haute performance, de sa capacité de suivi de courant précis et de définir de l'ensemble fini d'entrées de combinaisons de commutation possibles d'onduleur de puissance. Actuellement, l'algorithme de commande prédictif attire l'attention du chercheurs au développement, la vitesse, progrès des microprocesseurs modernes et aux technologies actuelles disponibles.

L'algorithme de commande prédictif utilise un modèle en temps discret du système a partir les équations du charge d'un moteur à induction représenté par la résistances et l'inductances de son bobinage pour prédire les valeurs futures du courant et de la tension de charge pour tous les vecteurs de tension possibles générés par l'onduleur. Le vecteur de tension qui minimise par une fonction de coût est encore finalement sélectionné.

Cette fonction de coût permet d'évaluer tous les vecteurs de tension au temps d'échantillonnage suivant et choisi la plus petite erreur. Un vecteur de tension optimal est sélectionné et l'état de commutation correspondant est appliqué au convertisseur pendant le temps d'échantillonnage suivant. Enfin, les résultats montrent que le modèle d'algorithme de commande prédictif est très efficace en termes de performance et bonne performance de la dynamique du système proposé.

Mots clés : Algorithme de commande prédictif, Modulation de largeur d'impulsion vectorielle (MLIV), Onduleur de pont en H en cascade multi-niveaux, Distorsion harmonique totale (DHT), Source de tension en courant continue, Etats de commutation.

Table of contents

Table of contents

Table of contents

Table of contents

List of tables

List of figures

CHAPTER I: State of the art on predictive control

CHAPTER II: Studies of the different topologies of multi-level inverters

CHAPTER III: Control strategies for three phase VSI and multi-level h-bridge inverter

List of figures

Publications

[1] RABIAI Attia, KOUZOU Abdellah, HAFAIFA Ahmed, "Current Model Predictive Control for Three-phase Multi-level H-Bridge inverter", in Electrotehnica, Electronica, Automatica (EEA), 2019, vol. 67, no. 2, pp. 05-16, ISSN 1582-5175.

URL: http://www.eea-journal.ro/ro/d/5/p/EEA67_2_1

[2] RABIAI Attia, KOUZOU Abdellah, HAFAIFA Ahmed, "Space vector pulse width modulation for three phase cascaded h-bridge inverter", published in the proceeding of The International Conference on Applied Smart Systems (ICASS) 2018. URL:https://ieeexplore.ieee.org/search/searchresult.jsp?newsearch=true&queryText=rabiai

International Conferences

[1] RABIAI Attia, KOUZOU Abdellah, HAFAIFA Ahmed, "Space vector pulse width modulation for three phase cascaded h-bridge inverter " ,The International Conference on Applied Smart Systems ICASS'2018, 24-25 November 2018, Medea, Algeria .

URL: http://www.univ-medea.dz/en/icass2018.

[2] RABIAI Attia, KOUZOU Abdellah, HAFAIFA Ahmed, " Predictive current control for three phase three level h-bridge inverter", The 2nd International Workshop on Signal Processing Applied to Rotating Machinery Diagnostics, SIGPROMD'2018 ,29-30 April 2018, Djelfa ,Algeria,

URL: http://www.univ-djelfa.dz/labo/laadi

[3] RABIAI Attia, KOUZOU Abdellah, HAFAIFA Ahmed, "Model predictive current control for three phase inverter". The 2nd International Conference on Power Electronics and their Applications (ICPEA 2015) 29-30 March 2015, Djelfa, Algeria.

URL: http://www.univ-djelfa.dz/labo/laadi

[4] RABIAI Attia, KOUZOU Abdellah, HAFAIFA Ahmed, "Model predictive current control for voltage source inverter ", The third International Conference on information processing and electrical engineering ICIPEE'2014, 24-25 November 2014, Tebessa, Algeria.

URL: http://www.univ-tebessa.dz/en/icipee2014

Research Projects

- Member of university research project (CNEPRU),Approved from 01 January 2015, Title: «Contribution au diagnostic des défauts dans les machines multi-phases et les convertisseurs d'électronique des puissance multi-phases». Project Code : J0202820140002.

Notations and Acronyms

A:

AC: Alternative Current.

C:

CF: Cost Function.

CHB: Cascaded H-bridge Inverter.

CMV: Common Mode Voltage.

D:

DC: Direct Current.

DMC: Dynamic Matrix Control.

DMPC: Discrete Model Predictive Control.

DT: Discrete Time.

E:

EHAC: Extended Horizon Adaptive Control.

EPSAC: Extended Prediction Self Adaptive Control.

F:

FC: Flying Capacitor Inverter.

FCH: Finite Control Horizon.

FSMPC: Finite Set Model Predictive Control.

G:

GPC: Generalized Predictive Control.

GTO: Gate Turn-Off Thyristor.

I:

IDCO-MC: Identification and Command Multivariable Controller.

IGBT: Insulated Gate Bipolar Transistor.

M:

MAC: Model Algorithmic Control.

MBPC: Model-Based Predictive Control.

MC: Multi-level converters.

MOESET: Metal Oxide Semiconductor Field Effect Transistor.

MPC: Model Predictive Control.

MPHC: Model Predictive Heuristic Control.

MURHAC: Multi-predictor Receding Horizon Adaptive Control.

MUSMAR: Multi Step Multivariable Adaptive Control.

N:

NGPC: Nonlinear Generalized Predictive Control.

NMPC: Nonlinear Model Predictive Control.

NPC: Neutral Point Clamped Inverter.

NRHC: Nonlinear Receding Horizon Control.

P:

PCT: Polynomial Chaos Theory.

PFC: Predictive Functional Control.

PLC: Programmable Logic Controller.

PWM: Pulse Width Modulation.

R:

RF: Reference Trajectory.

S:

SMOC: Shell Multivariable Optimizing Controller

SPWM: Sinus Pulse Width Modulation.

ST: Sampling Time.

SVPWM: Space Vector Pulse Width Modulation.

T:

THD: Total Harmonic Distortion.

U:

UPC: Unified Predictive Control.

List of Symbols and Measurement Units

v: Voltage [V]

i: Current [A]

L: Inductance [H]

R: Resistance [Ω]

f: Frequency [Hz]

T_s: Sampling time [s]

N: Number of parallel inverters

j: Complex number

k: Number of levels

$[\bullet]^T$: The transpose of a matrix

$\min_{x \in X} J$: Minimum value of J over X.

$|\quad|$: Absolute value

$\Re$: Element of real numbers.

General Introduction

In the last years, multilevel inverter topologies have been introduced and considered for several applications, especially in medium and high power conversion. It was proved that these inverter topologies could ensure the generation of high-quality voltage waveforms based on power semiconductor switches combinations that are operating at a frequency near the fundamental. Hence, the efficiency of the conversion can be increased remarkably.

Although, these topologies can be also used in low-power applications where the switching frequency of the power switches not restricted in such case. Additionally, multilevel inverters feature several DC links, making possible the independent voltage control. This characteristic advantage allow maintaining the efficiency at an increased level in the case of mismatch of the input voltage DC suppliers, especially with renewable energy source applications.

Among the available multilevel inverter topologies, the cascaded h-bridge multilevel inverter constitutes a promising alternative, providing a modular design that can be extended to allow a transformer-less power conversion. This topology benefits from the use of power semiconductors with a lower rating than the standard two-level configurations, hence; a low cost investment can be guaranteed. On the other side, several advantages can be achieved such as:

1. Lower total harmonic distortion «THD» of the output currents and the output voltage,
2. Requirements of smaller output filters,
3. Ability to transfer more power,
4. Smaller dv/dt stresses, which allows the increase the lifetime of many electrical components.

Last but not the least, h-bridge multilevel topologies feature several freedom degrees that make possible the operation of the inverters even under faulty conditions, increasing, in this way, the reliability of the conversion of the system in which it is included. In spite of all these characteristics, the cascaded H-bridge multilevel topology has also some disadvantages، such as:

1. The unbalance of the DC input voltages,v_{dc}
2. Huge number of switching gates control,S_i
3. Appearance of common mode voltage, especially under faults of one or more power switches in different branches of the inverter.

In order to properly operate a cascaded H-bridge inverter a discrete model predictive control is proposed to be achieved in this thesis based on more possible models that can be occurred in specified

applications, where the independent control of the DC-link voltages and the control of the output currents are necessary.

In the approach presented in this thesis, the main goal is the real-time maintenance of the control mode of the inverter to ensure the continuous operation of the system without interruption during a defined period of time. This proposal is a suitable and adequate solution, especially in application under medium and high power conversion with renewable energy sources in grid-connected applications or sensitive industrial plants applications to sudden power supply trip or breakdown.

The presented discrete model predictive control (DMPC) will be based on a set of model predictive control (MPC) of eventual models belonging to the operation of the system to ensure a high reliability and time-maintenance of the whole system.

This thesis work is divided into four chapters organized as follows:

In the first chapter the methodology of predictive control has been described: A brief history of this control strategy. The manner in which constraints are formulated in predictive control is described and the main elements that appear in these methodologies, i.e., the prediction model and the objective function. The principles elements were mentioned in addressing the most common constraints in practice.

The second chapter presents a state of the art on multi-level inverter, its fundamental topologies, the advantages and disadvantages of each topology in term of using the number of components such as the number of switches and capacitors then in term of harmonic reducing and signal quality. Finally its applications in different sectors and filed such as the electricity grid and the industry..e.g.

The third chapter, is devoted to presentation of mathematical equations of the space vector modulation and model predictive control and the relationship between the tow controls where the predictive control based on the voltage vectors to selecting the optimal voltage then applied to the inverter system:

In the last chapter, we will present the simulation results of the application of the predictive control on the two-level voltage source inverter and three-level half-bridge inverter using MATLAB software where we can see by the simulation results the effectiveness of the predictive control represented by the quality of the load currents waveforms and dynamic performance of the system.

Finally, this work will be concluded with a general conclusion through which the main results obtained will be presented and the perspectives to be considered as a follow-on to this work will be provided.

Chapter I

State of the art on predictive control

I.1 Introduction

Predictive control is an advanced control technique of the automatic. Its purpose is to control complex industrial systems and a variety of applications, including robotic systems, electrical machinery, and the monitoring and control of biotechnology processes. The principle of this technique is to use a dynamic model of the process inside the controller in real time in order to anticipate the future behavior of the process.

Predictive control differs from other control techniques in that it must be solved online; it consists in optimizing, from the inputs or outputs of a system, the predicted future behavior of the system considered. The prediction is made from an internal model of the system over a finite time interval called the prediction horizon. The solution of the optimization problem is a control vector whose first input of the optimal sequence is injected into the system. The problem is again resolved on the next time interval using updated system data.

This control strategy has shown its efficiency, flexibility and success in industrial applications, even for systems with low sampling time. The application of the predictive control in the field of numerical controls has given good results in terms of speed and accuracy.

This chapter aims to provide a brief history of this approach, to summarize the principles of all predictive control techniques.

I.2 Historical summary of the development of predictive control

In the early 1960s, Propov was one of the first to explicitly propose a form of model-based predictive control using a linear programming method. The idea is to insert, in the control algorithm, an element of prediction concerning the evolution of the process outputs, given by a model [1].

The computer then determines, at the present sampling instant, the sequence of commands to be applied over a prediction horizon, at the next sampling period, only the first component of this sequence is actually applied to the process and the resolution starts again in the same way taking into account the new process measurements and so on.

The first generation of predictive control applied in an industrial environment was initiated by Richalet, where the problem of Model Predictive Heuristic Control is formulated, later called Model Algorithmic Control [2] [3].

Cutler and Ramaker, developed what would later become known as dynamic matrix control. In these approaches, the model is of the black box type, the objective is to pursue a reference but the constraints are not yet taken into account [4].

These algorithms have a huge impact on the control of industrial processes and allow to define an example of predictive control based on a model. A dynamic process model is used in both contributions (the impulse response in the first and the index response in the second) to quantify the effect of control actions on the output, the controls are computed to minimize the predicted error under execution restrictions (objective function). The optimization is repeated at each sampling period, also based on the measured process data.

These techniques quickly became popular especially in chemical industrial processes due to the simplicity of the algorithm and the fact that a model derived from the impulse or index response is used, which requires a fewer number of parameters than state space formulation or input-output formulation (transfer function). These are more intuitive approaches that require less information for identification.

A complete status of these applications in the petrochemical sector during the eighties ,most of the applications are centered in the field of multivariate systems with restrictions[5]. At the same time and independently, some European academic research groups, with a strong history in adaptive control, have started to develop work based on the ideas of predictive theory for models formulated from an input-output representation of the system (transfer function).

The Extended Prediction Self Adaptive Control are developed to provides a constant control signal for the entire prediction horizon, which is applied from the beginning of the computation of the control that optimizes the chosen cost criterion [6].

The basic idea of the Extended Horizon Adaptive Control is to calculate at each instant the sequence of control signals to try to keep the future output as close as possible to the setpoint for a time horizon greater than the present delay on the process[7].

Currently, the Generalized Predictive Control developed by Clarke and Mohtadi, is the most popular method[8]. A summary of these methods and their most important features can be found in Clarke and all and De Keyser and all [9], [10].

The second generation, which appeared in the early 1980s, the interest in Predictive Control has gradually increased and other methodologies have appeared in the specialized literature on control. Among them, the most important are: Multi Step Multivariable Adaptive Control [11], Multi-predictor Receding Horizon Adaptive Control [12], Predictive Functional Control [13] and Unified Predictive Control [14].

The 1990s marked an increase in the number of predictive control applications. There are several real-world applications that work successfully [10], in the chemical process industry as well as in robotics. This has always been accompanied by strong research activity, [15]

Despite the extensive development of predictive control during the late 1970s and 1980s, it was not until the early 1990s that the study of predictive control stability and robustness began to be addressed.

Predictive control can also be formulated in the context of state variable representation [16]. This not only allows the use of the theorems and results existing in state space theory, but also facilitates the extension of predictive control theory to more complex cases such as systems with stochastic disturbances, noise on measurement variables or multivariable control.

Given the high computational load required by the quadratic programming algorithms in the Model Predictive Control strategy, many authors are beginning to investigate the possibility of obtaining a fast solution that provides a mostly sub-optimal result in the optimization problem. In this category we can mention the work of Bemporad and al[17], Ramirez and Camacho[18]. An explicit solution is presented for the case of state feedback for nominal systems. It is shown that the obtained control law can be considered linear in piecewise terms.

This approach has the disadvantage of the number of regions into which the state space must be divided, which increases combinatorially as the prediction horizon increases. This requires a significant amount of research time to determine the appropriate working region, which is not suitable for many practical application cases.

I.3 Predictive control methodology

The principle of predictive control consists in creating for the system to be controlled an anticipatory effect with respect to a trajectory to be followed that is known in advance, based on the prediction of the future behaviour of the system and minimising the deviation of these predictions from the trajectory in the sense of a certain cost function, while respecting operating constraints. This idea is simple and practised quite systematically in everyday life.

For example, the driver of a vehicle knows the desired reference trajectory in advance (the road) over a finite control horizon (his visual field), and by taking into account the characteristics of the car (mental model of the vehicle's behaviour), he decides which actions (accelerating, braking or turning the steering wheel) must be performed in order to follow the desired trajectory. Only the first driving action is performed at each moment, and the procedure is repeated again for the next actions.

The model predictive control (MPC) has a number of advantages as compared to other methods, including :

a. It can be used to control a wide variety of processes, from those with simple dynamics to those with more complex dynamics, for example, delay systems, or unstable systems.

b. The relatively easy adjustment of its parameters makes it accessible to people with limited knowledge of automation.

c. The multivariate case is easily processed.

d. Its predictive character allows to compensate for delays and dead times.

e. The treatment of constraints imposed on the system to be controlled can be included in the obtaining of the control law.

f. It is very efficient when the instructions or trajectories to be followed are known in advance (which is the case in several industrial processes such as digital machines and robots).

Predictive control law is determined by solving an optimal finite-horizon control problem as shown in the following figure I.1.

Starting from a reference path to be followed that is known in advance, by performing the following steps at each sampling period:

1. Calculate predictions of the output variables y over a prediction horizon N_p.
2. Minimize a finite horizon criterion based on: future prediction errors, deviations between the predicted system output and the future setpoint.
3. Obtain a sequence of future commands on a command horizon less than or equal to N_p.
4. Apply only the first value of this sequence to the system.
5. Repeat these steps at the next sampling period, using the principle of the receding horizon.

The following figure I.1 is summarized the precedent steps:

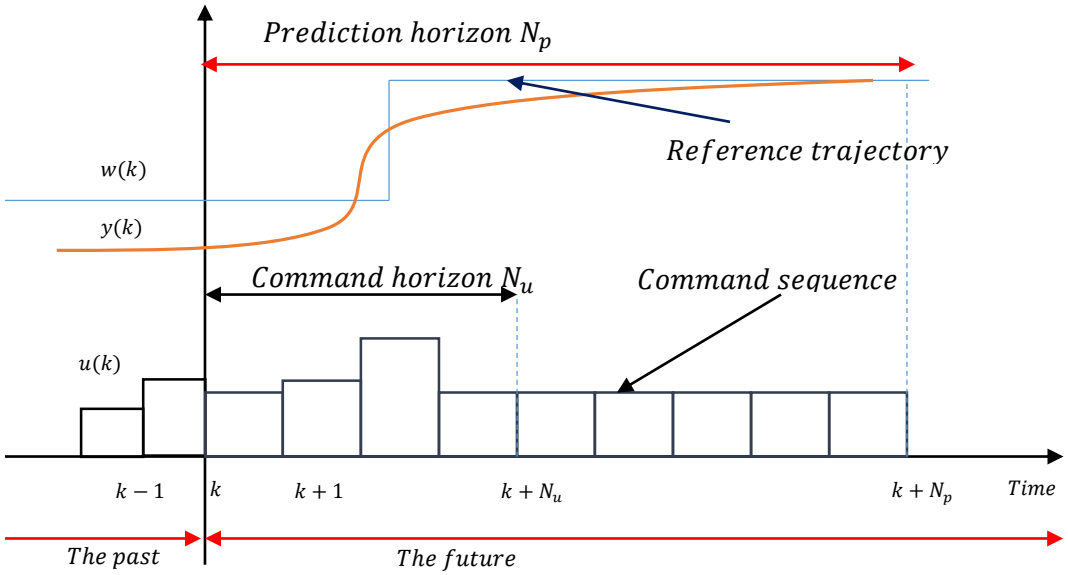

Figure I.1 Predictive control methodology.

Where,

k is the discrete time.

$u(k)$ is the input of the system at time k.

$w(k)$ is system reference at time k.

$y(k)$ is the output of the system at time k.

The operating principle of predictive control can be characterized as follows:

1. At each instant k, by having a model of knowledge of the output of the system, a prediction of the output is made for a certain horizon N_p, (the prediction horizon), the predicted outputs are denoted $y(k+i/k)$ where $k = 1,2,\dots,N_p$.
2. The prediction of the output, is made by calculating the vector of future control signals $[u(k+i/k), i = 0,1,\dots,N_p-1]$ through optimization of an objective function.This function (usually convex) forces to make the future output as near as possible to the reference trajectory known setpoint $w(k+i)$, while reducing the efforts of the control. Constraints on the output or on the control may also be imposed.
3. The first element $u(k)$ of the vector of the optimal control signal $u(k+i/k)$ and

$i = 0,1, \dots, N_p - 1$ from the previous problem is applied to the system and the rest is rejected because at the next instant the new output $y(k+1)$ is available and consequently step 1 is repeated. This is known as the concept of the receding horizon.

Remark :

In the general case of a constrained system, minimizing the predictive criterion requires the effective resolution of an online optimization problem.

Only the predictive control of time-invariant linear systems, restricted to the unconstrained case, does not require the effective resolution of this online optimization problem, because the corrector is in turn linear invariant and its analytical description can be obtained off-line.

I.4 Elements of the predictive control

Figure I.2 shows the fundamental structure common to all predictive control strategies.

All predictive control algorithms have:

1. The prediction model.
2. The objective function to calculate the optimal control strategy.

The differences are the type of the objective function, the prediction error processing and the prediction model.

I.4.1 The prediction model

The model plays a decisive role in the calculation of the order. It must reproduce with an a sufficient degree of accuracy the dynamic characteristics of the process at future points in time $y(k+i/k)$ using the past values of the order, the output and the optimum values of the future order $u(k+i/k)$.

Different predictive control strategies use different models to represent the relationship between the output and input of the system.

Input signals include manipulated variables (or control) and measurable disturbances that can be processed by feed forward compensation.

In addition, components not considered by the system model, including the effect of non-measurable inputs, noise and modeling errors, must be considered.

Thus, the model can be divided into two parts: the process model and the disturbance model. The predictions of the output will be a function of the both.

I.4.1.1 The process model

In the classical approach of predictive control any form of modeling, and most often linear, is used. Impulse response or step response are the most common, but there are also representations by transfer function and state function.

a. The impulse response

it appears in the MAC algorithm and in the special cases of generalised predictive control and extended prediction self adaptive control, especially for stable systems. The truncated model to be used for prediction is the one obtained from the impulse response of the system:

$$y(k + i/k) = \sum_{j=1}^{N_u} h_j \, \Delta u(k + i - j/k) \qquad (\text{I}.1)$$

$y(k + i/k)$ is the prediction of the output in $(k + i)$ given its knowledge in $k, u(k + i - j/k)$ is the input in $(k + i - j)$, h_j are the values of the output at each sampling period when a pulse signal of amplitude 1 is input.

b. The Index response

The Index response is used in the dynamic matrix control algorithm, and this case is quite similar to the previous one except that the input signal is a step.

Again, the truncated model, for stable systems, is used for output prediction.

$$y(k + i/k) = \sum_{j=1}^{N_u} j_j \, \Delta u(k + i - j/k) \qquad (\text{I}.2)$$

$y(k + i/k)$ is the prediction of the output in $(k + i)$ given its knowledge in k, j_j are the parameters obtained at the output of the system when applying a step to the input.

Where $\Delta u(k) = u(k + 1) - u(k)$ is the change in the input of the system.

c. The transfer function

The transfer function used in generalized predictive control, unified predictive control, extended prediction self-adaptive control, extended horizon adaptive control, multi-predictor receding horizon adaptive control and multi-step multivariable adaptive control among others. The prediction model is:

$$y(k + i/k) = \frac{B(Z^{-1})}{A(Z^{-1})} u(k + i/k) \quad (\text{I}.3)$$

This representation is also valid for unstable processes.

d. The state space model

It used in predictive functional control, it has the following representation:

$$x(k+1) = Ax(k) + Bu(k) \quad (\text{I}.4)$$
$$y(k) = Cx(k)$$

Where,

$x(k)$ is the state vector, $u(k)$ the inputs vector and $y(k)$ the outputs vector, A, B, and C are the matrixes of the system, the input and the output respectively.

I.4.1.2 Disturbance model

The selection of the model to be used to represent the disturbances affecting the system is as important as the selection of the process model.

A model of the system to predict the future evolution of the outputs on the prediction horizon N_p:

$$\hat{Y} = [\hat{y}(k)\hat{y}(k+1) \dots \hat{y}(k+N_p)] \quad (\text{I}.5)$$

a. Optimization method:

To calculate a sequence of commands on the control horizon N_u:

$$\theta = [u^*(k)u^*(k+1) \dots u^*(k+N_u)] \quad (\text{I}.6)$$

Which minimizes the optimization criterion« J » satisfying the constraints imposed by the user, knowing that:

$$u^*(k+i) = u^*(k+N_u) \text{ for } \leq i \leq N_p \quad \text{(I.7)}$$

b. The sliding horizon:

Which consists in moving the horizon from k to $(k+1)$ at each sampling period after the application of the first command $u^*(k)$ of the optimal sequence thus obtained.

Remark :

Generally, one of the main reasons for the success of the predictive control over the relatively slow processes is the time long enough to be able to solve the associated optimization problem before the end of the sampling period $[k; k+1]$.

On the other hand, if the system to be controlled is relatively fast, where the criterion associated with the optimization problem is non-convex, the sampling period is too short to allow the calculation of the desired command sequence.

Figure I.2 shows the basic structure of the predictive control strategy.

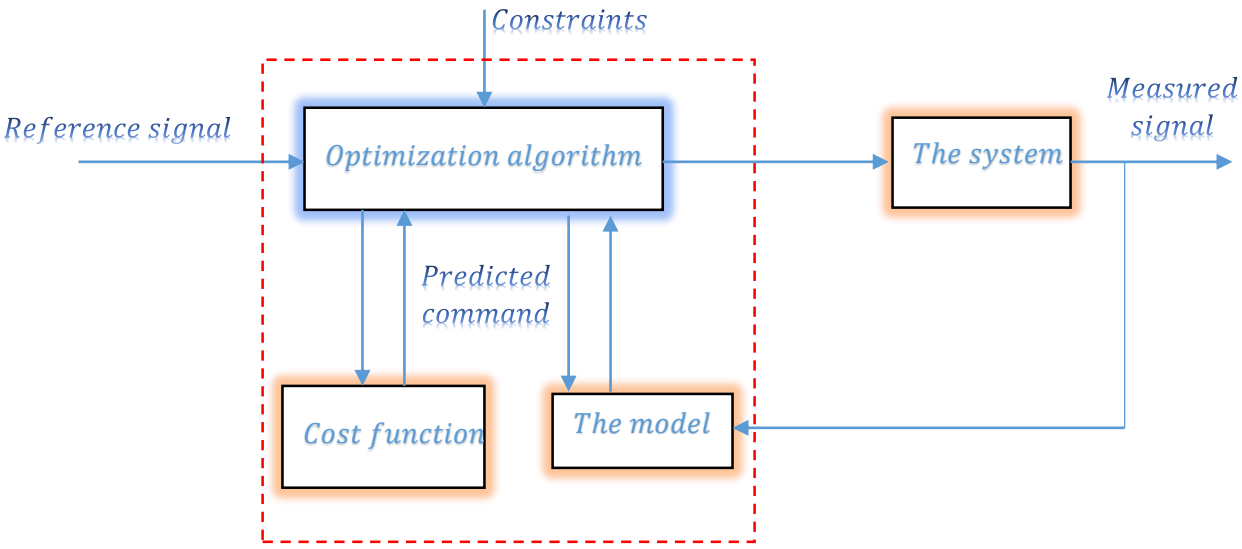

Figure I.2 Basic structure of a predictive control strategy.

For the implementation of the predictive strategy, the basic structure of figure I.2 is implemented.

A model is used to predict future system output, using current and past order values and future optimal orders.

The latter are calculated by an optimization method, which takes into account the cost function (which also depends on the future specifications), and possibly constraints.

Thus, the model of the system to be ordered plays a central role in predictive control. The chosen model must be able to take into account the dynamics of the process in order to accurately predict future outputs. The elements of the predictive control that must be involved in the design are discussed in the following paragraphs.

I.4.2 The objective function

The various predictive control algorithms offer different cost functions to obtain the control loop. The main objective is to ensure that the future output for the considered prediction horizon approaches the reference trajectory $w(k)$ in the best possible way while, at the same time, penalizing the necessary control effort $\Delta u(k)$.

The cost function (objective function)depends on the applied commands u (the system input), the system output variables y and the desired behavior w. All these quantities change with time.

A general expression of objective function adapted to this task is given by:

$$g(N_1, N_2, N_u) = E\left[\sum_{i=N_1}^{N_2} \sigma(i)\left[y\left(k+\frac{1}{k}\right) - w\left(k+\frac{i}{k}\right)\right]^2 + \sum_{i=1}^{Nu} \lambda(i)\left[\Delta u\left(k+i-\frac{1}{k}\right)\right]^2\right] \quad (\mathrm{I}.8)$$

Where,

N_1 and N_2 define the interval of time in which the output should approximate to the reference, If a high value of N_1 is taken it is because it is not important to observe an error in the first moments. In processes with delay d, there is no reason for N_1 to be smaller than this time since the output will not begin to react to the command applied in k before the time $(k+d)$.

In the same way, if the process is of non-minimal phase, this parameter allows eliminating from the objective function, the moments of time when the response is inverse, N_u is the control horizon. The coefficients σ and λ are values that penalize the future behavior, usually are used of the constant values or exponential values.

In some methods of predictive control, the second term, relating to control effort, is not taken into account.

Therefore, the problem of predictive control is the determination of the sequence of commands that allows minimizing the chosen performance criterion while ensuring a verification of the constraints.

A sequence of N_u Control is applied from the present moment k until the end of the control horizon, i.e. at $(N_u + k)$.

Then, the commands applied until the end of the prediction horizon $(N_p + k)$ are taken equal to the last element of the sequence.

This means that it has to make an estimation of the predictions of the values of output y at future sampling times based on the future values of input, this is the modeling step.

We call w the setpoint whose value is assumed to be known not only at the present instant k but also during the following sampling instants, with:

- $w\ (k\ +\ i)$ instruction applied at the moment $k\ +\ i$.
- $y(k\ +\ i)$ output predicted at the instant $k + i$.
- $N_u\ \leq\ N_p$ and $\Delta u\ (k\ +\ i)\ =\ 0, \forall\ i\ \geq\ N_u$.
    - ✓ N_u is the order horizon.
    - ✓ N_1 is the initialization horizon.
    - ✓ N_p is the prediction horizon $N_p = N_2 - N_1$.
    - ✓ λ is the weighting factor of the order.
- Δ is the difference operator $\Delta(k)\ =\ u(k+1)\ -\ u\ (k)$.

The coefficient λ makes it possible to give more or less weight to the control with respect to the output, so as to ensure convergence when the starting system presents a risk of instability [19].

For a continuous system, T is a continuous interval $[t, t\ +\ T]$ where T represent the future prediction time.

In this case where, using a non-linear predictor, there is no analytical solution, the solution of the predictive control problem is obtained, by a numerical optimization algorithm implemented on an computer, therefore, the problem is reduced to an optimization problem in finite dimension.

The optimization interval is a succession of temporal elements for which the objectives translate desired behaviors or only in successive segments of time, the objective function then becomes in discrete form :

$$J_{Q_K} = \sum_{Q_K}(.)\Delta Q_K \tag{I.9}$$

By discretizing this criterion, two values are naturally introduced into the predictive control:

- The length of the control sample sequences.
- The length on which the performance criterion is evaluated.

I.4.3 Reference trajectory

One of the great advantages of predictive control is that, if the future evolution of the reference trajectory is known, the system can start responding before the change is recognized.

The future evolution of the reference is well known in many applications.

In most methods, a reference trajectory is used that is not necessarily equal to the true reference. The true reference can be approximated by means of a first-order equation:

$$w(k + i) = \alpha w(k + i - 1) + (1 - \alpha) r(k + i) \qquad \text{(I.10)}$$

Where,

$i = 1, 2, \ldots, N_p$

I.4.4 Predictive control modeling

Different MPC strategies use different models to represent the relationship between output and input to the system. Let's give a quick overview of these types of modeling which can be done in two ways:

I.4.4.1 The knowledge model:

It is a matter of taking into account the physical phenomena involved: energy, mass balance, i.e.

The model is in this case rarely simple in terms of input-output. It is mainly non-linear, described by a set of differential equations with only the time variable as an independent variable. This model is described by partial differential equations.

The complexity of the model then depends on the desired descriptive requirements but more importantly on the level of precision required for the desired system behavior.

The importance of the various phenomena can be quantified and the model obtained makes it possible to simulate the process with other physical and dimensional characteristics.

On the other hand, it is obvious that the more the model is faithful to the process, in the physical sense of the term; the better will be the prediction of the evaluation of the behavior of the process.

However, the method requires precise knowledge in the field concerned.

I.4.4.2. Input-output global behavior model:

From a black box model, chosen a priori, it is a matter of making an estimate of its parameters.

These are determined based on experimental input-output data. The advantage of the approach may be simpler and faster than in the previous case.

Moreover, it can be very difficult to equate the behavior of many systems. The model has no physical meaning, especially if it is of a complex nature.

On the other hand, and contrary to the first method, it is more difficult to simulate the behavior of a process with other physical and dimensional characteristics.

Remark:

The choice of the method is of course made according to the precision of the objectives to be achieved and the information available. From a practical point of view, the identification method is still the most widely used, as it is the simplest and quickest implementation.

However, as the problems posed are increasingly complex and non-linear, the use of a non-linear representation is tending to expand.

The system model therefore plays a central role in predictive control. The chosen model must be able to account for the dynamics of the process to accurately predict future outputs and also must be simple to implement and understand.

Predictive methodology requires the definition of an N_p-step forward predictor that allows to anticipate the behaviour of the process in the future over a finite horizon.

To do this, from the form of the model, we determine the estimated output at time $(k+i)$, knowing the output at time k.

In this prediction structure, the past values of the inputs and outputs are used to predict the current output of the system.

The associated predictor is given by :

$$y_p(k) = f[y(k-1), \dots, y(k-n_a), u(k-n_k), \dots, u(k-n_b-n_k+1)] \quad \text{(I.11)}$$

The vector of past output and input measurements is written as follows:

$$\varphi(k) = f[y(k-1), \dots., y(k-n_a), u(k-n_k), \dots, u(k-n_b-n_k+1)] \quad \text{(I.12)}$$

n_a , n_b and n_k: are respectively the system commands and the time delay.

I.5 The optimization

Contrary to the linear case where the problem is convex, non-linear predictive control requires the solution of a non-linear non-convex problem.

Formulating the problem of optimization under constraints in the form of a problem without constraints but penalized.

I.5.1 Types of constraints

The different methodologies of predictive control make it possible to anticipate the violation of restrictions given their predictive nature.

A. constraints on control signal amplitude:

Restrictions on the amplitude of the control signal, which are quite frequent in practice (to take into account, for example, saturation effects of actuators), can be expressed by means of the following inequality:

$$u_{min} < u(\bullet) < u_{max} \tag{I.13}$$

These constraints are to be satisfied on all the optimization horizon :

$$u_{min} < U(k) < u_{max} \tag{I.14}$$

Where $U(k)$ the dimension vector of N_u

$$U(k) = [u(k)\ u(k+1) \dots u(k+N_u-1)]^T \tag{I.15}$$

B. constraints on the rate of change of the control signal:

The restrictions on the increase of the control signal take a very simple form, and can be expressed by means of the inequality:

$$\Delta u_{min} \leq u(k+1) - u(k) \leq \Delta u_{max} \tag{I.16}$$

Where

$$\Delta u_{min} \leq \Delta u(k) \leq \Delta u_{max} \quad \text{(I.17)}$$

And $\Delta u(k) = u(k+1) - u(k)$

C. **Output amplitude constraints:**

It is very frequent to find as a desired specification in controlled processes that their output is in a range around a desired path, for example, in cases of following a certain profile with a certain tolerance.

This type of condition can be introduced for the control system so that the output of the system is at all times within the range formed by the specified path more or less the tolerance this translates into an inequality of the form:

$$y_{min} \leq y(k) \leq y_{max} \quad \text{(I.18)}$$

D. **constraints on the rate of change of the output signal**

Constraints on increasing the output signal can be expressed by means of inequality:

$$\Delta y_{min} \leq \Delta y(k) \leq \Delta y_{max} \quad \text{(I.19)}$$

Where: $\Delta y = y(k+1) - y(k)$

I.5.2 Optimization under constraints

For a constrained optimization problem, noting:

$$\theta = [u(k)u(k+1) \dots u(k+(N_u-1)]^T \quad \text{(I.20)}$$

The optimization argument, in an instant k, the problems presented are reduced to the following:

$$\min g(\theta) \ \ with \begin{cases} j_{i_{min}} \leq j_i(\theta) \leq j_{i_{max}} & i = 1, \dots, m \\ h_i(\theta) = 0 & i = 1, \dots, r \\ g: \Re^{Nu} \rightarrow \Re \end{cases} \quad \text{(I.21)}$$

Where:

m is the number of constraints $j(\theta)$ of any type inequality.

r is the number of constraints $h(\theta)$of any type equality.

The constraints described above (I. 14), (I. 17), (I. 18) and (I. 19) can be written as:

$$j_{i_{min}} \leq j_i(\theta) \leq j_{i_{max}} \tag{I.22}$$

I.5.3 Concept of feasibility

Feasibility is the existence of a solution to the constrained optimization problem that reflects the control problem. It is a question of verifying that the control, solution of the algorithm, allows to ensure the stability of the process in closed loop [20]. This notion of feasibility is important in the context of real-time use. it call the feasibility domain, the set of solutions verifying the constraints. it note :

$$C = \left\{\theta / j_{i_{min}} \leq j_i(\theta) \leq j_{i_{max}} \ \wedge \ h_i(\theta) = 0\right\} \tag{I.23}$$

Note that in the predictive control approach, the resolution of the problem (I. 21) must be performed several times at a given time and changes at each time.

The principle is to replace the primal problem by a penalized problem. Starting from the problem (I. 21), we define a penalty function with positive values l related to the constraints.

It is then added, by weighting a positive penalty coefficient M, to the performance criterion J, thus defining the new cost function g_{tot} to be minimized. The new unconstrained but penalized problem is:

$$\begin{cases} \min g_{tot}(\theta) = g(\theta) + M \cdot l(g_i(\theta), h_i(\theta)) \\ \theta \in \Re^{Nu} \end{cases} \tag{I.24}$$

The principle is then to search the solution to this penalized optimization problem and to choose the weight M so that the quantity $M \cdot l(g_i(\theta), h_i(\theta))$ is sufficiently taken into account during the resolution of the problem.

There is no general method for taking constraints into account. Using the penalty functions $P(\theta)$ we end up with the following problem without constraints. If no violation of the constraints occurs, that is, if all constraints are satisfied, then $P(\theta)$ is set to zero; otherwise $P(\theta)$ is set equal to a positive value [21], as follows:

$$P(\theta) = M \cdot \left[\sum_{i=1}^{m} \left(g_i(\theta)\right)^2 + \sum_{i=1}^{r} \left(h_i(\theta)\right)^2\right] \tag{I.25}$$

Where, M is a positive penalty setting.

After the reformulation of the predictive control optimization problem, the calculation steps of the MPC remain the same:

1. At each moment k, having a model of knowledge of the output of the system, we make the prediction of the output for a certain prediction horizon N_p , the predicted outputs are indicated by $y(k+i\ /\ k)$ where $k = 1,2, \dots N_p$.
2. The prediction of the output, is used to calculate the vector of future control signals $u(k+i\ /\ k), i = 0,1,2 \dots N_u - 1$ through the optimization of an objective function g_{tot} .
3. The first element $u(k)$ of the optimal control signal vector $u(k+i\ /\ k), i = 0,1,2 \dots N_u - 1$, from the previous problem is applied to the system and the rest is rejected because at the next instant the new output $y(k+1)$ is available and as a consequence the step one is repeated according to the concept of the receding horizon.

I.5.4 Choice of horizons

As previously described, the difficulty of continuous time has been circumvented by a discretization of time and the command argument over a finite time. This introduced the horizons of prediction N_p and command N_u.

The problem known in predictive control since its origins is their optimal determination. In the case of linear models, there are methods for fixing these parameters since it is easier to establish the responses of such systems in the case of setpoint tracking whose dynamics are of the same order as those of the linear system to be controlled [20]. In the general case, this remains an open problem since an optimal horizon depends on the dynamics of the setpoint to be tracked, but also on the influence of the constraints on the behaviour of the process [22].

I.6 The prediction horizon N_p:

The choice of the prediction horizon N_p plays an important role both in terms of the amount of information provided to the algorithm and in terms of the numerical feasibility of the optimization problem. Its determination is based on physical considerations related to the behaviour of the open-loop model, the objective to be achieved and the constraints taken into consideration. However, if

there is not yet a method for choosing the optimal prediction horizon for the problem, the choice of a time-varying prediction horizon may be better than with a constant horizon N_p [22].

On the other hand, during the prediction horizons, it must be possible to predict the future behaviour of the system by including possible deviations from the model due or not to the control. Therefore, a compromise has to be found for this parameter between a large prediction period ensuring control over a longer time and a small horizon guaranteeing better predictions because of the more adapted information concerning the future deviation between the process and its model.

I.7 The order horizon N_u:

As for the choice of the control horizon N_u, a high value allows a priori, by having more degrees of freedom, to reach more difficult objectives. However, the choice of $N_u = 1$ is recognized as sufficient in most cases.

I.8 The weighting factor λ:

The weighting factor λ can be interpreted as the balance of the scale.

If $\lambda = 0$, only in the quadratic criterion the difference between the setpoint and the predicted output is minimized. This can result in a very strong control which can cause the actual process to deviate. On the other hand, if is very high, then the control is over-weighted and is no more dynamic enough to better follow the setpoint.

I.9 Conclusion

In this chapter, the methodology of predictive control has been described. A brief presentation was given of the most important characteristics of the main predictive control methods. The main elements that appear in these methodologies, i.e., the prediction model and the objective function, have been described. The principles elements were mentioned in addressing the most common constraints in practice. A discretization of time and another concerning the control argument then allowed this problem to be posed in finite dimension. This also made it possible to enter the essential adjustment parameters of the predictive control. The closed-loop control structure has been presented to integrate into the problem of optimization under constraints in finite dimension not only the measurements emissions from the process, but also its future behavior through the model.

Chapter II

The different topologies of multi-level inverters

II.1 Introduction

The multi level inverter technology has become a very important alternative in the field of medium voltage high power energy control. The inverter is referred to as « multi level » when it generates an output voltage composed of at least three levels. This type of inverter has essentially two advantages. On the one hand, multi level topologies make it possible to limit the voltage constraints undergone by power switches; each component, when it is in the off state, supports a fraction of the full DC bus voltage that is lower the higher the number of levels. On the other hand, the output voltage delivered by the multi level inverters has interesting spectral qualities.

Multiplying the number of intermediate levels reduces the amplitude of each rising or falling edge of the output voltage. The amplitude of the harmonic lines is therefore even lower. In the more specific case of modulation technic, the use of a multilevel inverter in combination with appropriate controls of the power components also makes it possible to suppress certain families of harmonic lines.

This chapter presents a brief history and some advantages of multi-level inversion topologies. As well as the most important topologies: the neutral point clamped inverter (NPC), flying capacitor inverter(FC) and cascaded h-bridge inverter (CHB) with separate sources of DC voltage, with their strengths, weaknesses, and application to industrial fields, and concludes the chapter with a comparison of these three topologies.

II.2 History and benefits of multi-level inverter

II.2 .1 Historical overview

The history of multi-level conversion begins in the early of 1970s [23]. The first topology described is a series of h-bridges to synthesize an alternating output voltage in the form of a staircase.

Then in the early of 1980s, the neutral point clamped inverter (NPC) is appeared[24]. This topology is considered the first multi level converter for medium power applications. Since the fact the neutral point clamped inverter (NPC) effectively multiplies the voltage level without requiring a matching voltage precise, the neutral point clamped topology reigned in the 1980s.

The application of the neutral point clamped inverter and of its extension to multi-level inverters has been published by Baker R [25]. Since then, many studies have been proposed to study its properties and possible evolutions of this topology.

Although the multi-level cascaded h-bridge inverter was invented first, its applications did not prevail until the mid of 1990s [26].Two important patents have been published to indicate the superiority of cascaded h-bridge inverter for training of the motors [27],[28].

Due to the high demand for high-power and medium-voltage inverters, the multi-level cascade h-bridge inverter attracted enormous interest.

In the 1990s, research was focused on new structures and they are carried to serial multicellular inverters, also known in the literature as a flying capacitor inverter (FCI) [23].

Moreover, it was at the end of the 90s that the multicellular inverter, this topology is a continuation of the reflection on the serial multicellular inverters .These topology can be considered as the basic topology of the multi-level inverter. Many of the properties of these basic topology are common to new topology discovered.

II.2.2 Multi-level inverter benefits

A multi-level inverter has several advantages over a conventional three phase two-level inverter that uses the pulse width modulation strategy (PWM) with a high switching frequency [29].

The attractive technical features of a multi-level inverter can be briefly summarized as follows:

1. **The Staircase waveform quality:** The multi level inverters not only can generate output voltages with very low deformations, but also can reduce dv/dt stress; for this reason, the electromagnetic problems can be reduced.
2. **The common mode voltage (v_{nN}):** Multi-level inverters produce a smaller common mode voltage; for this reason, the bearing load of a motor connected to a multi-level inverter can be reduced. In addition, the common mode voltage v_{nN} can be eliminated by using advanced modulation strategies[30].
3. **The input currents:** The multi level inverters can draw an input current with a low deformation rates.
4. **Switching frequency:** The multi level inverters can operate at the fundamental frequency and high switching frequency of pulse width modulation.

It should be noted that a low switching frequency usually means a low switching loss so the efficiency is higher.

Unfortunately, the multi level inverters have some inconveniences. One particular disadvantage is the large number of semiconductor switches required.

Although evaluated switches with reduced voltage can be used in the multilevel inverters, each switch requires a gate control circuit. This can make the overall system more expensive and complex.

We present below, the main multilevel inverter topologies discussed in the literature, as well as its main strengths and weaknesses.

II.3 Different multi-level inverter topologies

There are three most important topologies:

1. The Neutral point clamped inverters,
2. The flaying capacitor inverters,
3. The cascaded h-bridge inverters.

Before continuing the discussion in this topic, it should be noted that the multi level inverter is used to refer to an electronic power circuit that could operate in inverter or rectifier mode. However, the illustrated topologies can also be implemented as well for rectifier.

II.3.1 The neutral point clamped multi level inverter

A. Nabae and H. Akagi introduced this multi-level inverter topology in 1981[24].

The objective was to reduce the amplitude of the harmonics injected by the inverter into the load for motor power applications.

This topology, known as a neutral point clamped inverter (NPC), does not use an isolation transformer and the distribution of the DC input voltages to the various switches in series is ensured by the clamp diodes connected to capacitive midpoints.

Figure II.1 shows the electrical schema corresponding to a leg when it generic N level inverter.

To obtain a voltage of N levels, $(N\ -1)$ capacities are required.

The voltages across the capacitors are all equal to $v_{dc}/(N\ -1)$, v_{dc} is the total voltage of the DC bus.

Each pair of switches ($S_n,\ \bar{S}_n$,with $n\ =\ 1, \dots, (N\ -1)$) forms a switching cell, so the two switches are controlled in a complementary way.

A series of $(N\ -1)$ capacitors allows to create a set of $(N\ -2)$ capacitive midpoints having voltage of $v_{dc}/(N\ -1)$, $2v_{dc}/(N\ -1)$, up to $v_{dc}(N\ -2)/(N\ -1)$.

The intermediate voltage levels on the output voltage can therefore be created by connecting each of these points to the output, by acting on the control signals ($S_1, \bar{S}_1, S_2, \bar{S}_2, \dots S_{N-1}, \bar{S}_{N-1}$) of the power switches.

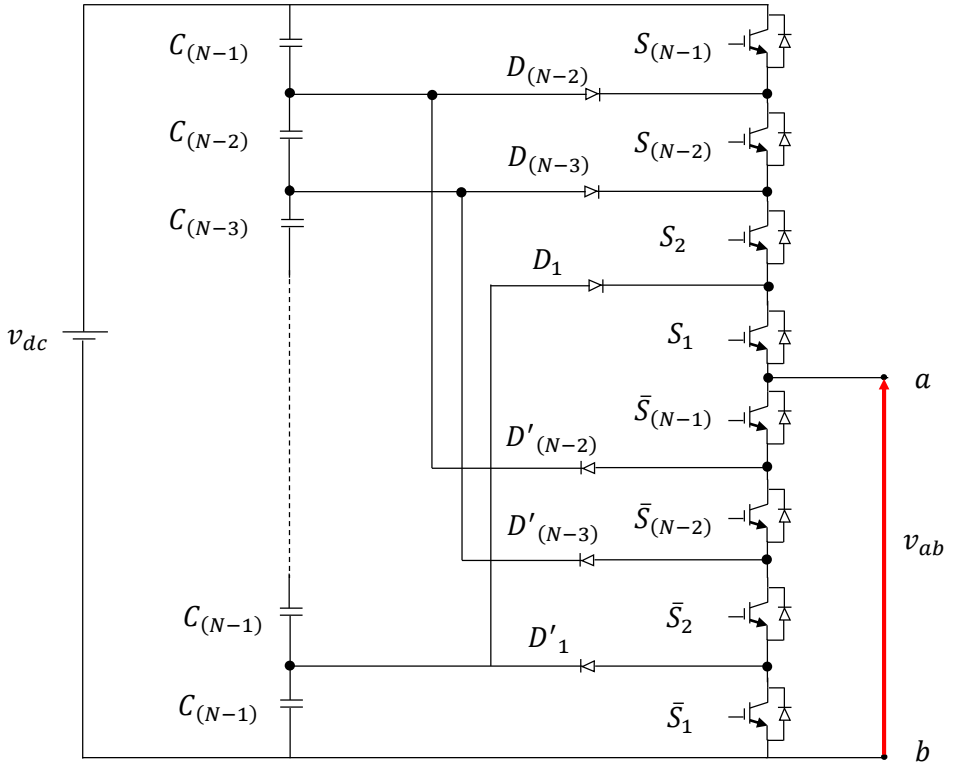

Figure II.1 A leg of N level neutral point clamped inverter.

Each leg of this inverter has four controllable switches and six diodes, as shown in figure II.2.

A direct voltage v_{dc} between terminals a and b is supplies this assembly. The three possible switching states allow to deliver three distinct and positive levels between terminals a and b.

Each phase/leg has two levels consisting of two switches of the type $IGBT$, S_{1H} and S_{1B} , with antiparallel diodes. Two additional diodes D_{1H} and D_{1B} are used to connect the intermediate level v_{1H} and v_{1B} to the midpoint n_1.

When the two levels are controlled simultaneously in the same way, the diodes D_{1H} and D_{1B} don't conduct and this assembly then functions as a two $IGBT's$ switch generating the two levels: $0\ V$ and v_{dc} between N and b. When S_{1H} and S_{2B} are conducting, and consequently S_{1B} and S_{1H} are blocked, the diode D_{1H} connects the midpoint n_1 to the nodes v_{1H} and v_{ab} for the output currents. The diode D_{1B} connects the midpoint n_1 to the nodes v_{1B} and v_{ab} for the incoming currents.

This means connecting the midpoint n_1 with the output voltage v_{ab} , independently of the current sign and allows to generate an intermediate level $v_{ab} = v_{dc}/2$ between a and b.

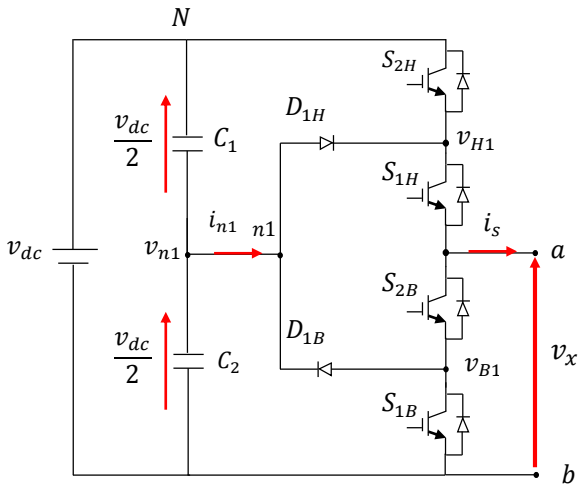

Figure II.2 A leg of three level neutral point clamped inverter.

The complementary command of the intermediate state leads to conduit the output v_{ab} to the level N for an incoming current and to null level for an outgoing current.

This state is therefore undefined and therefore not allowed in normal inverter commutation. The possible switching states are summarized in table I.1.

Table 1.1: Possible states of three level NPC inverter

Voltage levels	***Switching stats***				i_{C_f}
	S_{1H}	S_{2H}	S_{1B}	S_{1B}	
$+\boldsymbol{v_{dc}}$	1	1	0	0	2
0	0	0	1	1	1
$-\boldsymbol{v_{dc}}$	1	0	0	1	0
Infinite	0	1	1	0	x

When S_{1H} and S_{2H} are clamped, the potential of point v_{1H} is maintained at a value higher or equal to that of the midpoint v_{n1}.

Nothing prevents the potential of v_{1H} from rising higher than the potential of the midpoint, which leads to the breakdown of the switch S_{1H}, which is designed to block the intermediate half voltage 'v_{dc}'. The same is true for the same reason for S_{2B}.

A resistor was placed between v_{1H} and v_{1B} ensures that the blocked voltage is distributed between the two switches. The assembly can then be done using components clamping the half voltage supply 'v_{dc}' [31].

This property can pose problems in the stabilization of the potentials of capacitive midpoints.

Indeed, a single leg supplying a unidirectional current source is not capable of imposing the same intermediate voltage level indefinitely.

This is because the configuration of the corresponding phase will require the charging current to pass through the capacitors always in the same direction.

However, this disadvantage can be mitigated when using a three phase inverter, because in this case the capacitive midpoints are shared by all three phases, the zero sequence currents component can be used at the control level to balance the capacitors [32].

Concerning the accounting of the number of components, active and passive, a three phase N level neutral point clamped (NPC) inverter has :

- $(N\ -1)$ capacitors for the creation of capacitive midpoints. Each capacitor must be dimensioned for a voltage equal to $v_{dc}/(N-1)$ and for a current equal to the maximum load current;
- $6(N\ -1)$ power switches of the fully controlled semiconductor plus the diodes being mounted head to tail;
- $6(N\ -2)$ clamp diodes.

Each leg of the inverter is seen as a switch whose positions allow the potential of point 'a' to be modified.

As shown in figure II.3(a), this point is connected each time to one of the voltages across the capacitors, which are sometimes connected in series.

An example of the switching configuration is shown in figure II.3(b) and figure II.3(c), when the discontinuous line switches are open.

Figure II.3 shows the principle and switching mechanism of a five levels NPC inverter with:

a. The principle for which the action of the power semiconductors is represented by an ideal switch with several positions. Each position represents a voltage level.

b. The inverter generates the 1^{st} voltage level $v_{ab}\ =\ v_{C4}\ =\ \frac{v_{dc}}{4}$.

c. The inverter generates the 3^{rd} voltage level $v_{ab}\ =\ v_{c4}+v_{c3}+v_{c2}\ =\ \frac{3\,v_{dc}}{4}$.

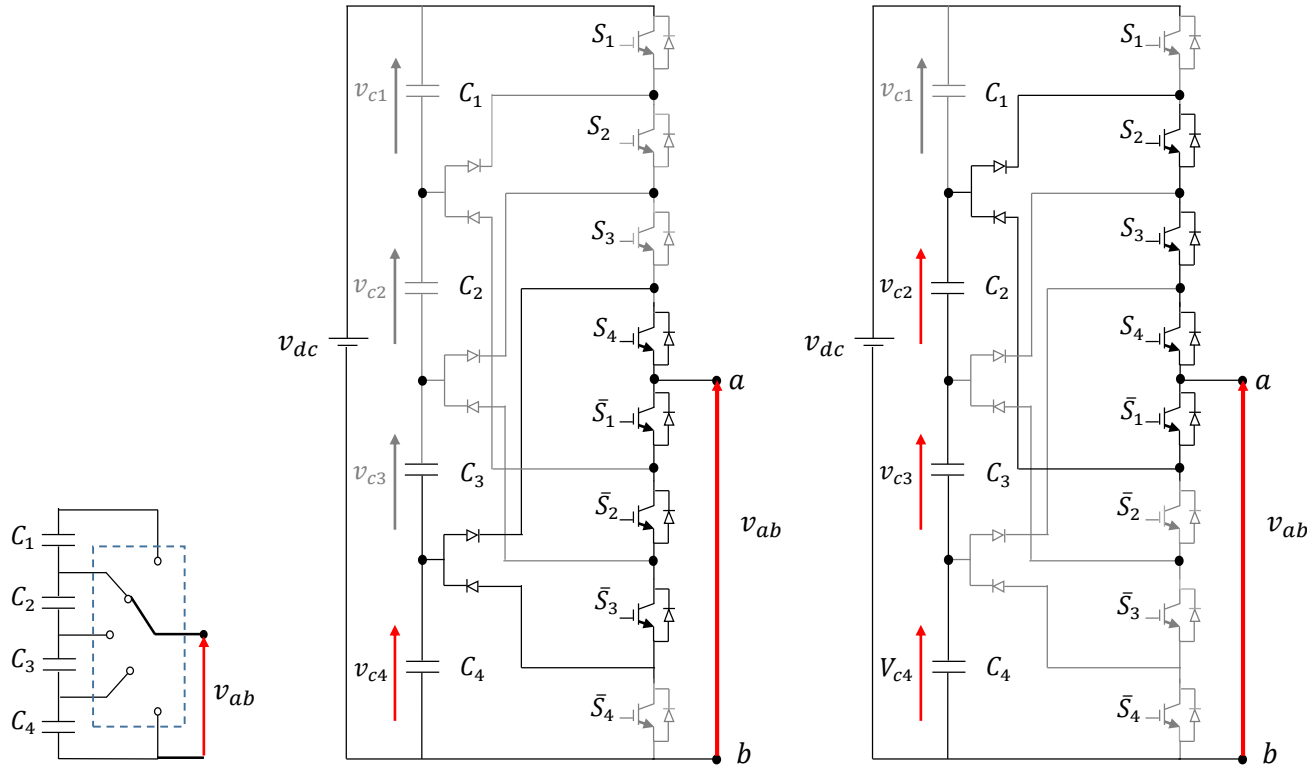

(a)The principle topology of NPC inverter (b) Five level inverter: the voltage level 1 (c) Five level inverter: the voltage level 3

Figure II.3 Neutral point clamped inverter topologies

II.3.1.1 Advantages

The main advantages and inconveniences of multi-level NPC inverters are as follows:

- The resulting three level waveforms has a better spectral quality compared to that of a three phase standard inverter, which makes passive filters less voluminous, even non-existent;
- It is configurable to obtain a high number of levels, allowing you to reduce the voltage blocked by each switch; this is given by $v_{dc}/(N\ -\ 1)$;
- For a three phase inverter all phases are shared the DC bus, which reduces the capacitors. For this reason, a back-to-back topology is no only possible but also practical for uses such as interconnection back-to-back high voltage or a variable speed drive;
- The capacitors can be recharged as a group;
- The flow of reactive energy can be controlled [33].

II.3.1.2 Inconveniences

- When the number of levels is great than three, the balance of voltages across the capacitors becomes difficult, as it is intimately related to the power factor of the load at the modulation index.
- The inequality of the reverse voltages carried by the diodes;
- The inequality of switching between switches located outside the structure compared to others;
- The number of diodes becomes excessively high with the increase in levels[33];
- It is more difficult to control the power flow of each inverter[33].
- Indeed, the voltage blocked by each diode depends on its position in the system.

For N level inverter, there are two diodes whose voltage to be blocked. One solution to this problem is to insert a large number of diodes in series. Assuming that the inverse voltage of the diodes is the same, the number of diodes required increases very quickly with the number of levels, which complicates the implementation of the circuit and makes it unreliable at the same time. Depending on the application, it is necessary to insert more diodes in series in the part of the circuit requiring the blocking of high voltages; so that it is possible to find for two given voltage levels, a different number of diodes connected in series, in order to respect their blocking voltage. Figure II.4 shows the pyramidal scheme of interconnection

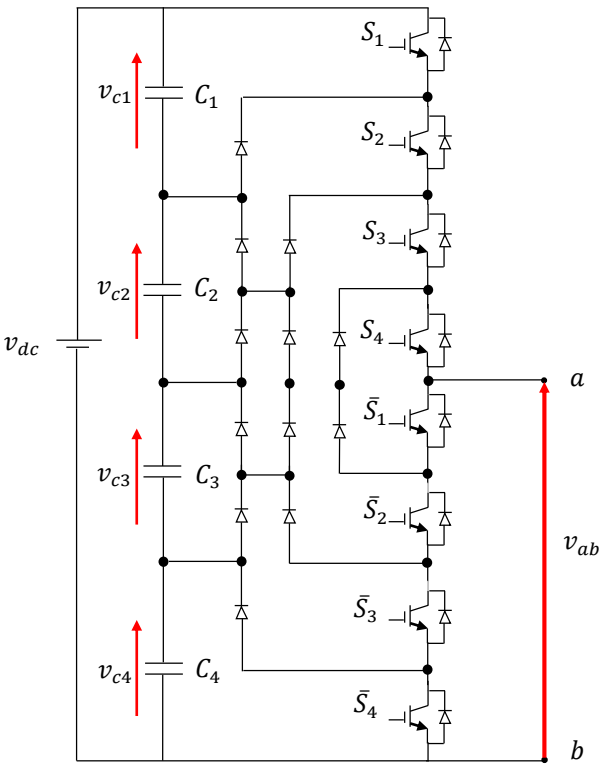

Figure II.4 pyramidal scheme of interconnection neutral point clamped topology

Depending on the desired voltage level, the diodes connect mutually in series so that each of them blocks the same voltage, $v_{dc}/(N\ -1)$.

The switches at the ends of each leg and their complements undergo few switches, while those located around point 'a' undergo more. If the inverter is designed to be used with the same average duty cycle for all power switches, it is therefore necessary to oversize those located inside the leg, so that they can support the switching rate [34].

Due to the uneven conduction time of the switches, the loading or unloading time of the capacitors is affected. The voltage wave undergoes a change due to the non-uniformity of its value between two consecutive levels, as well as an increasing in the dv/dt. This topology therefore requires rigorous control the equilibrium of the voltages across the capacitors [34].

II.3.1.3 Other variants of neutral point clamped inverter topology

There are several variants of multi-level NPC inverters whose configuration is a modification of the basic NPC topology. These allow, for example, to postpone some limitations of the basic topology, such as the inequality of reverse tensions supported by the diodes [35]. Figure II.5 shows other variants on the NPC topology.

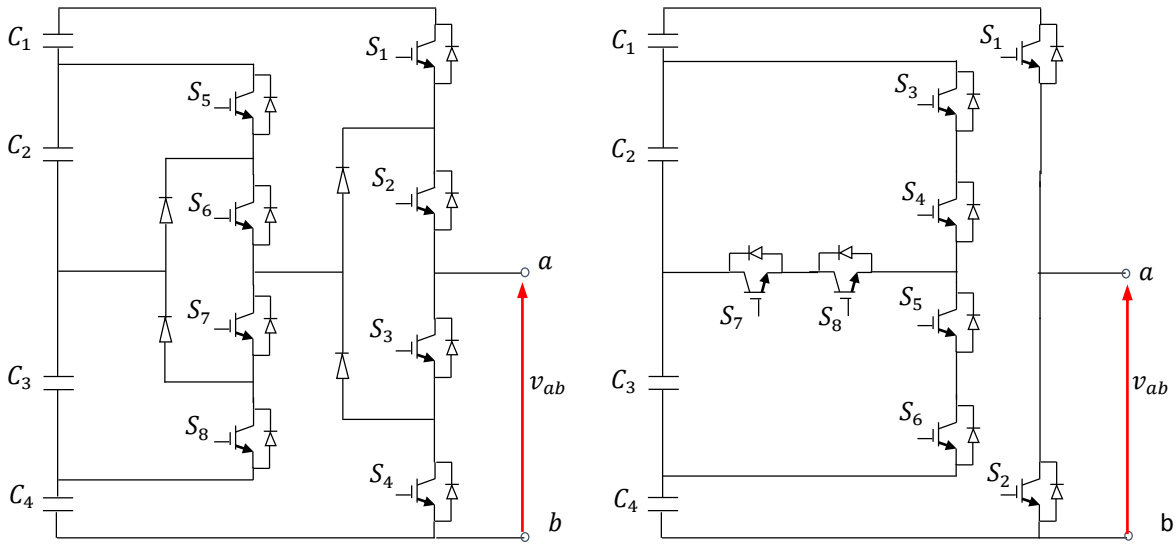

(a) Connection of two single phase NPC inverters (b) NPC Inverter with Bidirectional switches

Figure II.5 Other variants on the NPC inverter topology

Figure II.5 (a) shows a connection of two NPC inverters, and allows a voltage with five different values , but does not solve the problem of unequal blocking voltages that the switches must support. This variant is better suited for low power applications. It has the same number of switches as five level NPC inverter topology, but access to the neutral point is through bi-directional switches and the switches do not support the same voltage. This variant is also better suited for low power applications [35], [36].

II.3.2 Flying capacitor multi-level inverter

This topology was introduced in 1992 by T.Meynard and H.Foch . The topology of the multilevel flying capacitor inverter is similar to that of the multilevel NPC inverter except that instead of using clamp diodes, they are replaced by capacitors that play the role of flaying voltage sources from which it comes the name flying capacitor inverter [38].

Each phase of the N level flaying capacitor inverter is represented by the series connection of $(N-1)$ cells (figure II.6). Each cell consists of a pair of switches separated by a flying capacitor.

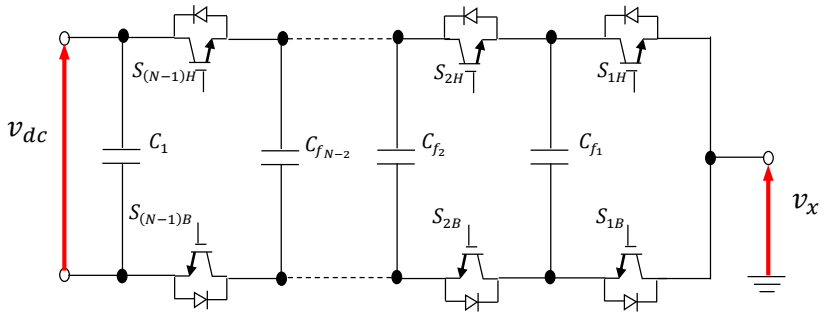

Figure II.6 A leg of N level flaying capacitor inverter

Therefore, globally there are $2(N-1)$ switches, a DC voltage source and $(N-2)$ flying capacitors charged by N level voltages.

A proper series connection of the flying capacitor with different voltage levels allows the inverter to produce a synthesized output voltage. This connection is made by setting the switch of each cell to the conduction state (ON). However, the two switches of the switching cell must never be in the passing state simultaneously (i.e. the switches of the same switching cell must be ordered in addition) for example (S_{1H}, S_{1B}), otherwise two consecutive capacitors with different voltage values would be connected in parallel, which results in a short circuit. The combination of switches and capacitors ensures that the voltage is always well defined through any shut switch.

Another inherent characteristic of this topology is the degree of freedom produced to balance the flying capacitors due to redundant switching states. These redundant states produce the same output voltage. it consider only the last two cells of the topology presented in figure II.6, the output voltage equal to $v_x = v_{dc}/(N-1)$ with the negative potential consideration of C_{f2}, which can be generated by setting the switches S_{2H} and S_{1B} or by the switches S_{2B} and S_{1H} .However, the current flowing through the capacitor is in the opposite direction.

Therefore, by choosing an appropriate state according to the direction of output current, the voltage of the flying capacitors can be controlled. Although the multicellular representation allows a simple analysis of the topology, the usual single phase flying capacitor inverter is shown in figure II.7.

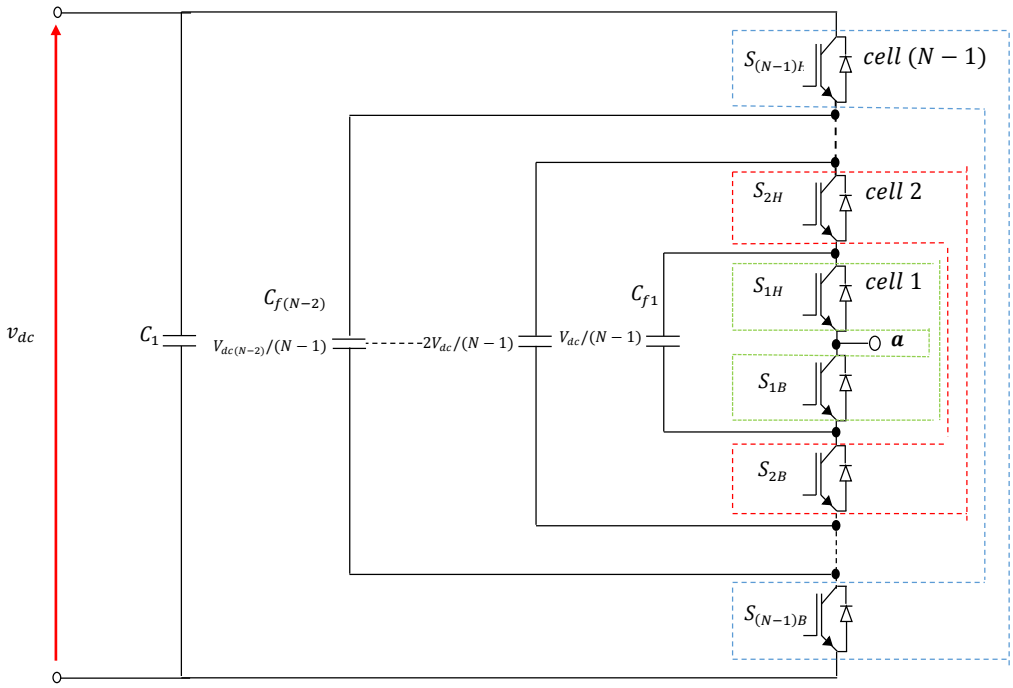

Figure III.7 Single phase N level flaying capacitor inverter

The switches S_{2H} and S_{1H} are in the passing state to have the positive voltage level $+v_{dc}/2$ then to have the negative voltage level $-v_{dc}/2$, the switches S_{1H} and S_{2B} are in the passing state, and to have the null voltage level , one of the following switch pairs S_{2B} and S_{1H} or S_{1B} and S_{2H} must be switched on.

This redundancy is used to balance the flying capacitor C_{f1}, since the floating output current considered at the point a, the first pair produces the negative current of the flying capacitor, while the second produces a positive current, as shown in table I.2.

Table I.2 Voltage levels of three level flying capacitor inverter.

Voltage levels	**Swathing stats**				i_{C_f}
	S_{1H}	S_{2H}	S_{1B}	S_{2B}	
$+v_{dc}/2$	1	1	0	0	0
0	1	0	0	1	$-i_a$
0	0	1	1	0	$+i_a$
$-v_{dc}/2$	1	0	0	1	0

For the five level inverter (Figure II.8 (b)), the flexibility is increased since there are more redundant states. The output voltage with respect to point a is synthesized by the following switching conditions:

1. For the voltage level $v_{ab} = v_{dc}/2$, all high switches are set to the passing state.
2. For the voltage level $v_{ab} = v_{dc}/4$, there are four possible combinations.
3. For the voltage level $v_{ab} = 0$, there are six possible combinations .
4. For the voltage level $v_{ab} = -v_{dc}/4$, there are four possible combinations;
5. For the voltage level $v_{ab} = -v_{dc}/2$, all low switches are set to the passing state;

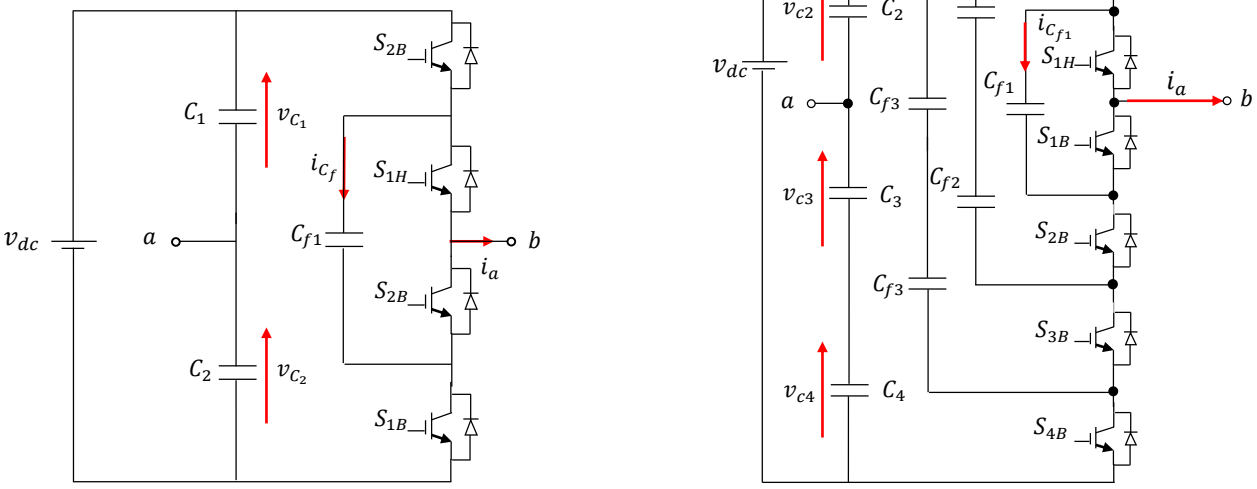

(a) Three level FC inverter (b) Five level FC inverter

Figure II.8 Flying capacitor inverter topologies

The main advantages and disadvantages of this topology are given as follows:

II.3.2.1 Advantages

- The clamping voltage of the switches is the same throughout;
- The concept can be easily applied to other types of power converters (DC to DC, AC to AC, AC to DC), both for unidirectional power transfer and bi-directional;
- Its modularity allows easy extension and adaptation of control strategies at a high number of levels;
- The availability of redundant states balances the voltage levels of the capacitors;
- For a large number of levels, the use of the filters is unnecessary;
- The possibility to control of active and reactive power;

II.3.2.2 Inconveniences

- The main disadvantage of this topology is the required number of capacitors, which can be a prohibitive volume. In addition, if the application in which the inverter is used requires non-zero initial voltages at the terminals of capacitors, a precharging control strategies must be associated with the control strategy adequate;
- The control is complicated to monitoring the voltage level for all capacitors.
- In addition, the complexity of starting up by preloading all the capacitors at the same voltage level;
- The control of the system becomes difficult with the level is increased.

II.3.3 Cascaded h-bridge multi level inverter

This family is the first described in the literature as a multi level inverter topology [39]. Indeed, The sequencing of several topologies at three levels allows to have at the output a multi-level voltage waveform[40]. The cascaded h-bridge multi-level inverter is simply the serial connection of several single phase h-bridge inverters with isolated DC voltage sources (Figure II.9).

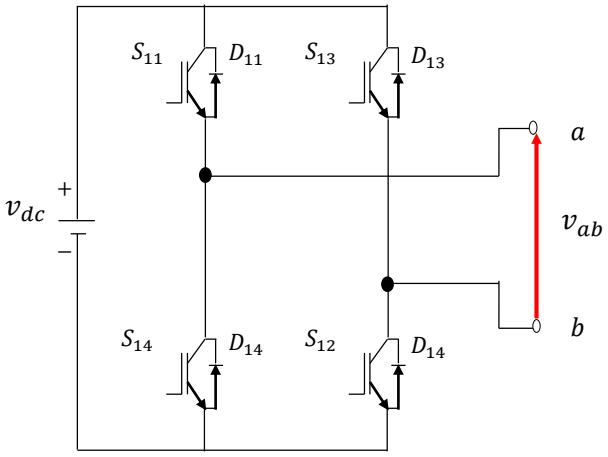

Figure II.9 Single phase h-bridge inverter.

Figure II.10(a) shows the schema of a multi level inverter based on the series connection of single phase inverters. The cells are connected in a star connection, but it is also possible to connect them in a triangle.

Each partial cell is supplied by a DC voltage source. If the separated DC sources have the same DC voltage level (v_{dc}), the phase voltage will be able to range from the level ($-c * v_{dc}$) to the level ($+c * v_{dc}$) that will have N levels. where $c = (N - 1)/2$ is the number of all h-bridges(cell) or the number of separate DC sources.

As the number of voltage sources (v_{dc}) increases, there would be more levels in the output voltage. Thus, the output voltage waveform will be more similar to the sinusoid, even without filtering [41].

Each single phase h-bridge inverter can generate three output voltage values: $0V$, $-v_{dc}$ and $+v_{dc}$.

The output voltages of each cell/bridge are summed up via the transformers T_f, whose transformer ratio can be chosen in order to obtain a desired maximum voltage value v_{ab}, from a DC sources. Figure II.10(a) shows the h-bridge circuit to generate an N level of one phase.

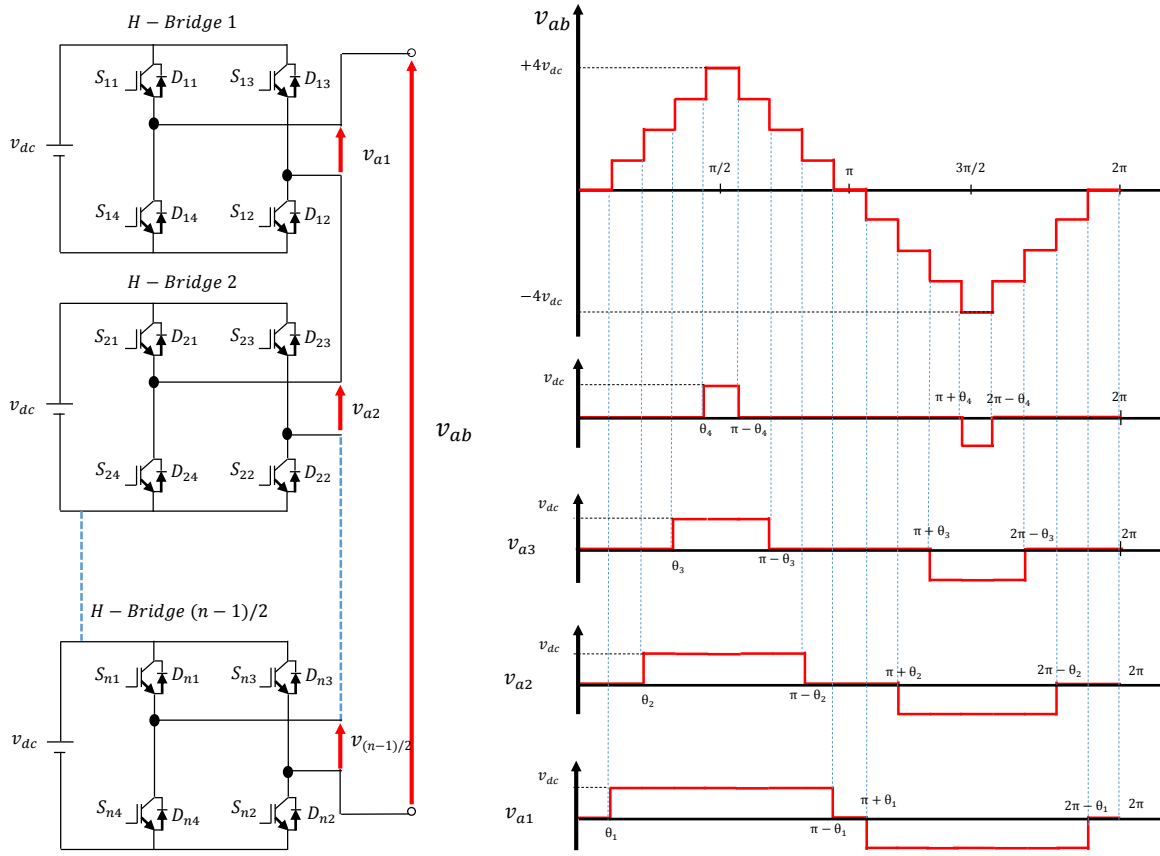

(a) A leg of N level CHB inverter

(b) The waveforms for a leg of 11 level CHB inverter

Figure II.10 Topology and waveforms of a multi level cascaded h-bridge inverter

Figure II.10(b) shows the waveforms obtained with a leg of 11 levels , for the two previous assemblies. In the assembly of Figure II.10(a), the alternating outputs of the three level h-bridge inverter are directly connected in series. Obviously, this requires isolated DC voltage sources.

In applications where the power source is already distributed by several PV modules, such as when the power source consists of several batteries, this requirement is naturally achieved.

However, if starting from a single DC bus, the generation of isolated DC sources must be done using galvanic isolated DC/DC converters, which can considerably increase the cost of the equipment.

In both installations, although the voltage levels generated are inherently stable (no rebalancing action is expected), this is achieved at the price of complexity and cost increased.

Indeed, to obtain an output voltage of N levels, it will be necessary to have $(N-1)/2$ h-bridge/cell inverter of 3 level single phase/leg. Each bridge must be dimensioned for load current divided by N.

The distinctive property of this topology in relation to the number of levels, which could theoretically extend to infinity, is a considerable advantage both from the point of view of equipment assembly and from the point of view of the inverter control strategies.

II.3.3.1 Advantages

This topology has several advantages as follow :

- The distinctive property of this topology is easily allows its extension to a high number of cells on each phase/leg, without any additional complexity;
- The natural balancing of voltages response is achieved, so that the control of the switches can be easily diverted;
- The switches support the same clamping voltage;
- It becomes possible to supply a high or medium load voltage from one or more low voltage power supplies.

II.3.3.2 Inconveniences

- It requires isolated DC sources for each h-bridge cell, which it limits the application possibilities;
- For a three phase systems, this type of inverter requires more power switches than a standard inverters.

II.4 Application of multi-level inverters in the industry

Multi-level inverters are receiving significant attention in industry and academia as one of the preferred conversion choices for high-power applications. They have successfully shaped their way in the industrial environment and can therefore be considered as a mature and proven technology. Currently, they are commercialized in standards and operate in a wide range of applications, such as compressors, extruders, pumps, fans, strawberries, rolling mills, conveyors, mills, furnace blowers, gas turbine starters, mixers, elevators, reactive energy compensation, marine propulsion, high voltage direct current $(HVDC)$ gearbox, hydro pumped storage, wind energy, and rail traction.

II.4.1 Application in the field of rail traction and electric vehicle

In rail traction, for example, some European transport networks provide a $15kV$ power supply. It uses a low voltage transformer frequency to adapt this voltage to static converters. Since, the problem of the galvanic isolation is bypassed.

For this purpose, the inverters are placed in parallel with the continuous side, their alternating sides going on primary windings distinct from a low frequency transformer (at the operating frequency of the load). The contributions of the different cells are added to the magnetic level of the transformer core, the secondary being made up of a single high voltage winding per phase. This type of inverter has been industrially manufactured for a power of $100\ MV$.

Other variants using low frequency transformers or motor windings to add voltages have been studied, including [42]. In electric vehicles, the use of multi level inverters is also possible. The exploitation of the topology based on the series connection of partial inverters becomes relatively easy, since each inverter is powered by a batteries of $48\ V$, thus ensuring the required galvanic isolation between all sources [43].

There is also the multi-level back-to-back converter with NPC structure for use in large drives of hybrid electric vehicles for heavy trucks.

The configuration of control system of an electric vehicle motor using a cascaded inverter topology, this configuration functions in two modes: In car running mode, in this mode the power flow is flowing from the batteries to the motor through the cascaded inverter.

In battery charging mode, the cascade converters act as rectifiers, and the power flow flows from the charger to the batteries. The cascaded inverters can also act as rectifiers to help recover the vehicle's kinetic energy if regenerative braking is used.

The application of the cascaded inverter as a boost on electric and hybrid electric vehicles can have the advantage of eliminating the bulky inductor of conventional dc/dc boost converters, which increases the power [43].

II.4.2 Application in the supply of on board networks and propulsion of maritime buildings

In maritime buildings, the limitation of available space poses enormous problems for the realization of an electrical power supply with a reduced size and weight. Multi-level conversion techniques can be used to supply ships.

A medium frequency transformer provides the connection between each elementary module of the rectifier and an output inverter[44].

Despite the high number of phases of asynchronous machines encountered in the propulsion of some American warships and despite their power (around 20 MW per engine), investigations have also been conducted on the use of multi-level converters to reduce the total harmonic distortion.

In [45], the authors conducted an evaluation between cycloconverters and other topologies, including the multi-level NPC inverter, for marine propulsion with variable speed in the 30MW range and they concluded that the NPC inverter frequency is more efficient than the cycloconverter. However, more efficient and less cumbersome, and which could be replaced by the NPC inverter due to the improvement of its power quality.

Figure II.11 shows a simplified diagram of an oil tanker power generation, distribution and charging systems with a redundant electrical system. Two 6.15MW back-to-back NPC inverters each driving a synchronous motor.

In addition, the tanker uses a multi-engine system with several engines powered by the same converter, for example, to drive both pumps for loading/unloading cargo and propulsion engines.

Since cargo pumps and propulsion engines are normally not used simultaneously, the front NPC converter is active and shared between the two units, which reduces the overall cost of the system.

Another important development of multi-level inverters for the propulsion of ships was motivated more on the engine side by multi-phase machines.

Over the past decade, multi-phase machines have become increasingly popular due to several interesting advantages such as high reliability, fault tolerance, improved torque performance, and higher power, making them particularly suitable for marine / ship propulsion systems. Therefore, the combination of multiphase and multi-level technologies adds a series of benefits that are useful for this application[46], [47], [48].

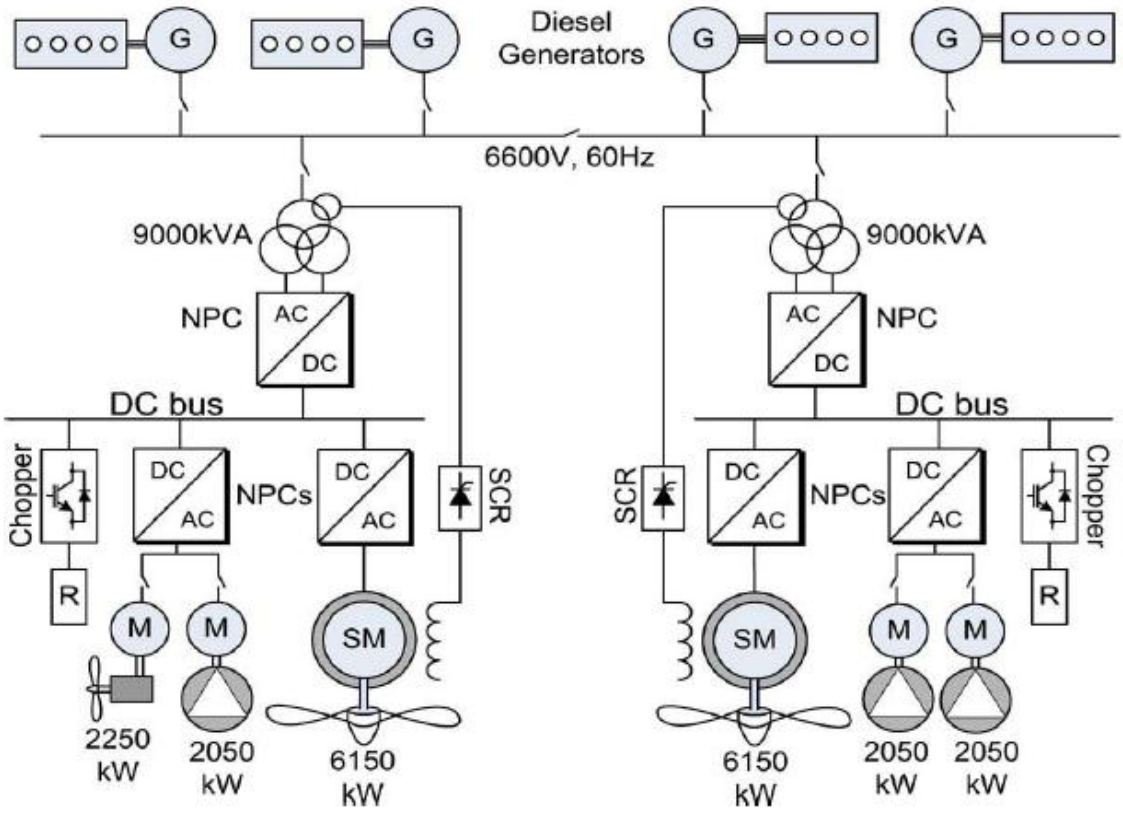

Figure II.11 Generator of an oil tanker with three level two NPC Back-to-Back converters.

II.4.3 Application in the field of electricity grids

Because they can provide medium or high voltage, multi-level inverters are also suitable for improving the quality of the voltage in electrical networks.

Production and injection of energy into the electricity grid, a allows multi-level inverters to be used as an interface between photovoltaic modules and the electricity grid.

The most suitable multi-level topologies for this type of installation are NPC topology and especially the cascaded h-bridge topology [49]. However, the NPC topology can be used as an interface between a high speed turbo alternator and the power grid[50].

On long distance of transmission lines, it is often necessary to compensate for reactive power. When properly controlled, multi-level inverters offer the possibility of adjusting the voltage amplitude and phase shift, but also the impedance of the transmission line. They can therefore play the role of static compensators. For this reason, the multi-level cascaded inverter is more suitable for reactive compensation [51]. Since each h-bridge can equilibrate its DC source without requiring additional

isolated power sources. Alstom has marketed a multi-level, cascaded h-bridge inverter for reactive energy compensation.

On the other hand, for the multi level flaying capacitor inverter, voltage balancing is relatively complicated, so it cannot be used in reactive energy compensation.

II.4.4 Application in the area of power supply for electrical machines

In industrial applications, medium and high power electrical machines require a medium voltage power supply. The use of multi-level inverters in this case is also more appropriate. In such systems, the semiconductors can only support a low voltage, compared to that required by the machine. The voltage quality in terms of harmonics is better, thus reducing the adverse effects on the life of the machine and the life of the potential grid that supplies it.

In addition, from low-voltage cells (such as batteries, fuel cells or photovoltaic cells), it becomes possible to supply a medium voltage machine. For this reason, the three level NPC topology is widely used in medium voltage applications using IGBTs with cooling by forced air. These applications cover a wide range of high power loads including fans, pumps, blowers, compressors, and conveyors. However, the multi level NPC structure has a great interest in speed variation.

Initially the multi level converter with a multi level flaying capacitor inverter topology was proposed for high voltage of the DC to DC conversion advantageous for speed variation[. It is easy to balance the voltages for such applications because the charge current is continuous. Currently it is widely used in inverters and marketed as a variable speed drive[50].

Another type of multi level inverter was introduced the first time for applications of the electric motor drives, which is the cascaded topology, in the which DC sources are isolated and separated for each h-bridge/cell. However, in industrial applications such as the supply of high-power compressors , the supply network is often high voltage ($10kV$, $11kV$, $33kV$, $35kV$,$33KV$, $270KV$…).

The presence of a low-frequency transformer is almost unavoidable, in order to adapt the mains voltage to that of the machines, it taking into account the limitation in blocking voltage of current semiconductors.

The transformer in this case, facilitates the obtaining of isolated sources with a transformer[52]. Its size, cost and maintenance (including cooling) are no longer a problem, since it this is a stationary application.

II.5 Comparison of different multi level inverter topologies

The topologies such as NPC inverters and embedded cell inverters divide their supply voltage: The output voltage is smaller than or equal to the input DC voltage. They are capable of operating from a continuous power supply unique. On the other hand, the structures such as series cell inverters raise their supply voltage, so the maximum output voltage is greater than each of the supply voltages; it is less than or equal to the sum of the supply voltages [33].

Contrary to other topologies, cell power supplies cannot be obtained from a single continuous power supply without additional converters. In most cases, transformers are required to obtain the necessary power supplies. The parallel coupling of transformers on the «side supply» and the addition of the « load side » voltages leads to an increase in the voltage.

Although the choice of multi-level topology is directly related to the application and list of characteristics, in order to minimize losses, volume and costs, usually the number of components plays the most important role [53].

For a three-level approach, the analysis shows that neutral point clamped inverters (NPC), flaying capacitor inverters (FC) and cascaded h-bridge inverters (CHB) require the same number of switches, however they differ in the elements and the number of DC sources required.

For applications where only one continuous source is available, the neutral point clamped inverters(NPC) and flaying capacitor inverters(FC) topologies are advantageous compared to the cascaded H-bridge topologies, which require a special transformer to provide the various continuous independent sources.

On the one hand, when the different sources are available the cascaded H-bridge topology could be considered a suitable solution since it requires the minimum number of components [49]. This first comparison based on the number of components allows us to draw some conclusions and to separate the fields of application of these different converters. The NPC inverters are interesting for three-phase applications requiring few levels. The energy stored at the intermediate level can be reduced.

Structures allowing direct conversion, such as NPC and embedded cells, are advantageous for applications with active power exchange, where galvanic isolation is not required between power exchange sources. Inverters of cascaded cell are very advantageous for single-phase applications without the need for active power. when galvanic isolation is not required between power exchanging sources.

Cascaded multilevel inverters are very advantageous for single-phase applications without active power supply. They are suitable even for very high voltages.

They are also preferred for applications where galvanic isolation with medium or high-frequency transformers is required. Table II.3 summarized the big different between topologies of inverters in terms of components and their applications.

Table II.3 comparison of power components between different topologies of inverters

$\boldsymbol{Inverter\ topology}$ / $\boldsymbol{Components}$	$\boldsymbol{Diode\ clamped\ inverter\ (NPC)}$	$\boldsymbol{Flying\ capacitor\ inverter\ (FC)}$	$\boldsymbol{Cascaded\ h-bridge\ inverter\ (CHB)}$
DC Bus capacitor	$(N-1)$	$(N-1)$	0
Clamping diode per phase	$(N-1)\ (N-2)$	0	0
Power semi-conductor switches	$2(N-1)$	$2(N-1)$	$2(N-1)$
Balancing capacitor per phase	0	$(N-1)\ (N-2)/2$	0
Voltage unbalancing	Average	high	Very small
main diodes	$2(N-1)$	$2(N-1)$	$2(N-1)$
Flying capacitor number	0	$(N-1)\ (N-2)$	0
Isolated DC source	1	1	$(N-1)$
Applications of different inverter	▪ Static VAR compensation ▪ Variable speed motor drives ▪ High voltage system interconnections ▪ High voltage DC and AC transmission lines	▪ Induction motor control using DTC (Direct Torque Control) circuit ▪ Static VAR generation ▪ Both AC-DC and DC-AC conversion applications ▪ Converters with Harmonic distortion capability ▪ Sinusoidal current rectifiers	▪ Motor drives ▪ Active filters Electric vehicle drives ▪ DC power source utilization Power factor compensators Back to back frequency link systems ▪ Interfacing with renewable energy resources.

II.6 Conclusion

Due to the ability to use more than two voltage levels to synthesize a sinusoidal voltage, the use of multi level inverters has been increased by industry since the introduction of the three level inverter. In addition to improving spectrum quality, when compared to standard two level topology, multi level inverters use power devices with a low voltage ratio and lead to reduced switching losses and electromagnetic effects. Among the multi level topologies mentioned, some inverter structures include the neutral point clamped inverter topology(NPC), the flying capacitor inverter topology (FC) and cascaded h-bridge inverter topology (CHB) that use the same basic concept instead of diodes, there are capacitors. However, although these concepts have been used extensively by industry, the practical number of levels is limited by the required number of connected clamping elements in series. The Approaches that eliminate the need for clamping elements were emerging in recent years. The cascaded h-bridge inverter performs the multi level voltage by connecting the single phase h-bridge inverters in series. However, it requires that an isolated voltage sources for each single phase/cell, which can limit the use of such a topology in some applications.

Although the majority of the multi level topologies presented so far differ in the structure of their circuits, they all require appropriate control of the voltages of DC bus capacitor or in some cases flying capacitors. The industrial application of these topologies differs from one domain to another and from one topology to another. Each structure is advantageous in one area and it has disadvantages in another, there is no multi-purpose topology each structure to its field of application. Finally, this chapter compares multi-level topologies in terms of number of components and DC voltage sources.

Chapter III

Control Strategies for Three Phase VSI and Multi-Level H-Bridge Inverter

III.1 Introduction

The control strategies of multi-level converters use the commonalities that these different topologies have in common. Among these commonalities are the achievement of redundancies between states and output voltage levels from the interconnection of conventional switch cells and the use of power storage elements. In this chapter, we will present the principles of control which are common to all these converters and which are based on pulse width modulation (PWM).

In the case of multi-level converters, it is often preferable to split the signal realization into two parts. In this sense, we usually use a modulator and a control command generator.

The modulator, based on the comparison of a low-frequency signal and high-frequency carrier signals, is independent of the multi-level structure under consideration and depends only on the number of output levels, whereas the control command generator can change according to the chosen structure. The generation of the appropriate duty cycles for the control of the external and internal variables of the converter will be carried out by linear controllers.

In this chapter a theoretical study of two level voltage source inverter and multi-level cascaded h-bridge inverter using space vector pulse width modulation control and predictive control.

III.2 Multi-level inverter control principle

The generation of the control commands for a multi-level converter is usually done in two steps:

1. **The first step** is to generate the succession of output voltage levels from a comparison between a low-frequency signal and a regularly phase-shifted carrier signal at high frequency. The output of this first step consists of ideal multilevel waveforms.
2. **The second step** of the control principle will create switching commands related to each switch according to the studied topology and the desired voltage levels. This step will also allow energy management in the storage elements and the distribution of switching losses across the switch set.

Figure III.1 shows the principle of control command generation where the modulation block represents the modulator used to obtain the desired voltage levels and the generation block selects the next state of the converter.

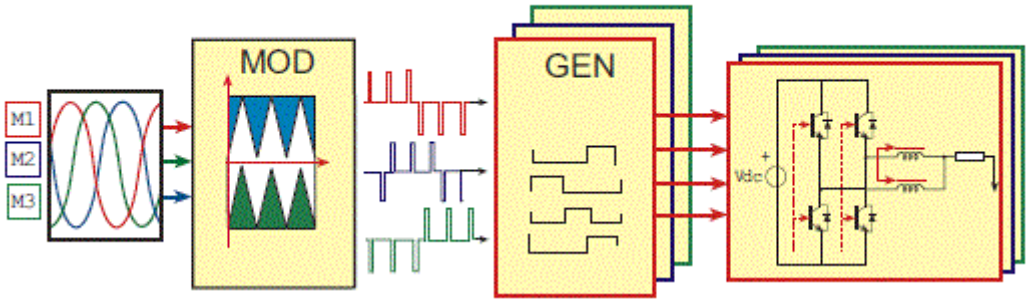

Figure III.1 Multilevel converter control architecture.

III.3 Multi-level modulator

In this chapter, we will detail the advantages of using a generic modulator when generate control commands for a multilevel converter. The most commonly used multilevel modulator is the space vector pulse width modulation . This modulator is processed and applied to the different connections between the switching cells .

III.3.1 Presentation of the two-level voltage source inverter

The DC to AC converter is a voltage inverter. It consists of three legs (a, b, c) each composed of two transistors and two antiparallel diodes. The eight voltage vectors applied to the inverter correspond to the different switch configurations shown in figure III.2.

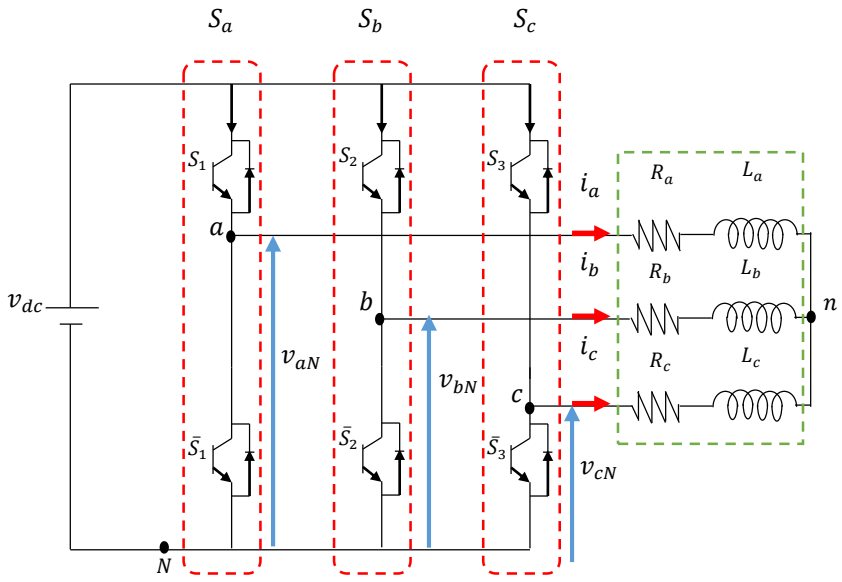

Figure III.2 Three-phase voltage source inverter topology

III.3.2 Description and operation of two-level three-phase inverter

The model of the converter in stationary reference frame abc can be written:

$$\begin{cases} v_{an}(t) = L\frac{di_a(t)}{dt} + Ri_a(t) \\ v_{bn}(t) = L\frac{di_b(t)}{dt} + Ri_b(t) \\ v_{cn}(t) = L\frac{di_c(t)}{dt} + Ri_c(t) \end{cases} \quad \text{(III.1)}$$

Where,

i_a, i_b and i_c are the currents associated to the loads.

R and L are the load resistance and load inductance respectively, without considering equivalent series resistor.Table III.1 shows the parameters of this inverter.

Table III.1 three phase voltage source inverter parameters

Parameter	Value
DC link voltage, v_{dc}	200 V
Inductance, L	20 mH
Resistance, R	10 Ω
Sampling time, T_s	1 μs
frequency, f	50 Hz

$v_{an}(t)$, $v_{bn}(t)$ and $v_{cn}(t)$ are the load voltages, can be defined as:

$$\begin{cases} v_{an}(t) = v_{aN}(t) - v_{nN}(t) \\ v_{bn}(t) = v_{bN}(t) - v_{nN}(t) \\ v_{cn}(t) = v_{cN}(t) - v_{nN}(t) \end{cases} \quad \text{(III.2)}$$

$v_{aN}(t)$, $v_{bN}(t)$ and $v_{cN}(t)$ are respective three-phase inverter output voltages. Figure III.3 and figure III.4 show the load voltage, $v_{an}(t)$ and the line voltage, $v_{ab}(t)$ respectively.

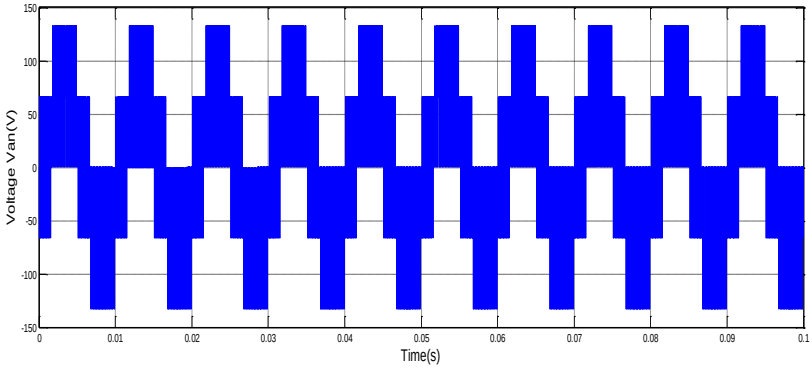

Figure III.3 The load voltage v_{an}

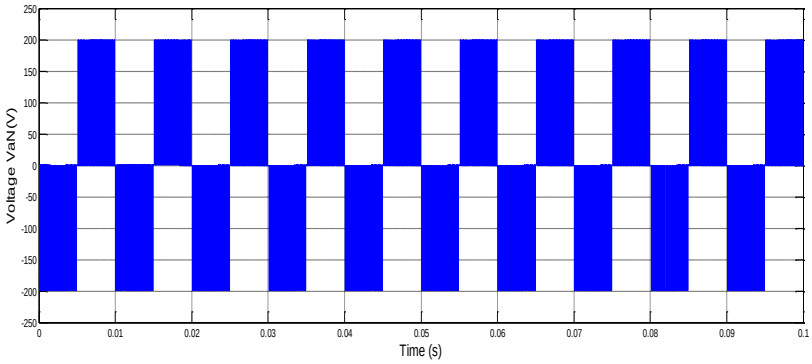

Figure III.4 The line voltage v_{ab}

$v_{nN}(t)$ is the common-mode voltage defined as:

$$v_{nN}(t) = \frac{1}{3} * \left(v_{aN}(t) + v_{bN}(t) + v_{cN}(t)\right) \quad \text{(III.3)}$$

The load voltages can be defined as:

$$\begin{cases} v_{an}(t) = \frac{1}{3}[v_{ab}(t) - v_{ca}(t)] \\ v_{bn}(t) = \frac{1}{3}[v_{bc}(t) - v_{ab}(t)] \\ v_{cn}(t) = \frac{1}{3}[v_{ca}(t) - v_{bc}(t)] \end{cases} \quad \text{(III.4)}$$

Where

$v_{ab}(t), v_{bc}(t)$ and $v_{ca}(t)$ are the phase to phase voltages can be written:

$$\begin{cases} v_{ab}(t) = v_{an}(t) - v_{bn}(t) \\ v_{bc}(t) = v_{bn}(t) - v_{cn}(t) \\ v_{ca}(t) = v_{cn}(t) - v_{an}(t) \end{cases} \quad \text{(III.5)}$$

Assuming that the system is balanced $v_{an}(t) + v_{bn}(t) + v_{cn}(t) = 0$ (III.6)

III.3.3 Vector modelling of two-level voltage source inverter

The output voltages $v_{aN}(t)$, $v_{bN}(t)$ and $v_{cN}(t)$ of inverter are determined by the switching states S_i (where $i = a, b, c$), which are supposed perfect (figure III.2) ,that define the values of the output voltages witch can be derived as:

$$v_{iN} = S_i . v_{dc} \tag{III.7}$$

If the top switches S_1, S_2 and S_3 are turns "on" (separately or together) , then the phase voltages v_{aN} , v_{bN}, v_{cN} equal to $+v_{dc}$. Else the top switches S_1, S_2 and S_3 are turns "off" the phase voltages (v_{aN}, v_{bN}, v_{cN}) is equal to null value ($v_{iN} = 0V$)(table III.2).

- $S_i = 1$ if the top switch is closed (on) and the bottom switch is open(off),
- $S_i = 0$ if the top switch is open (off) and the bottom switch is closed (on).

Different combinations of the three states (S_a,S_b,S_c) because The bottom switches are complementary to the upper switches, means eight possible states of the vector $\overrightarrow{V_s}$:
$000, 001, 010, 011, 100, 110, 110, 111$, two between them correspond to the zero vector(000,111). The zero vectors are placed in the origin of the axis (Figure III.5).

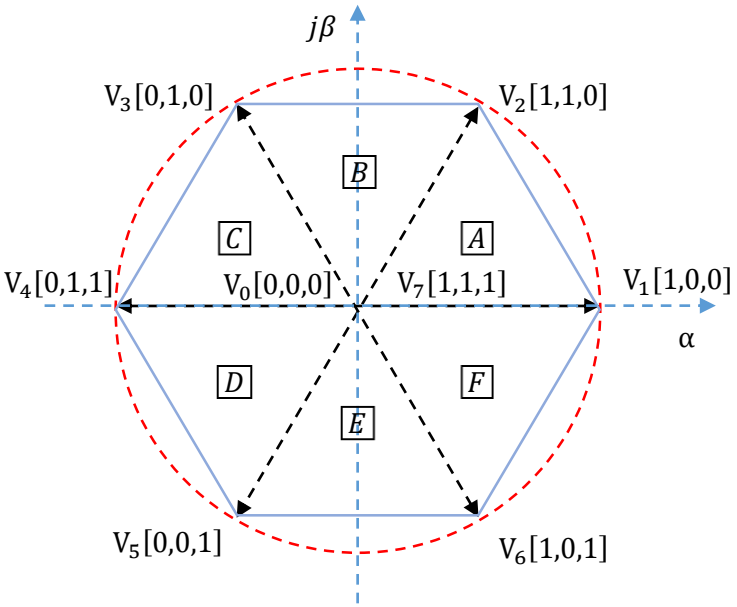

Figure III.5 Two-level inverter space vectors diagram in $\alpha\beta$ coordinate.

$$\overrightarrow{V_s} = \frac{2}{3} v_{dc} \left[S_a + S_b e^{j\frac{2\pi}{3}} + S_c e^{j\frac{4\pi}{3}} \right] \tag{III.8}$$

$$\begin{cases} \overrightarrow{V}_0 \Leftrightarrow [S_a, S_b, S_c] = [0,0,0] \\ \overrightarrow{V}_7 \Leftrightarrow [S_a, S_b, S_c] = [1,1,1] \end{cases} \tag{III.9}$$

Table III.2 switching states for each phase/leg.

Switching states	S_a			S_b			S_c		
	S_1	$\overline{S}_1$	v_{aN}	S_2	$\overline{S}_2$	v_{aN}	S_3	$\overline{S}_3$	v_{aN}
1	on	off	$+v_{dc}$	on	off	$+v_{dc}$	on	off	$+v_{dc}$
0	off	on	0	off	on	0	off	on	0

III.4 Space vector modulation control

III.4.1 Space vector pulse width modulation principle

The principle of space vector modulation consists in reconstructing the voltage vector V_{ref} from eight voltage vectors. Each of these vectors corresponds to a combination of the switch states of a three-phase voltage inverter; it is not based on separate calculations of the modulations by each of the inverter legs.

This technique follows this steps:

- The reference vector V_{ref} is calculated globally and approximated over a modulation period T_s by a medium voltage vector.
- For each phase, the modulation period T_s centered on the period whose mean value is equal to the value of the reference voltage at the sampling time.
- All half-bridge switches have the same status at the centers and ends of the period.
- A combinatorial analysis of all possible switch states allows the voltage vector V_{ref} to be calculated.

The reference vector V_{ref} is approximated on the modulation period, by the generation of an average vector elaborated by the application of the available vectors (Table.III.3).

It consists in considering the three-phase system as a two-phase system, and applying a Clarke transformation to it to bring it back into the $\alpha\beta$-plan.

This vector is not directly achievable by the inverter switches, but the three nearest configurations (located on the summits and in the center of the hexagon) can be searched and applied successively for an adequate fraction of the sampling period, so as obtain in average value the desired vector.

The three-phase system of voltages to be generated for the current sampling time can then be represented as a single vector in this plane (figure III.6).

$$\begin{bmatrix} v_{an} \\ v_{bn} \\ v_{cn} \end{bmatrix} = \frac{2}{3} \cdot \begin{bmatrix} 1 & 0 \\ -\frac{1}{2} & \frac{\sqrt{3}}{2} \\ -\frac{1}{2} & -\frac{\sqrt{3}}{2} \end{bmatrix} \cdot \begin{bmatrix} V_\alpha \\ V_\beta \end{bmatrix} \quad \text{(III.10)}$$

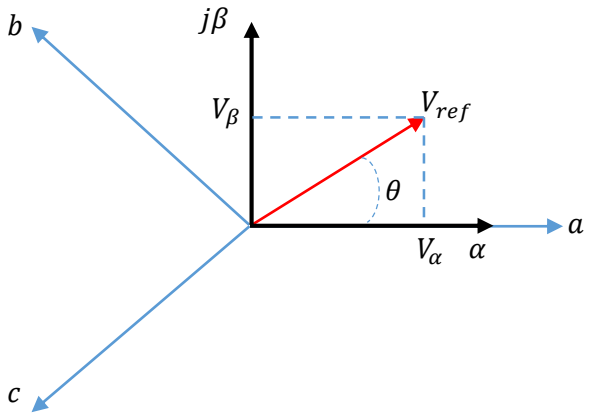

Figure III.6 The reference vector in the two and three dimensional plane.

Table III.3 All switching states and its corresponding voltage vectors.

Vector	S_a	S_b	S_c	V_a	V_b	V_c	V_α	V_β	***Magnitude***	***Angle***
V_0	0	0	0	0	0	0	0	0	0	0
V_1	1	0	0	$\frac{2}{3}v_{dc}$	$-\frac{1}{3}v_{dc}$	$-\frac{1}{3}v_{dc}$	$\frac{2}{3}v_{dc}$	0	$\frac{2}{3}v_{dc}$	0
V_2	1	1	0	$\frac{1}{3}v_{dc}$	$\frac{1}{3}v_{dc}$	$-\frac{2}{3}v_{dc}$	$\frac{1}{6}v_{dc}$	$\frac{1}{2}v_{dc}$	$\frac{2}{3}v_{dc}$	$\frac{\pi}{3}$
V_3	0	1	0	$-\frac{1}{3}v_{dc}$	$\frac{2}{3}v_{dc}$	$-\frac{1}{3}v_{dc}$	$-\frac{1}{6}v_{dc}$	$\frac{1}{2}v_{dc}$	$\frac{2}{3}v_{dc}$	$\frac{2\pi}{3}$
V_4	0	1	1	$-\frac{2}{3}v_{dc}$	$\frac{1}{3}v_{dc}$	$\frac{1}{3}v_{dc}$	$-\frac{2}{3}v_{dc}$	0	$\frac{2}{3}v_{dc}$	π
V_5	0	0	1	$-\frac{1}{3}v_{dc}$	$-\frac{1}{3}v_{dc}$	$\frac{2}{3}v_{dc}$	$-\frac{1}{6}v_{dc}$	$-\frac{1}{2}v_{dc}$	$\frac{2}{3}v_{dc}$	$\frac{4\pi}{3}$
V_6	1	0	1	$\frac{1}{3}v_{dc}$	$-\frac{2}{3}v_{dc}$	$\frac{1}{3}v_{dc}$	$\frac{1}{6}v_{dc}$	$-\frac{1}{2}v_{dc}$	$\frac{2}{3}v_{dc}$	$\frac{5\pi}{3}$
V_7	1	1	1	0	0	0	0	0	0	0

III.4.2 Definition of the reference vector

These are the instantaneous phase voltages:

$$\begin{cases} v_{an}(t) = v \cdot \sin\big(\omega(t)\big) \\ v_{bn}(t) = v \cdot \sin(\omega(t) - \frac{2\pi}{3}) \\ v_{cn}(t) = v \cdot \sin(\omega(t) - \frac{4\pi}{3}) \end{cases} \quad \text{(III.11)}$$

The reference vector V_{ref} can be defined in several ways in the voltage plane. The magnitude and angle (determining in which sector the reference vector is located) of the reference vector are:

$$\big|V_{ref}\big| = \sqrt{V_\alpha^2 + V_\beta^2} \quad \text{(III.12)}$$

$$\theta = tan^{-1}(\frac{V_\beta}{V_\alpha}) \quad \text{(III.13)}$$

$$V_{ref} = \big|V_{ref}\big| \cdot e^{j\theta t} \quad \text{(III.14)}$$

The reference voltage can then be expresses as:

$$V_{ref} = V_\alpha + jV_\beta = \frac{2}{3}\Big[v_{an} + v_{bn}e^{j\frac{2\pi}{3}} + v_{cn}e^{j\frac{4\pi}{3}}\Big] \quad \text{(III.15)}$$

$$V_{ref} = V_\alpha + j \cdot V_\beta = \frac{2}{3}(v_{an} + a \cdot v_{bn} + a^2 \cdot v_{cn}) \quad \text{(III.16)}$$

Where a is given by $a = e^{j\frac{2\pi}{3}}$

Inserting the phase shifted values for v_{an}, v_{an} and v_{an} gives:

$$V_{ref} = V_\alpha + jV_\beta = \frac{2}{3}\Big[v_{an} + cos\left(\frac{2\pi}{3}\right)v_{bn} + cos\left(\frac{2\pi}{3}\right)v_{cn}\Big] + \frac{2}{3}j\Big[\sin\left(\frac{2\pi}{3}\right)v_{bn} - \sin\left(\frac{2\pi}{3}\right)v_{cn}\Big] \quad \text{(III.17)}$$

$$V_{ref} = \frac{2}{3}(\frac{3}{2}v_{an} + j\frac{\sqrt{3}}{2}(v_{bn} - v_{cn}) \quad \text{(III.18)}$$

The reference vectors on the $\alpha\beta$-axis can then be described as:

$$\begin{bmatrix} V_\alpha \\ V_\beta \end{bmatrix} = \frac{2}{3}\begin{bmatrix} 1 & -\frac{1}{2} & -\frac{1}{2} \\ 0 & \frac{\sqrt{3}}{2} & -\frac{\sqrt{3}}{2} \end{bmatrix} \cdot \begin{bmatrix} v_{an} \\ v_{bn} \\ v_{cn} \end{bmatrix} \quad \text{(III.19)}$$

$$V_\alpha = \frac{2}{3}\Big[v_{an} - \frac{1}{2}v_{bn} - \frac{1}{2}v_{cn}\Big] \quad \text{(III.20)}$$

$$V_\beta = \frac{2}{3}\Big[\frac{\sqrt{3}}{2}v_{bn} - \frac{\sqrt{3}}{2}v_{cn}\Big] \quad \text{(III.21)}$$

III.4.3 Sector determination

The voltage vector $\vec{V}_{ref}$ is of amplitude $\sqrt{V_\alpha^2 + V_\beta^2}$ rotating in the anticlockwise direction with an angular speed θ, which follows at any time in one of the six vectors, as shown in figure III.7.

The angle and the magnitude are determining by Clarke transformation, they determining in which the reference vector is located (Figure III.7).

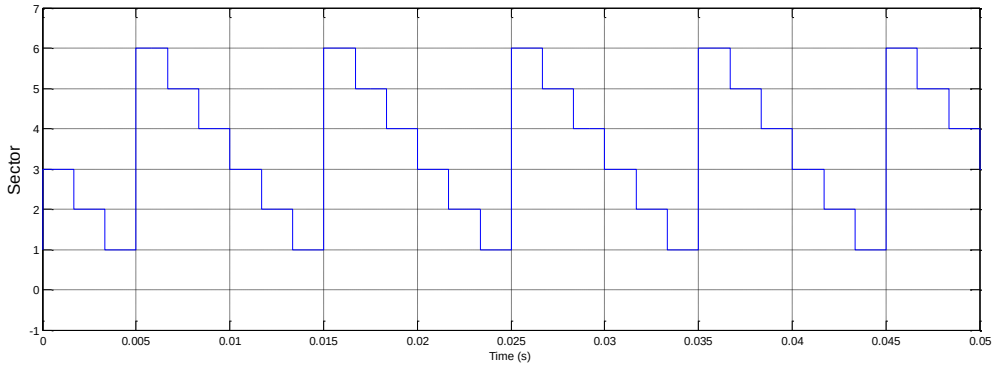

Figure III.7 Sector identification

III.5 Approximation of voltage vector control

III.5.1 Duration times

The control voltage vector $\vec{V}_{ref}$ is approximated, over the modulation period T_s, by the generation of a mean voltage vector $\vec{V}_i$ $(i = 0, \dots, 7)$ elaborated by applying the adjacent active vectors $\vec{V}_i$ and $\vec{V}_{i+1}$ and the zero vectors $\vec{V}_0$ and $\vec{V}_7$.

For this purpose, the reference vector $\vec{V}_{ref}$ is sampled at the frequency $f_s = \frac{1}{T_s}$.

The sampled value of $\vec{V}_{ref}$ is then used to solve the following equations:

$$\vec{V}_{ref} = \frac{1}{T_s}\left(T_0 \cdot \vec{V}_0 + T_i \cdot \vec{V}_i + T_{i+1} \cdot \vec{V}_{i+1}\right) \quad \text{(III.22)}$$

With,

$$T_s = T_0 + T_i + T_{i+1} \quad \text{(III.23)}$$

T_0 is the time of application of the zero vectors (V_0, V_7).

$\vec{V}_i$ and $\vec{V}_{i+1}$ are the two vectors that delimit the sector (i) of the reference vector $\vec{V}_{ref}$.

Therefor, for the sector one ($0 \leq \theta \leq \pi/3$), $\vec{V}_{ref}$ can be defined with V_0, V_1 and V_2.

$\vec{V}_{ref}$ in terms of the duration time can be considered as:

$$V_{ref} = \frac{T_0}{T_s} \cdot V_0 + \frac{T_1}{T_s} \cdot V_1 + \frac{T_2}{T_s} \cdot V_2 \quad \text{(III.24)}$$

With its magnitude and angle the position of V_{ref}, V_0, V_1 and V_2 can be described as:

$$V_{ref} = V_{ref} e^{j\theta} = V_{ref}(\cos(\theta) + j\sin(\theta)) \quad \text{(III.25)}$$

$$V_0 = 0 \quad \text{(III.26)}$$

$$V_1 = \frac{2}{3} v_{dc} \quad \text{(III.27)}$$

$$V_2 = \frac{2}{3} v_{dc} e^{j\frac{\pi}{3}} = \frac{2}{3} v_{dc} (\cos\left(\frac{\pi}{3}\right) + j sin(\frac{\pi}{3})) \quad \text{(III.28)}$$

The real part : $T_s V_{ref} \cos(\theta) = T_1 \frac{2}{3} v_{dc} + T_2 \frac{1}{3} v_{dc}$

The imaginary part : $T_s V_{ref} \sin(\theta) = T_2 \frac{1}{\sqrt{3}} v_{dc}$

T_1 and T_2 is then given by:

$$T_1 = T_s \frac{\sqrt{3} V_{ref}}{v_{dc}} \sin\left(\frac{\pi}{3} - \theta\right) = T_s m \sin(\frac{\pi}{3} - \theta) \quad \text{(III.29)}$$

$$T_2 = T_s \frac{\sqrt{3} V_{ref}}{v_{dc}} \sin(\theta) = T_s m \sin(\theta) \quad \text{(III.30)}$$

m is the modulation index with $m = \frac{\sqrt{3} V_{ref}}{v_{dc}}$.

The general equations to receive the duration times in each sector by choosing "n" as the number of the sector ($i = 1,2,3,4,5,6$) are given by:

$$T_i = T_s \cdot m \cdot \left[\sin(\frac{\pi}{3} i)\cos(\theta) - \cos(\frac{\pi}{3} i)\sin(\theta)\right] \quad \text{(III.31)}$$

$$T_{i+1} = T_s \cdot m \cdot \left[\cos(\frac{\pi}{3}(i-1))\sin(\theta) - \sin(\frac{\pi}{3}(i-1))\cos(\theta)\right] \quad \text{(III.32)}$$

Table III.4 Duration times for each sector

Sectors	***Duration times***		
	T_1	T_2	T_0
1	$T_s \cdot m \cdot \sin(\frac{\pi}{3} - \theta)$	$T_s \cdot m \cdot \sin(\theta)$	$T_s - T_1 - T_2$
2	$T_s \cdot m \cdot \sin(\frac{2\pi}{3} - \theta)$	$T_s \cdot m \cdot \sin(\theta - \frac{\pi}{3})$	$T_s - T_2 - T_3$
3	$T_s \cdot m \cdot \sin(\pi - \theta)$	$T_s \cdot m \cdot \sin(\theta - \frac{2\pi}{3})$	$T_s - T_3 - T_4$
4	$T_s \cdot m \cdot \sin(\frac{4\pi}{3} - \theta)$	$T_s \cdot m \cdot \sin(\theta - \pi)$	$T_s - T_4 - T_5$
5	$T_s \cdot m \cdot \sin(\frac{5\pi}{3} - \theta)$	$T_s \cdot m \cdot \sin(\theta - \frac{4\pi}{3})$	$T_s - T_5 - T_6$
6	$T_s \cdot m \cdot \sin(2\pi - \theta)$	$T_s \cdot m \cdot \sin(\theta - \frac{5\pi}{3})$	$T_s - T_6 - T_1$

III.5.2 Definition of the state vector sequences

The desired voltage vector is obtained as an average value over a modulation period by successive application of the adjacent state vectors $\vec{V}_i$, $\vec{V}_{i+1}$ and the zero vectors $\vec{V}_0$ and $\vec{V}_7$.

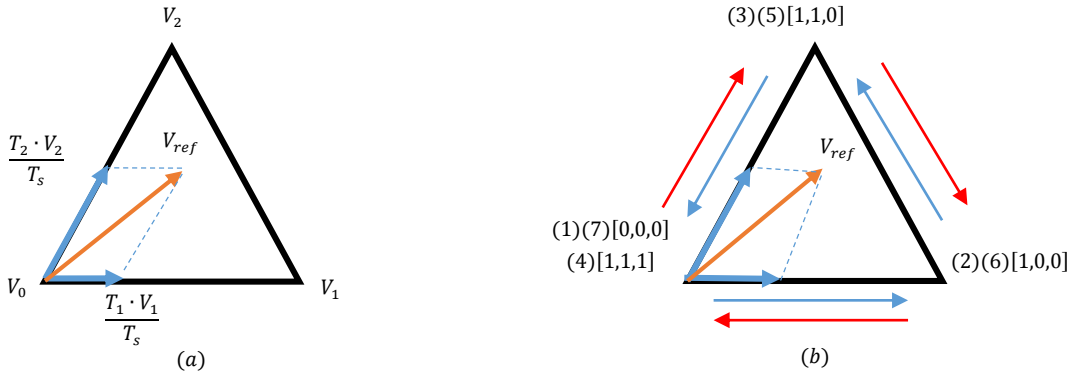

Figure III.8 Space vector diagram for sector 1 (a) the duty cycle for each vector (b) its switching states.

$\vec{V}_i$ and $\vec{V}_{i+1}$ delimit the sector of the plane in which $\vec{V}_{ref}$ is located.

In addition, in order to reduce switching, the zero vectors to be applied are selected as follows:

- $\overrightarrow{V_0}$ is used before and after odd vectors
- $\overrightarrow{V_7}$ is used before and after even vectors

For the sector« A » it goes through these switching states: $\vec{V}_0[000]$-$\vec{V}_1[100]$-$\vec{V}_2[110]$-$\vec{V}_7[111]$-$\vec{V}_7[110]$-$\vec{V}_2[100]$-$\vec{V}_1[000]$, one round then back again.

The succession of voltage vectors can be represented by the diagram in figure III.9.

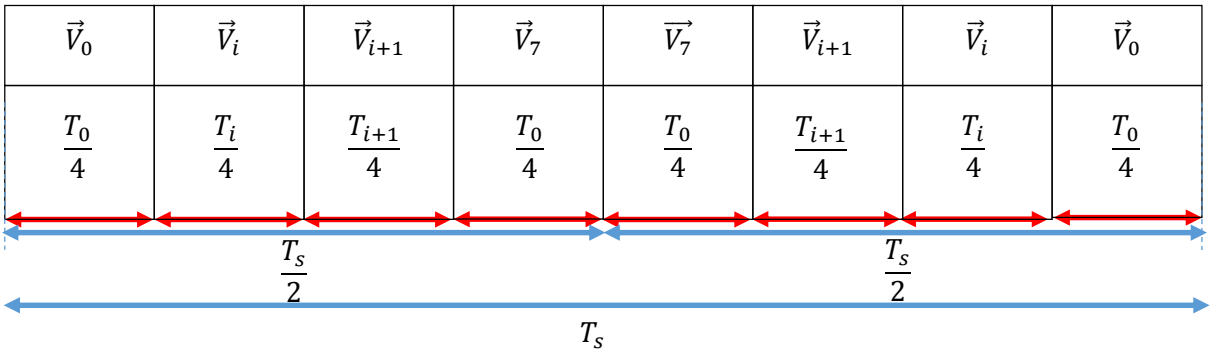

Figure III.9 Time sequences for application of vectors in a sampling period T_s.

III.5.3 The dwell times

Figure III.10 (a) and (b) shown The dwell times T_1, T_2 and T_3 and the phase voltages v_{an}, $v_{bn}$and v_{cn} respectively for all sector A, B, C, D, E and F respectively . For each sector there are 7 switching states for each cycle. It always start and finish with a zero vector.

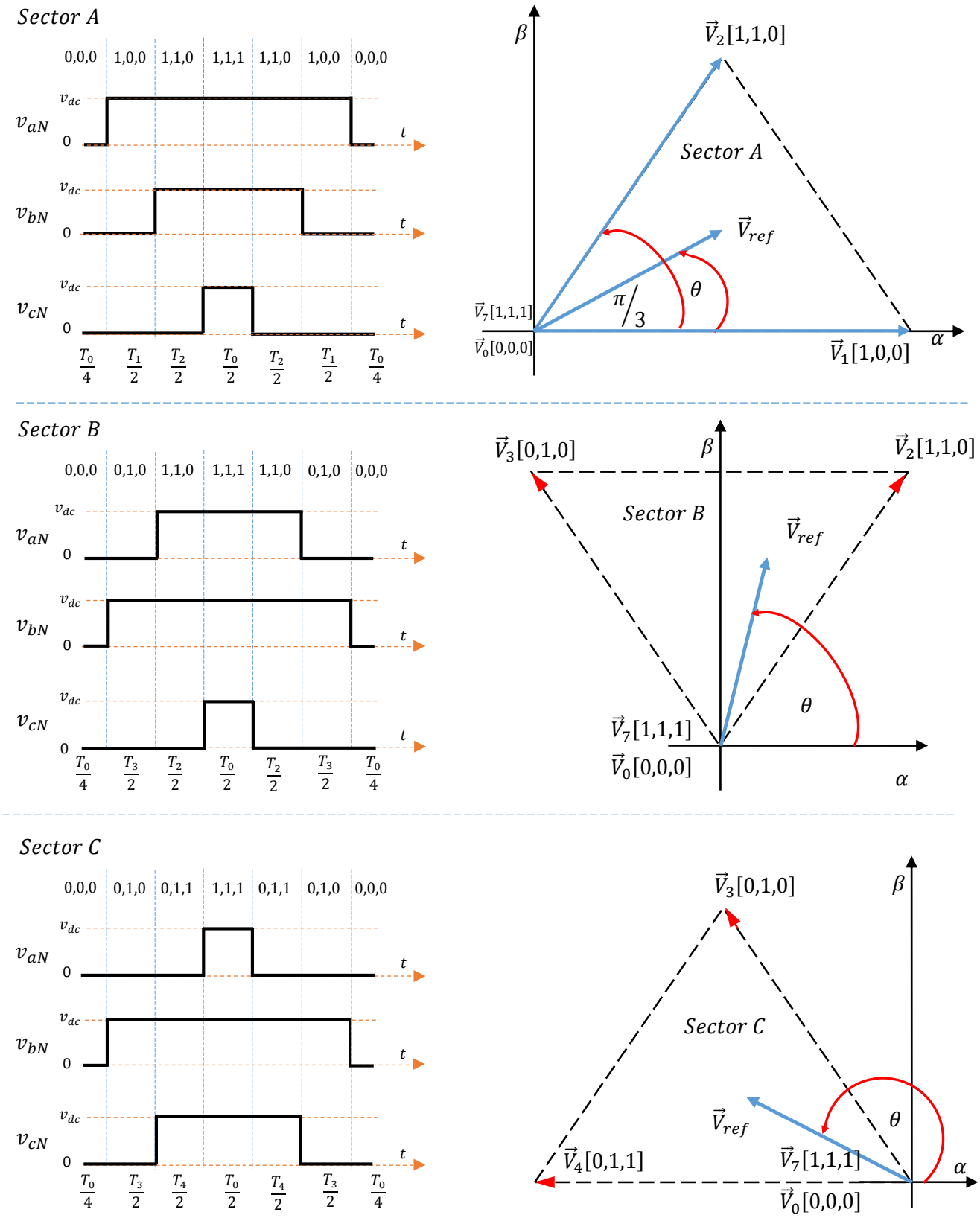

Figure III.10 (a) Phase voltages v_{aN}, v_{bN} ,v_{cN} and its switching states for the sectors: A,B,C

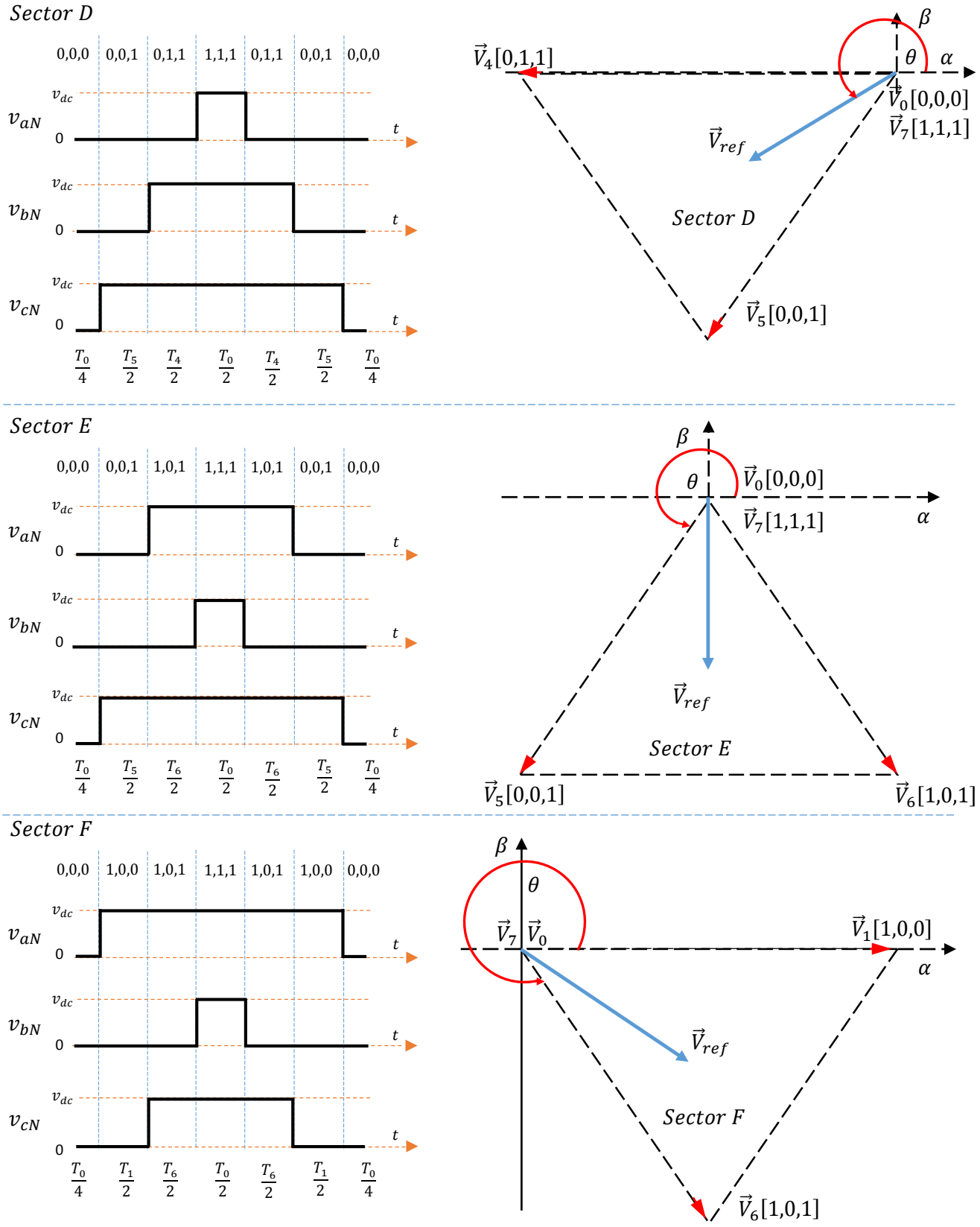

Figure III.10(b) Phase voltages v_{aN}, v_{bN} ,v_{cN} and its switching states for the sectors: D,E,F

III.6 Basic principle of space vector PWM of a three-level h-bridge inverter

The diagram representing the topology of a three-phase h-bridge inverter given in figure III.11.

This inverter topology produces three voltage levels ($-v_{dc}$, 0,$+$ v_{dc}) depending on the voltage of the DC source v_{dc} and the state variable S_i, where 'i' is the phase indicator ($i = a, b, c$). S_{i1}, S_{i2}, S_{i3}, and S_{i4} are switches for phase/cell 'i', and v_{iN} is the phase voltage between the phase 'i' and the fictive point N.

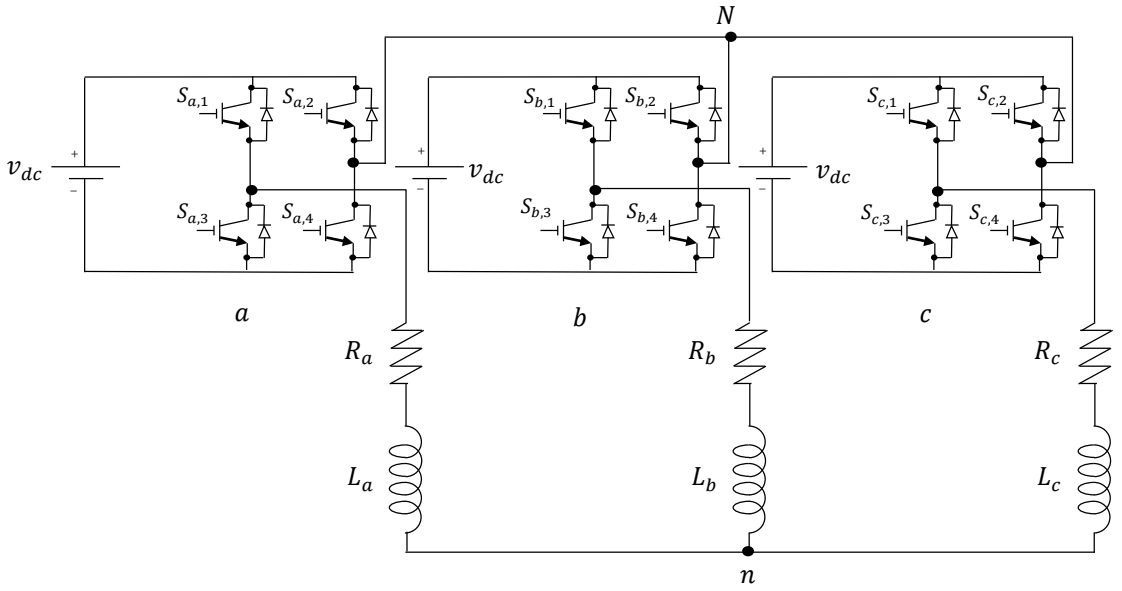

Figure III.11 Three-phase three level h-bridge inverter topology

Table III.5 Three-phase h-bridge inverter parameters

Parameters	Values
DC link voltage, v_{dc}	100 V
Inductance, L	10 mH
Resistance, R	0.5 Ω
Sampling time, T_s	10 μs
frequency, f	50 Hz

III.6.1 The switching stats

Considering the C combinations states of the state variable S_i ($S_i = +1, 0, -1$), it obtain the $\boldsymbol{C^p}$ possible combinations states for a three-level inverter (where p: is the number of phases.

The operating principle is shown in table III.6 in order to obtain the three desired voltage levels from one phase/leg (figure III.12) [54]. The inverter must ensure that the complementary between the switch pairs: (S_{i1}, S_{i3}) and (S_{i2}, S_{i4}).

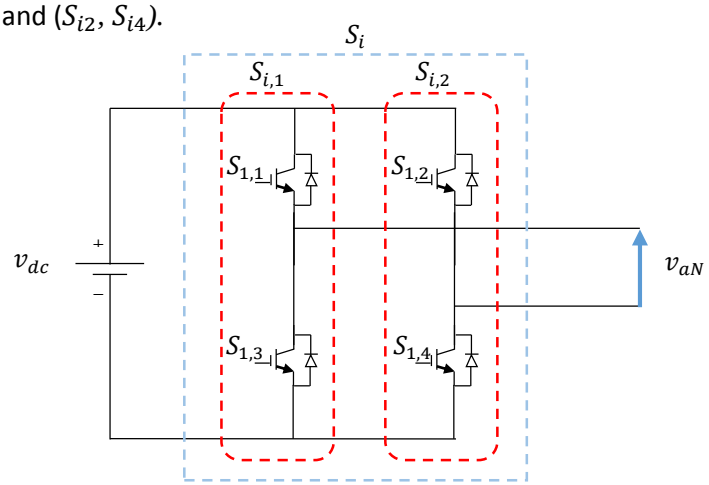

Figure III.12 Single-phase h-bridge inverter

Table III.6 switching stats of three-phase h-bridge inverter

switching states		S_i $(i = a, b, c)$	v_{iN}
$S_{i,1}$	$S_{i,2}$		
1	0	+1	$+v_{dc}$
1	1	0	**0**
0	0	0	**0**
0	1	−1	$-v_{dc}$

v_{iN} is dependent to the DC voltage v_{dc} by the equation:

$$v_{iN} = v_{dc}(S_{i,1} - S_{i,2}) \quad \text{(III.33)}$$

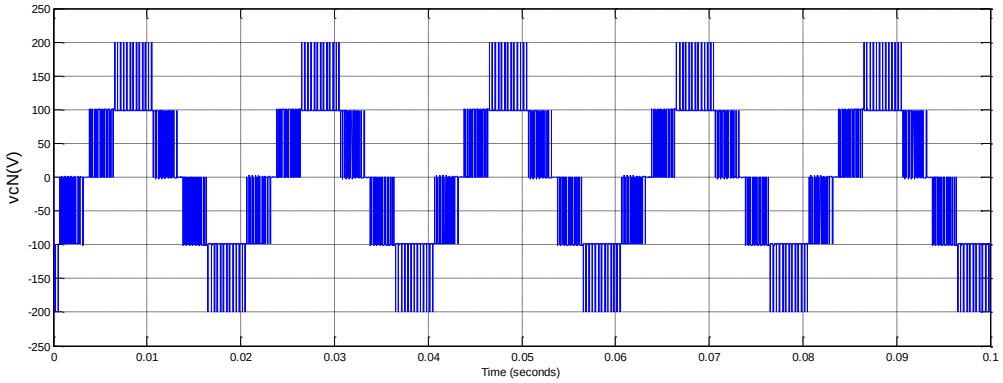

Figure III.13 The line voltage v_{bc}

The simple voltage v_{in} between the phase and the neutral point is a function of the voltage v_{iN}:

$$v_{in}(t) = v_{iN}(t) - v_{nN}(t) \quad \text{(III.34)}$$

Where,

$v_{nN}(t)$ is the common-mode voltage

And $i = a, b, c$

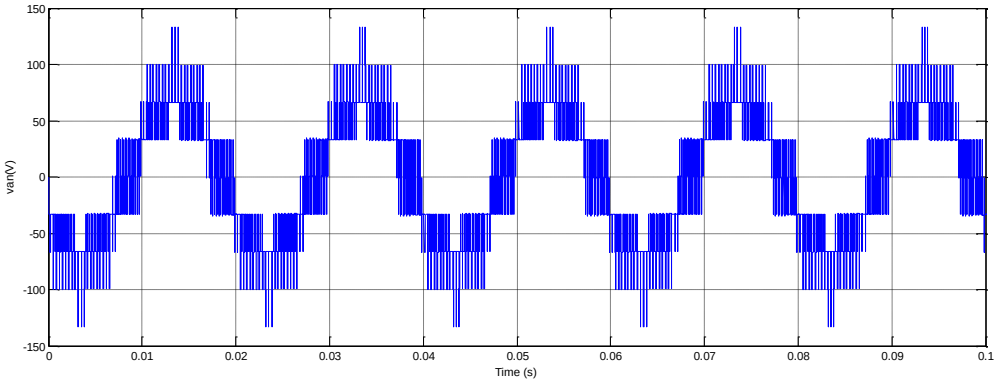

Figure III.14 The load voltage v_{cn}

Assuming that the system is balanced, the sum of v_{in} is equal to zero:

$$v_{an}(t) + v_{bn}(t) + v_{cn}(t) = 0 \quad \text{(III.35)}$$

By the expressions (III.34) and (III.35) it is found:

$$v_{nN}(t) = \frac{1}{3}[v_{aN}(t) + v_{bN}(t) + v_{cN}(t)] \quad \text{(III.36)}$$

By replacing the (III.36) in (III.34), we obtain the following system:

$$\begin{bmatrix} v_{an}(t) \\ v_{bn}(t) \\ v_{cn}(t) \end{bmatrix} = \begin{bmatrix} \frac{2}{3} & \frac{-1}{3} & \frac{-1}{3} \\ \frac{-1}{3} & \frac{2}{3} & \frac{-1}{3} \\ \frac{-1}{3} & \frac{-1}{3} & \frac{2}{3} \end{bmatrix} \cdot \begin{bmatrix} v_{aN}(t) \\ v_{aN}(t) \\ v_{aN}(t) \end{bmatrix} \quad \text{(III.37)}$$

By applying the Clarke transformation to the vector it find:

$$\begin{bmatrix} V_\alpha \\ V_\beta \end{bmatrix} = \frac{2}{3} \begin{bmatrix} 1 & -\frac{1}{2} & -\frac{1}{2} \\ 0 & \frac{\sqrt{3}}{2} & -\frac{\sqrt{3}}{2} \end{bmatrix} \begin{bmatrix} v_{an} \\ v_{bn} \\ v_{cn} \end{bmatrix} \quad \text{(III.38)}$$

Figure III.15 shows the representation of twenty-seven voltage vectors for a three-level inverter.

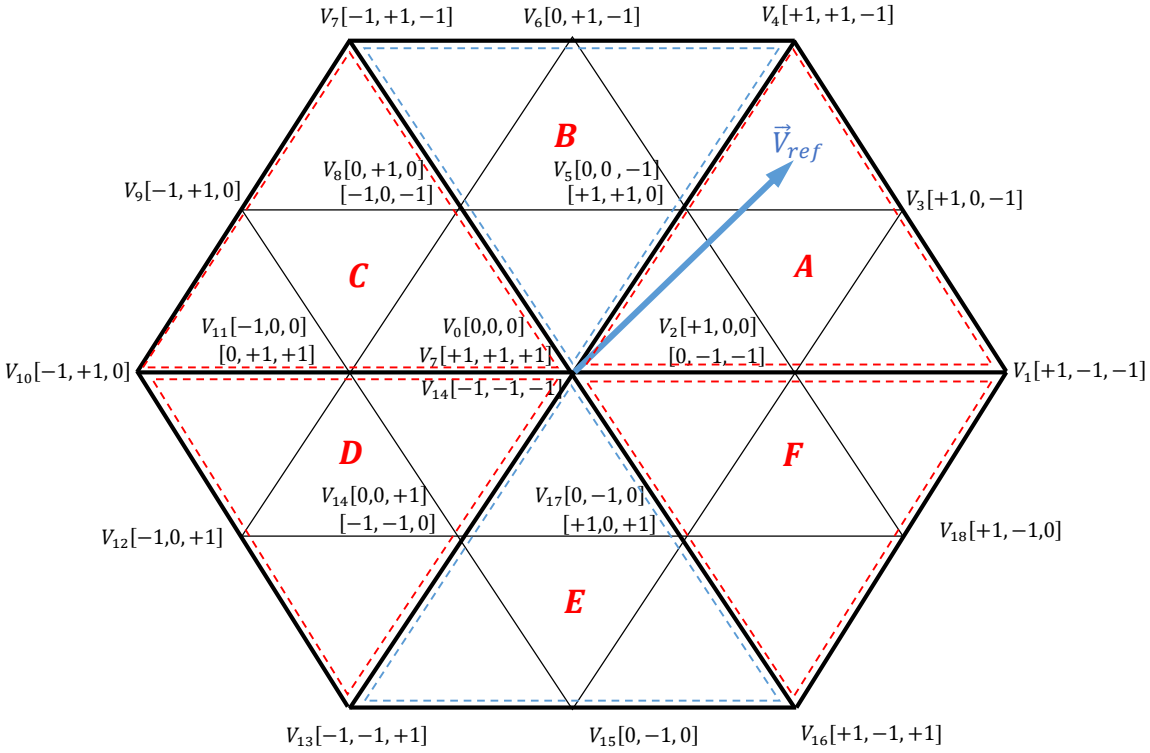

Figure III.15 Voltage vectors for a three-level inverter.

The surface of the hexagon can be divided into six sectors (A to F), each sector is divided into four regions (1 to 4) giving quite twenty-four regions.

Depending on the size of the voltage vectors, we divide them into four groups:

- Zero voltage vectors:V_0, V_7 and V_{14}, which are in the middle of the diagram. These vectors connect the three phases at the same voltage level.
- The small (short) voltage vectors: V_2, V_5 , V_8, V_{11}, V_{14} and V_{17}, which can be obtained by two different vectors.
- The medium voltage vectors: V_3, V_6, V_9, V_{12}, V_{15}, and V_{18}, which always have an output connected to the middle point of the DC bus.
- The large (Long) voltage vectors: V_1, V_4, V_7, V_{10}, V_{13} and V_{16}, which generate the amplitude of the largest output voltage.

As in two-level voltage inverters, the vector pulse width modulation technique applied to multi-level inverters follows the same calculation steps (figure III.7) [55]:

- Determination of the duty cycles of the switching vectors T_a, T_b and T_c for each region.

- Determination of the switching period of each switch: $\boldsymbol{S_a}$: $[S_{a1}, S_{a2}]$,$\boldsymbol{S_b}$: $[S_{b1}, S_{b2}]$, $\boldsymbol{S_c}$: $[S_{c1}, S_{c2}]$.

Table III.7 The different vectors corresponding to different switching states

Vector group	Vector number	Switching stats			v_{aN}	v_{bN}	v_{cN}	v_{an}	v_{bn}	v_{cn}	V_α	V_β	$\lvert\vec{V}_{ref}\rvert$	θ
		S_a	S_b	S_c										
Small vectors	V_2	1	0	0	v_{dc}	0	0	$v_{dc}/3$	$-v_{dc}/6$	$-v_{dc}/6$	$v_{dc}/3$	0	$1/3$	0
		0	-1	-1	0	$-v_{dc}$	$-v_{dc}$	$v_{dc}/3$	$-v_{dc}/6$	$-v_{dc}/6$				
	V_5	1	1	0	v_{dc}	v_{dc}	0	$v_{dc}/6$	$v_{dc}/6$	$-v_{dc}/3$	$v_{dc}/6$	$v_{dc}/2\sqrt{3}$	$1/3$	$\pi/3$
		0	0	-1	0	0	$-v_{dc}$	$v_{dc}/6$	$v_{dc}/6$	$-v_{dc}/3$				
	V_8	0	1	0	0	v_{dc}	0	$-v_{dc}/6$	$v_{dc}/3$	$-v_{dc}/6$	$-v_{dc}/6$	$v_{dc}/2\sqrt{3}$	$1/3$	$2\pi/3$
		-1	0	-1	$-v_{dc}$	0	$-v_{dc}$	$-v_{dc}/6$	$v_{dc}/3$	$-v_{dc}/6$				
	V_{11}	0	1	1	0	v_{dc}	v_{dc}	$-v_{dc}/3$	$v_{dc}/6$	$v_{dc}/6$	$-v_{dc}/3$	0	$1/3$	π
		-1	0	0	$-v_{dc}$	0	0	$-v_{dc}/3$	$v_{dc}/6$	$v_{dc}/6$				
	V_{14}	0	0	1	0	0	v_{dc}	$-v_{dc}/6$	$-v_{dc}/6$	$v_{dc}/3$	$-v_{dc}/6$	$-v_{dc}/2\sqrt{3}$	$1/3$	$-2\pi/3$
		-1	-1	0	$-v_{dc}$	$-v_{dc}$	0	$-v_{dc}/6$	$-v_{dc}/6$	$v_{dc}/3$				
	V_{17}	1	0	1	v_{dc}	0	v_{dc}	$v_{dc}/6$	$-v_{dc}/3$	$v_{dc}/6$	$v_{dc}/6$	$-v_{dc}/2\sqrt{3}$	$1/3$	$-\pi/3$
		0	-1	0	0	$-v_{dc}$	0	$v_{dc}/6$	$-v_{dc}/3$	$v_{dc}/6$				
Medium vectors	V_3	1	-1	-1	v_{dc}	$-v_{dc}$	$-v_{dc}$	$v_{dc}/2$	0	$-v_{dc}/2$	$v_{dc}/2$	$v_{dc}/2\sqrt{3}$	$1/\sqrt{3}$	$\pi/6$
	V_6	1	1	-1	v_{dc}	v_{dc}	$-v_{dc}$	0	$v_{dc}/2$	$-v_{dc}/2$	0	$v_{dc}/\sqrt{3}$	$1/\sqrt{3}$	$\pi/3$
	V_9	-1	1	-1	$-v_{dc}$	v_{dc}	$-v_{dc}$	$-v_{dc}/2$	$v_{dc}/2$	0	$-v_{dc}/2$	$v_{dc}/2\sqrt{3}$	$1/\sqrt{3}$	$5\pi/6$
	V_{12}	-1	1	1	$-v_{dc}$	v_{dc}	v_{dc}	$-v_{dc}/2$	0	$v_{dc}/2$	$-v_{dc}/2$	$-v_{dc}/2\sqrt{3}$	$1/\sqrt{3}$	$-5\pi/6$
	V_{15}	-1	-1	1	$-v_{dc}$	$-v_{dc}$	v_{dc}	0	$-v_{dc}/2$	$v_{dc}/2$	0	$-v_{dc}/\sqrt{3}$	$1/\sqrt{3}$	$-\pi/2$
	V_{18}	1	-1	1	v_{dc}	$-v_{dc}$	v_{dc}	$v_{dc}/2$	$-v_{dc}/2$	0	$v_{dc}/2$	$-v_{dc}/2\sqrt{3}$	$1/\sqrt{3}$	$-\pi/6$
Large vectors	V_1	1	0	-1	v_{dc}	0	-v_{dc}	$-v_{dc}/3$	$2v_{dc}/3$	$-v_{dc}/3$	$2v_{dc}/3$	0	$2/3$	0
	V_4	0	1	-1	0	v_{dc}	$-v_{dc}$	$v_{dc}/3$	$v_{dc}/3$	$v_{dc}/3$	$v_{dc}/\sqrt{6}$	$v_{dc}/\sqrt{3}$	$2/3$	$\pi/3$
	V_7	-1	1	0	$-v_{dc}$	v_{dc}	0	$-v_{dc}/3$	$-v_{dc}/3$	$2v_{dc}/3$	$-v_{dc}/3$	$v_{dc}/\sqrt{3}$	$2/3$	$2\pi/3$
	V_{10}	-1	0	1	$-v_{dc}$	0	v_{dc}	$-2v_{dc}/3$	$-2v_{dc}/3$	$v_{dc}/3$	$-2v_{dc}/3$	0	$2/3$	π
	V_{13}	0	-1	1	0	$-v_{dc}$	v_{dc}	$-v_{dc}/3$	$-v_{dc}/3$	$-v_{dc}/3$	$-v_{dc}/3$	$-v_{dc}/\sqrt{3}$	$2/3$	$-2\pi/3$
	V_{16}	1	-1	0	v_{dc}	$-v_{dc}$	0	$v_{dc}/3$	$v_{dc}/3$	$-2v_{dc}/3$	$-v_{dc}/3$	$-v_{dc}/\sqrt{3}$	$2/3$	$-\pi/3$
zero vectors	V_0	0	0	0	0	0	0	0	0	0	0	0	0	0
	V_7	1	1	1	0	0	0	0	0	0	0	0	0	0
	V_{14}	-1	-1	-1	0	0	0	0	0	0	0	0	0	0

III.6.2 The duty cycles

todescribe the reference voltage vector V_{ref}, we use the space vector transformations:

$$\vec{V}_{ref} = \frac{2}{3}\left(V_{aN} + V_{aN}e^{j\frac{2\pi}{3}} + V_{cN}e^{j\frac{4\pi}{3}}\right) \quad \text{(III.39)}$$

$$\vec{V}_{ref} = Ve^{j\theta t} \quad \text{(III.40)}$$

V_{ref} can be described with the three nearest voltage vectors $[\vec{V}_a, \vec{V}_b, \vec{V}_c]$. This selection is based on the magnitude of the reference vector $\vec{V}_{ref}$ and its angle θ. For one cycle:

$$\vec{V}_{ref} = T_a \cdot \vec{V}_a + T_b \cdot \vec{V}_b + T_c \cdot \vec{V}_c \quad \text{(III.41)}$$

We take the case where the reference vector is in sector A and its region 1,2,3 and 4.

III.6.2.1 The duty cycles in the first region

If the vector V_1 is chosen as the reference vector, the voltage vectors on the axis can be described as:

$$\begin{cases} V_a = V_2 = \frac{1}{\sqrt{6}} \\ V_b = V_5 = \frac{1}{\sqrt{6}} \cdot e^{\frac{\pi}{3}j} \\ V_c = V_0 = 0 \end{cases} \quad \text{(III.42)}$$

Figure III.16 represent the projection of the reference vector when it is in first region of sector A.

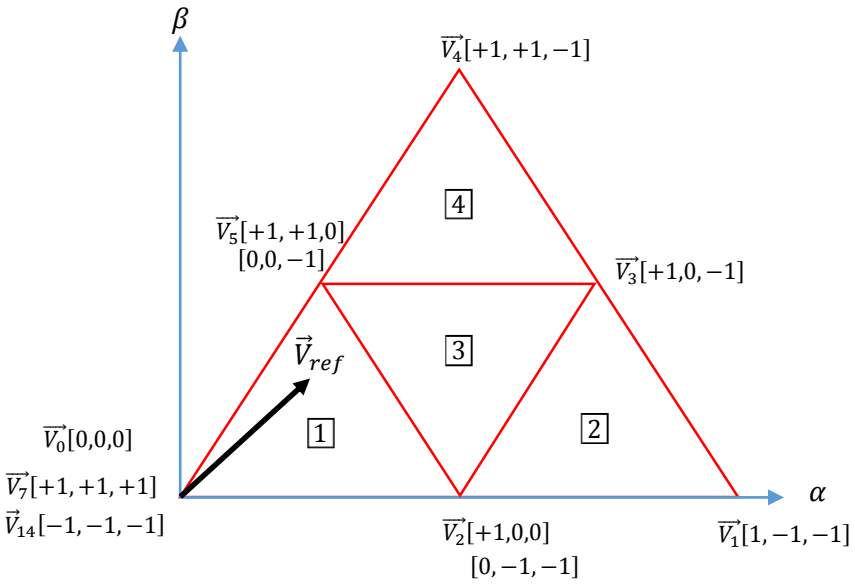

Figure III.16 Projection of the reference vector in the first region.

The adjacent vectors are: V_0, V_2 and V_5

$$T_s \cdot \vec{V}_{ref} = T_a \cdot \vec{V_0} + T_b \cdot \vec{V_2} + T_c \cdot \vec{V_5} \quad \text{(III.43)}$$

V_{ref} in forms of the real and imaginary axis:

$$T_s \cdot \left|\vec{V}_{ref}\right| \cdot \begin{bmatrix}\cos(\theta)\\ \sin(\theta)\end{bmatrix} = T_2 \cdot \frac{1}{\sqrt{6}} \cdot v_{dc} \cdot \begin{bmatrix}\cos(0)\\ \sin(0)\end{bmatrix} + T_5 \cdot \frac{1}{\sqrt{6}} \cdot v_{dc} \cdot \begin{bmatrix}\cos(\frac{\pi}{3})\\ \sin(\frac{\pi}{3})\end{bmatrix} \quad \text{(III.44)}$$

Dividing the equation into real and imaginary part eases the calculations of the duty cycles:

The real part:

$$T_s \cdot V_{ref} \cdot \cos(\theta) = \frac{v_{dc}}{\sqrt{6}} \cdot T_b + \frac{v_{dc}}{2\sqrt{6}} \cdot T_c \quad \text{(III.45)}$$

The imaginary part:

$$T_s \cdot V_{ref} \cdot \sin(\theta) = \frac{v_{dc}}{2\sqrt{2}} \cdot T_c \quad \text{(III.46)}$$

$$T_s = T_a + T_b + T_c \quad \text{(III.47)}$$

from the equation (III.46) it obtain:

$$T_c = \frac{2\sqrt{2} \cdot T_s \cdot V_{ref}}{v_{dc}} \sin(\theta) \quad \text{(III.48)}$$

We replace the expression of T_c in (III.45), it find:

$$T_b = \frac{2\sqrt{2} T_s V_{ref}}{v_{dc}} \cdot \sin\left(\frac{\pi}{3} - \theta\right) \quad \text{(III.49)}$$

By replacing the expression of $T_b$and T_c in (III.47),it find

$$T_a = T_s - T_b - T_c = T_s \left[1 - \frac{2\sqrt{2} T_s V_{ref}}{v_{dc}} \sin\left(\frac{\pi}{3} + \theta\right)\right] \quad \text{(III.50)}$$

m is the modulation index , $m = \frac{2\sqrt{2} \cdot V_{ref}}{v_{dc}}$.

The duty cycles is then given in form of:

$$\boxed{\begin{array}{c} T_a = T_s \left[1 - m \cdot \sin\left(\frac{\pi}{3} + \theta\right)\right] \\ T_b = m \cdot T_s \cdot \sin\left(\frac{\pi}{3} - \theta\right) \\ T_c = m \cdot T_s \cdot \sin\theta \end{array}} \quad \text{(III.51)}$$

III.6.2.2 The duty cycles in the second region

Figure III.17 represents the projection of the reference vector in the second region of sector A.

The vectors concerning are: $\vec{V}_1$, $\vec{V}_2$ and $\vec{V}_3$.

$$T_s \cdot \vec{V}_{ref} = T_a \cdot \overrightarrow{V_2} \cdot + T_b \cdot \vec{V}_1 + T_c \cdot \overrightarrow{V_3} \quad \text{(III.52)}$$

$$T_s \cdot \left|\vec{V}_{ref}\right| \cdot \begin{bmatrix}\cos\theta\\ \sin\theta\end{bmatrix} = T_a \cdot \frac{1}{\sqrt{6}} \cdot v_{dc} \cdot \begin{bmatrix}1\\ 0\end{bmatrix} + T_b \cdot \sqrt{\frac{2}{3}} \cdot v_{dc} \cdot \begin{bmatrix}1\\ 0\end{bmatrix} + T_c \cdot \frac{1}{\sqrt{2}} \cdot v_{dc} \begin{bmatrix}\cos\frac{\pi}{6}\\ \sin\frac{\pi}{6}\end{bmatrix} \quad \text{(III.53)}$$

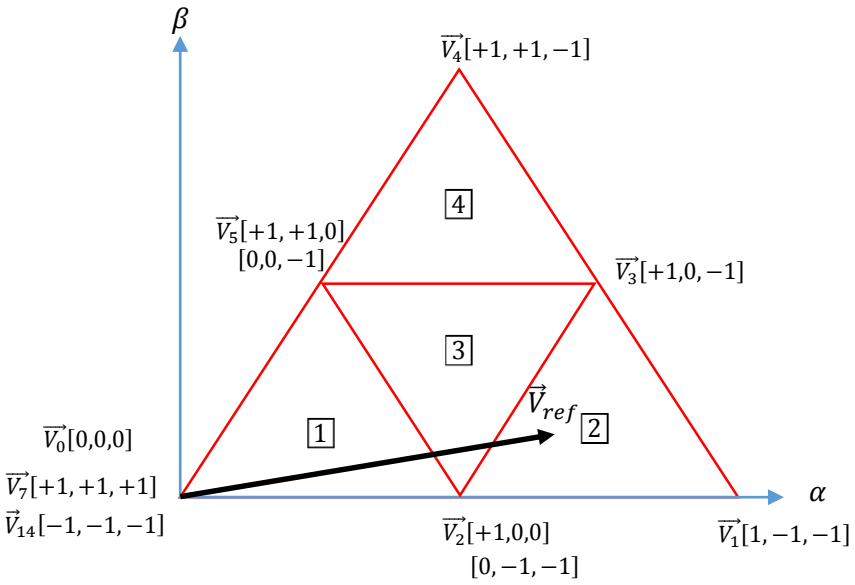

Figure III.17 Projection of the reference vector in the second region.

From imaginary part of (III.53), it find:

$$T_c = \frac{2\sqrt{2}\cdot T_s \cdot V_{ref}}{v_{dc}} \sin\theta \tag{III.54}$$

And $$T_b = T_s - T_a - T_b \tag{III.55}$$

By replace the expression of T_b and T_c in (III.40) we find :

$$T_a = T_s\left[2 - \frac{\sqrt{2}T_s V_{ref}}{v_{dc}} \cdot \sin\left(\frac{\pi}{3} + \theta\right)\right] \tag{III.56}$$

From the equation (III.55):

$$T_b = T_s\left[\frac{2\sqrt{2}V_{ref}}{v_{dc}} \sin\left(\frac{\pi}{3} - \theta\right) - 1\right] \tag{III.57}$$

$$\boxed{\begin{array}{c} T_a = m \cdot T_s\left[2 - m \cdot \sin\left(\frac{\pi}{3} + \theta\right)\right] \\ T_b = T_s\left[m \cdot \sin\left(\frac{\pi}{3} - \theta\right) - 1\right] \\ T_c = m \cdot T_s \cdot \sin\theta \end{array}} \tag{III.58}$$

III.6.2.3 The duty cycles in the third region

Figure III.18 represents the projection of the reference vector in the third region of sector A.

The adjacent vectors are: V_2 , V_3 and V_5

$$T_s \cdot \vec{V}_{ref} = T_a \cdot \vec{V_2} \cdot + T_b \cdot \vec{V_5} + T_c \cdot \vec{V_3} \tag{III.59}$$

$$T_s \cdot |\vec{V}_{ref}| \cdot \begin{bmatrix}\cos\theta \\ \sin\theta\end{bmatrix} = T_a \cdot \frac{1}{\sqrt{6}} \cdot v_{dc} \cdot \begin{bmatrix}1 \\ 0\end{bmatrix} + T_b \cdot v_{dc} \cdot \begin{bmatrix}\cos\frac{\pi}{3} \\ \sin\frac{\pi}{3}\end{bmatrix} + T_c \cdot \frac{1}{\sqrt{6}} \cdot v_{dc} \begin{bmatrix}\cos\frac{\pi}{6} \\ \sin\frac{\pi}{6}\end{bmatrix} \quad \text{(III.60)}$$

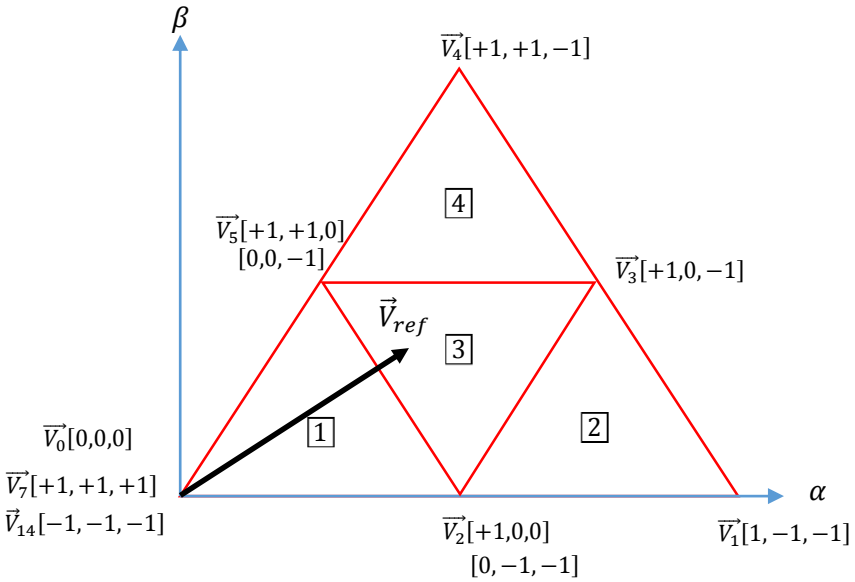

Figure III.18 projection of the reference vector in the third region.

From the imaginary part of equation (III.60):

$$T_c = \frac{2\sqrt{2}\cdot T_s \cdot V_{ref}}{v_{dc}} \sin\theta - T_b \quad \text{(III.61)}$$

By replace the expression of T_c in (III.61) it find :

$$T_a = \left[1 - \frac{2\sqrt{2}\cdot T_s \cdot V_{ref}}{v_{dc}} \sin\theta\right] \quad \text{(III.62)}$$

Then, by replace the expression of T_a and T_c in the real part of equation (III.60):

$$T_b = T_s\left[\frac{2\sqrt{2}V_{ref}}{v_{dc}} sin\left(\frac{\pi}{3}+\theta\right) - 1\right] \quad \text{(III.63)}$$

$$\text{(III.61)} \Leftrightarrow T_c = \frac{2\sqrt{2}V_{ref}}{v_{dc}}\sin(\theta) - T_s\left[\frac{2\sqrt{2}V_{ref}}{v_{dc}}\sin\left(\frac{\pi}{3}+\theta\right) - 1\right] = T_s\left[\frac{2\sqrt{2}V_{ref}}{v_{dc}}\sin\left(\theta - \frac{\pi}{3}\right) + 1\right] \quad \text{(III.64)}$$

$$\boxed{\begin{array}{c} T_a = T_s[1 - m\cdot\sin(\theta)] \\ T_b = T_s\left[m\cdot\sin\left(\frac{\pi}{3}+\theta\right) - 1\right] \\ T_c = T_s\left[1 + m\cdot\sin\left(\theta - \frac{\pi}{3}\right)\right] \end{array}} \quad \text{(III.65)}$$

III.6.2.4 The duty cycles in the fourth region

Figure III.19 represents the projection of the reference vector in the fourth region of sector A.

The adjacent vectors are: V_3, V_4 and V_5

$$T_s \cdot \vec{V}_{ref} = T_a \cdot \vec{V_5} \cdot + T_b \cdot \vec{V_3} + T_c \cdot \vec{V_4} \quad \text{(III.66)}$$

$$T_s \cdot |\vec{V}_{ref}| \cdot \begin{bmatrix} \cos\theta \\ \sin\theta \end{bmatrix} = T_a \cdot \frac{1}{\sqrt{6}} \cdot v_{dc} \cdot \begin{bmatrix} \cos\frac{\pi}{3} \\ \sin\frac{\pi}{3} \end{bmatrix} + T_b \cdot \frac{1}{\sqrt{2}} \cdot v_{dc} \cdot \begin{bmatrix} \cos\frac{\pi}{6} \\ \sin\frac{\pi}{6} \end{bmatrix} + T_c \cdot \sqrt{\frac{3}{2}} \cdot v_{dc} \begin{bmatrix} \cos\frac{\pi}{3} \\ \sin\frac{\pi}{3} \end{bmatrix} \quad \text{(III.67)}$$

$$T_s = T_a + T_b + T_c \quad \text{(III.68)}$$

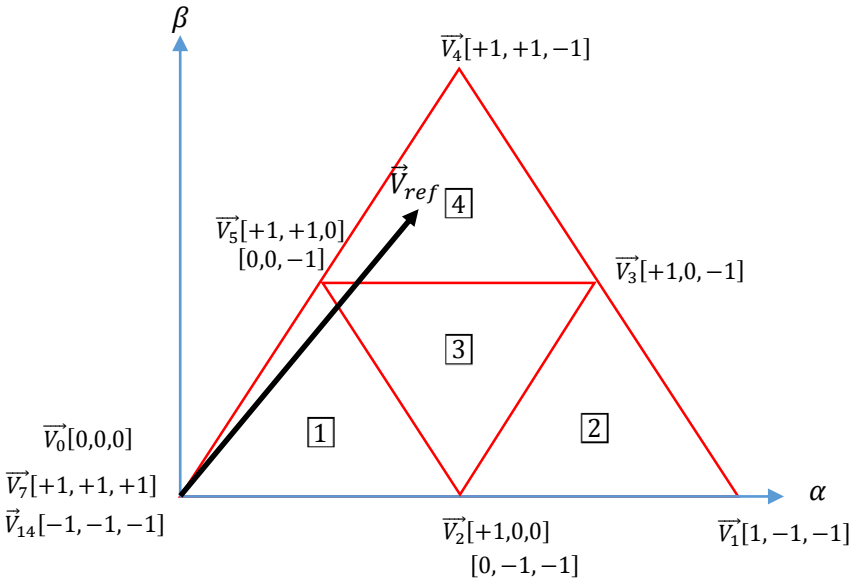

Figure III.19 Projection of the reference vector in the fourth region.

By use the expression of (III.67),,the expression of T_a is given by :

$$T_a = T_s \cdot \left[\frac{2\sqrt{2}}{v_{dc}} \cdot V_{ref} \cdot \sin(\theta - 1)\right] \quad \text{(III.69)}$$

By replace the expressions of T_a and (III.68) in (III.67), we obtain :

$$T_c = T_s \cdot \left[2 - \frac{2\sqrt{2} \cdot T_s \cdot V_{ref}}{v_{dc}} \sin\left(\theta + \frac{\pi}{3}\right)\right] \quad \text{(III.70)}$$

$$\boxed{\begin{aligned} T_a &= T_s[m \cdot \sin(\theta) - 1] \\ T_b &= m.T_s \cdot \sin\left(\frac{\pi}{3} - \theta\right) \\ T_c &= T_s \cdot \left[2 - m.\sin\left(\frac{\pi}{3} + \theta\right)\right] \end{aligned}} \quad \text{(III.71)}$$

In the same way, the switching times for the other sectors (from B to F) are calculated, and than are summarized in the following table III.8.

Table III.8 Time expressions of switching times for voltage vectors in different sectors and regions.

Sector	T_i	Region 1	Region 2	Region 3	Region 4
A	T_a T_b T_c	$m \cdot T_s \cdot \sin\left(\frac{\pi}{3}-\theta\right)$ $T_s\left[1-m \cdot \sin\left(\frac{\pi}{3}+\theta\right)\right]$ $m \cdot T_s \cdot \sin\theta$	$T_s\left[2-m \cdot \sin\left(\frac{\pi}{3}+\theta\right)\right]$ $m \cdot T_s \cdot \sin\theta$ $T_s\left[m \cdot \sin\left(\frac{\pi}{3}-\theta\right)-1\right]$	$T_s[1-m \cdot \sin(\theta)]$ $T_s\left[m \cdot \sin\left(\frac{\pi}{3}+\theta\right)-1\right]$ $T_s\left[1+m \cdot \sin\left(\theta-\frac{\pi}{3}\right)\right]$	$T_s[m \cdot \sin(\theta)-1]$ $m.T_s \cdot \sin\left(\frac{\pi}{3}-\theta\right)$ $T_s.\left[2-m \cdot \sin\left(\frac{\pi}{3}+\theta\right)\right]$
B	T_a T_b T_c	$T_s.m \cdot \sin\left(\theta-\frac{\pi}{3}\right)$ $T_s[1-m \cdot \sin(\theta)]$ $T_s.m.\sin\left(\frac{\pi}{3}+\theta\right)$	$T_s\left[m \cdot \sin\left(\frac{\pi}{3}+\theta\right)-1\right]$ $T_s.m \cdot \sin\left(\theta-\frac{\pi}{3}\right)$ $T_s[2-m \cdot \sin(\theta)]$	$T_s\left[1-m \cdot \sin\left(\frac{\pi}{3}+\theta\right)\right]$ $T_s[m \cdot \sin(\theta)-1]$ $T_s\left[1-m \cdot \sin\left(\theta-\frac{\pi}{3}\right)\right]$	$T_s[2-m \cdot \sin(\theta)]$ $T_s.m \cdot \sin\left(\theta+\frac{\pi}{3}\right)$ $T_s\left[m \cdot \sin\left(\theta-\frac{\pi}{3}\right)-1\right]$
C	T_a T_b T_c	$m \cdot T_s \cdot \sin\theta$ $T_s\left[1-m \cdot \sin\left(\theta-\frac{\pi}{3}\right)\right]$ $-T_s.m.\sin\left(\frac{\pi}{3}+\theta\right)$	$T_s\left[2-m \cdot \sin\left(\theta-\frac{\pi}{3}\right)\right]$ $T_s.m.\sin\left(\frac{\pi}{3}+\theta\right)$ $T_s[m \cdot \sin(\theta)-1]$	$T_s\left[1+m \cdot \sin\left(\theta+\frac{\pi}{3}\right)\right]$ $T_s\left[m \cdot \sin\left(\theta-\frac{\pi}{3}\right)-1\right]$ $T_s[1-m \cdot \sin(\theta)]$	$-T_s\left[1+m \cdot \sin\left(\frac{\pi}{3}+\theta\right)\right]$ $m \cdot T_s \cdot \sin\theta$ $T_s\left[2-m \cdot \sin\left(\theta-\frac{\pi}{3}\right)\right]$
D	T_a T_b T_c	$-m \cdot T_s \cdot \sin\theta$ $T_s\left[1+m \cdot \sin\left(\frac{\pi}{3}+\theta\right)\right]$ $T_s.m.\sin\left(\frac{\pi}{3}-\theta\right)$	$T_s\left[m \cdot \sin\left(\frac{\pi}{3}-\theta\right)-1\right]$ $-m \cdot T_s \cdot \sin\theta$ $T_s\left[2-m \cdot \sin\left(\theta+\frac{\pi}{3}\right)\right]$	$T_s\left[1-m \cdot \sin\left(\theta-\frac{\pi}{3}\right)\right]$ $-T_s\left[1+m \cdot \sin\left(\frac{\pi}{3}+\theta\right)\right]$ $T_s[1+m \cdot \sin(\theta)]$	$T_s\left[2+m \cdot \sin\left(\theta+\frac{\pi}{3}\right)\right]$ $T_s.m.\sin\left(\frac{\pi}{3}-\theta\right)$ $-T_s[1-m \cdot \sin(\theta)]$
E	T_a T_b T_c	$T_s.m.\sin\left(\frac{\pi}{3}+\theta\right)$ $T_s[1+m \cdot \sin(\theta)]$ $T_s.m.\sin\left(\frac{\pi}{3}-\theta\right)$	$T_s[2+m \cdot \sin(\theta)]$ $T_s.m.\sin\left(\frac{\pi}{3}-\theta\right)$ $-T_s\left[1+m \cdot \sin\left(\frac{\pi}{3}+\theta\right)\right]$	$T_s\left[1+m \cdot \sin\left(\frac{\pi}{3}-\theta\right)\right]$ $-T_s[1+m \cdot \sin(\theta)]$ $T_s\left[1+m \cdot \sin\left(\theta+\frac{\pi}{3}\right)\right]$	$T_s\left[m \cdot \sin\left(\theta-\frac{\pi}{3}\right)-1\right]$ $T_s.m.\sin\left(\theta+\frac{\pi}{3}\right)$ $T_s[2+m \cdot \sin(\theta)]$
F	T_a T_b T_c	$T_s.m.\sin\left(\frac{\pi}{3}+\theta\right)$ $T_s\left[1+m \cdot \sin\left(\frac{\pi}{3}-\theta\right)\right]$ $-m \cdot T_s \cdot \sin\theta$	$-T_s[1+m \cdot \sin(\theta)]$ $T_s.m.\sin\left(\frac{\pi}{3}+\theta\right)$ $T_s\left[2+m \cdot \sin\left(\theta-\frac{\pi}{3}\right)\right]$	$T_s[1+m \cdot \sin(\theta)]$ $T_s\left[m \cdot \sin\left(\frac{\pi}{3}-\theta\right)-1\right]$ $T_s\left[1-m \cdot \sin\left(\theta+\frac{\pi}{3}\right)\right]$	$T_s\left[2+m \cdot \sin\left(\theta-\frac{\pi}{3}\right)\right]$ $-m \cdot T_s \cdot \sin\theta$ $T_s\left[m \cdot \sin\left(\theta+\frac{\pi}{3}\right)-1\right]$

III.7 The modulation algorithm

After the determination of the duty cycles, the choice of a modulation algorithm is required according to the following criteria:

- The choice of zero vector if we would like to use V_0 (0,0,0),or V_7 (+1,+1,+1) or V_{14} (-1,-1,-1).
- Switching vector order.
- Divide the duty cycles of the switching vectors without presenting the additional switches.

There are four kinds of vector modulation algorithm mentioned as follows:

1. The Right aligned sequence.
2. The Symmetric sequence.
3. The alternating zero vector sequence.
4. The High current not-switched sequence.

in this thesis we used the symmetric sequence algorithm. because it is advantages compare to other modulation sequences among them the lowest total harmonic distortion (THD)[56]. Figure III.20 show the switching directions for three-levels inverter using space vector pulse width modulation by symmetrical sequence algorithm.

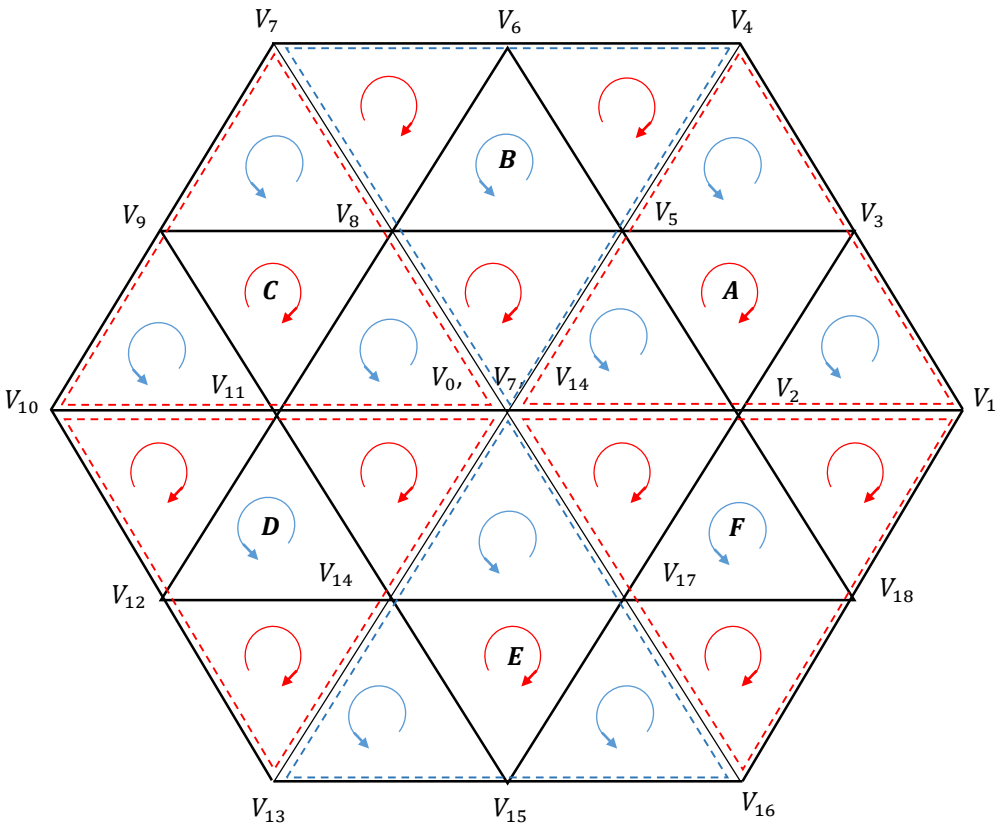

Figure III.20 The Switching times directions using symmetrical sequence modulation.

III.7.1 Sequencing of the switching times

In the same way, each switch in each phase/leg has its own output waveform as for the two-level inverter. For each of the sectors, it will be described the different waveforms achieved. Several selected properties must be taken into account in order to have a symmetrical pulse width modulation in terms of commutation. Each waveform is symmetrical in terms of half switching period.

III.7.1.1 Sequencing of switching states for sector A

a. Switching states of the first region

Figure III.21 shows the phase voltages v_{aN} , v_{bN} and v_{cN} for the first region in sector A for the three level inverter.

(S_{a1}, S_{a1}), (S_{b1}, S_{b1}) and (S_{c1}, S_{c1}) are the switching stats of the vectors V_0 , V_2 and V_5 respectively.

(S_{i1}, S_{i1}): are the switching times of the upper switches for cell i.

T_0, T_2 and T_5 are the switching times of the vectors V_0 , V_2 and V_5 respectively.

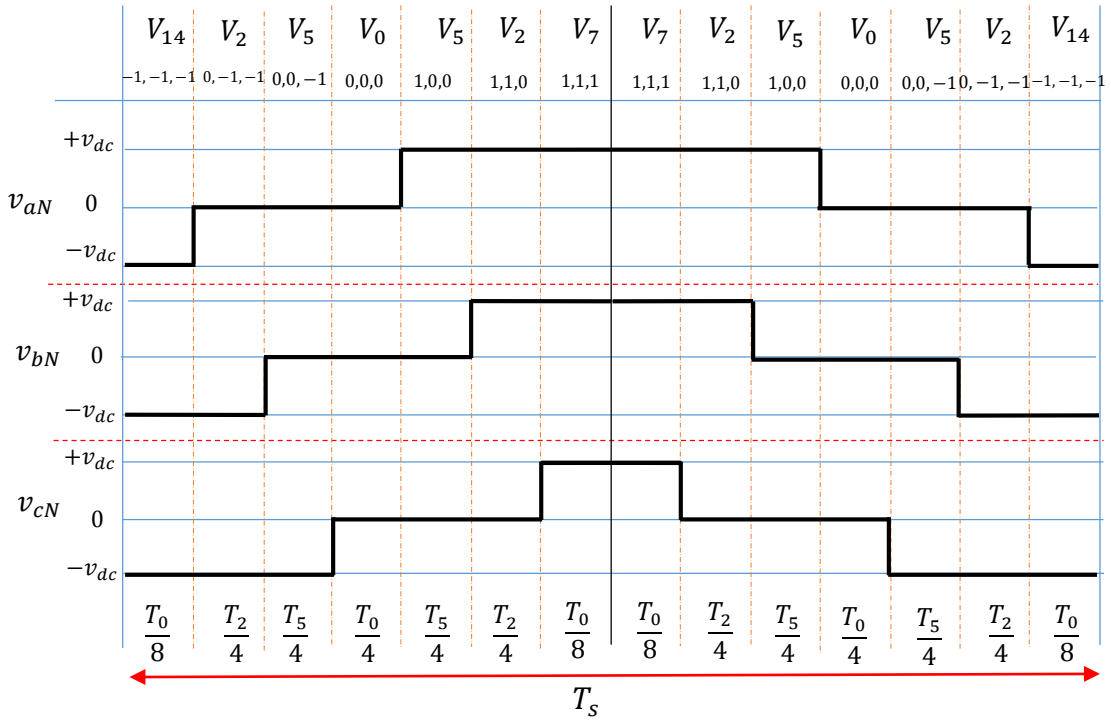

Figure III.21 The phase voltages v_{aN}, v_{bN} and v_{cN} in the first region « Sector A »

- $S_{a1} = 2.\left(\frac{T_0}{4} + \frac{T_2}{4} + \frac{T_5}{8}\right) \Rightarrow S_{a1} = \frac{T_a}{2} + \frac{T_c}{2} + \frac{T_b}{4}$

$$S_{a2} = 2.\left(\frac{T_a}{4} + \frac{T_c}{4} + \frac{T_b}{4} + \frac{T_a}{4} + \frac{T_c}{4} + \frac{T_b}{8}\right) \Rightarrow S_{a2} = S_{a1} + \frac{1}{2}(T_a + T_b + T_c)$$

- $S_{b1} = 2.\left(\frac{T_c}{4} + \frac{T_b}{8}\right) \Rightarrow S_{b1} = \frac{T_c}{2} + \frac{T_b}{4}$

  $S_{b2} = 2.\left(\frac{T_a}{4} + \frac{T_c}{4} + \frac{T_b}{4} + \frac{T_a}{4} + \frac{T_c}{4} + \frac{T_b}{8}\right) \Rightarrow S_{b2} = S_{b1} + \frac{1}{2}(T_a + T_b + T_c)$

- $S_{c1} = \frac{T_b}{4}$

- $S_{c2} = 2.\left(\frac{T_b}{4} + \frac{T_a}{4} + \frac{T_c}{4} + \frac{T_b}{8}\right) \Rightarrow S_{c2} = S_{c1} + \frac{1}{2}(T_a + T_b + T_c)$

b. Switching states of the second region

Figure III.22 shows the phase voltages v_{aN} , v_{bN} and v_{cN} for the second region in the sector A of three-level inverter.

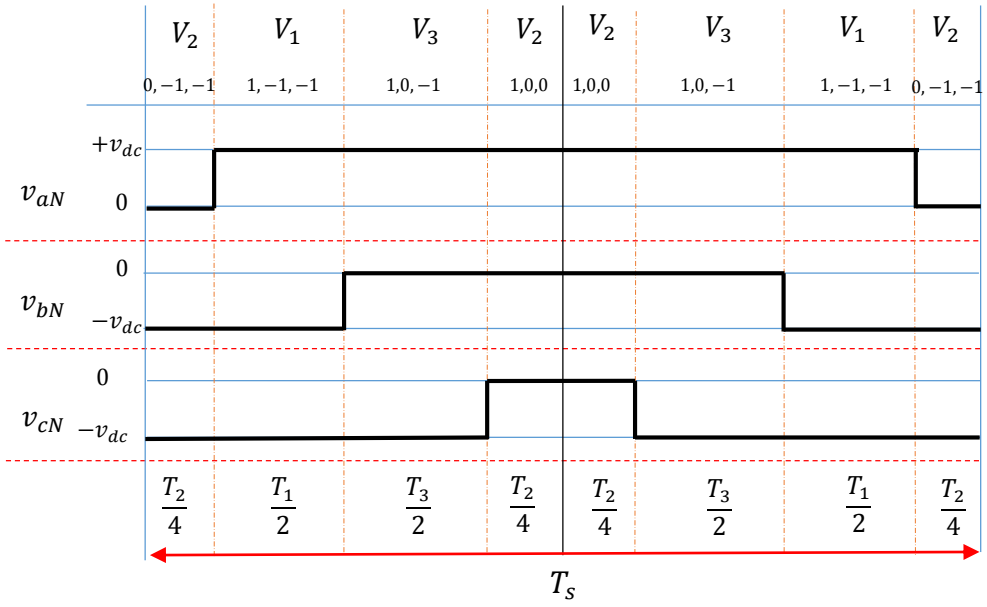

Figure III.22 The phase voltages v_{aN}, v_{bN} and v_{cN} in second region «Sector A»

- $S_{a1} = 2.\left(\frac{T_a}{4} + \frac{T_c}{2} + \frac{T_b}{2}\right) \Rightarrow S_{a1} = \frac{T_a}{2} + T_c + T_b$

  $S_{a2} = 2.\left(\frac{T_a}{4} + \frac{T_c}{2} + \frac{T_b}{2} + \frac{T_a}{4}\right) \Rightarrow S_{a2} = S_{a1} + \frac{T_a}{2}$

- $S_{b1} = 0$

  $S_{b2} = 2.\left(\frac{T_b}{2} + \frac{T_a}{4}\right) \Rightarrow S_{b2} = T_b + \frac{T_a}{2}$

- $S_{c1} = 0$

$$S_{c2} = \frac{T_a}{2}$$

c. Switching states of third region

Figure III.23 shows the phase voltages v_{aN}, v_{bN} and v_{cN} for the third region in sector A of three-level inverter.

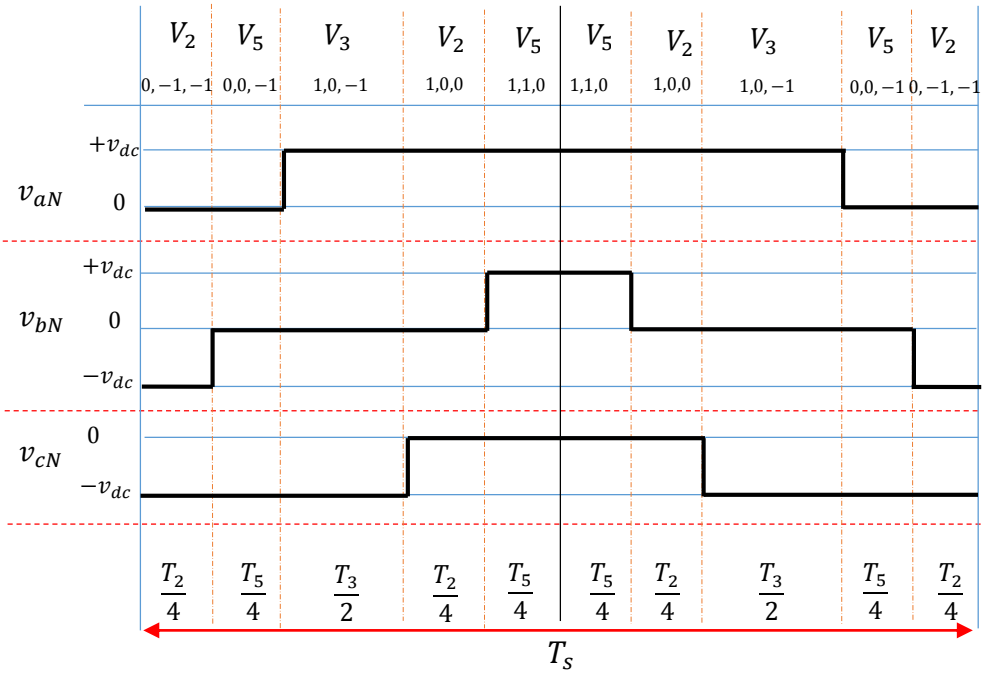

Figure III.23 The phase voltages v_{aN}, v_{bN} and v_{cN} in the third region «Sector A»

1. $S_{a1} = \frac{T_a}{2} + \frac{T_c}{2} + T_b$ $\quad S_{a2} = S_{a1} + \frac{1}{2}(T_a + T_c)$
2. $S_{b1} = \frac{T_c}{2}$ $\quad S_{b2} = S_{b1} + \left(T_b + \frac{T_a}{2} + \frac{T_c}{2}\right)$
3. $S_{c1} = 0$ $\quad S_{c2} = 2.\left(\frac{T_a}{2} + \frac{T_c}{2}\right)$

d. Switching states of fourth region

Figure III.24 shows the phase voltages v_{aN} , v_{bN}, v_{cN} for the third region in sector A of three-level inverter cells/arms .

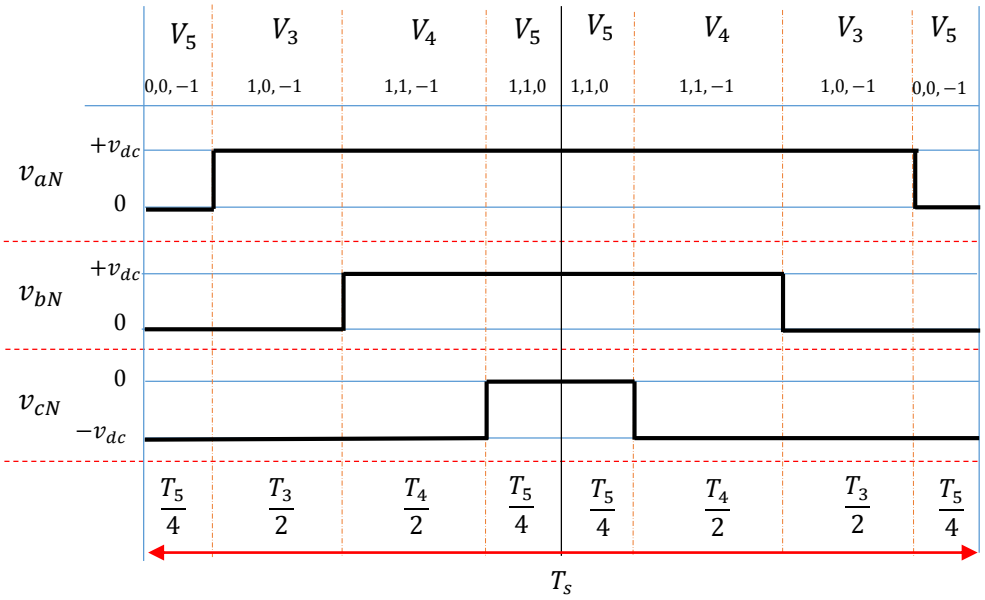

Figure III.24 the phase voltages v_{aN}, v_{bN} and v_{cN} in the fourth region « Sector A ».

1. $S_{a1} = \frac{T_c}{2} + T_a + T_b \qquad S_{a2} = S_{a1} + \frac{T_c}{2}$
2. $S_{b1} = \frac{T_c}{2} + T_a \quad S_{b2} = S_{b1} + \left(T_b + \frac{T_c}{2}\right)$
3. $S_{c1} = 0 \quad S_{c2} = \frac{T_c}{2}$

The switching times for the other sectors (from B to F) are calculated . it summarize in the following table III.9. Therefore, the switching times of the switches at the bottom for the three-inverter cells (S_{i3}, S_{i4}) in any region can be determined using these expressions:

$$\begin{cases} S_{i3} = T_s - S_{i1} \\ S_{i4} = T_s - S_{i2} \end{cases} \tag{III.72}$$

Table III.9 Switching times of the switches at the top of the three level h-bridge inverter.

sector		Region 1	Region 2	Region 3	Region 4
A	S_{a1}	$(T_a+T_c)/2+T_b/4$	$T_a+T_b+(T_c/2)$	$T_b+(T_a+T_c)/2$	$T_a+T_b+(T_c/2)$
	S_{a2}	$S_{a1}+(T_a+T_b+T_c)/2$	$S_{a1}+(T_a/2)$	$S_{a1}+(T_a+T_c)/2$	$S_{a1}+(T_c/2)$
	S_{b1}	$T_b/4+T_c/2$	0	$T_c/2$	$(T_a+T_c)/2$
	S_{b2}	$S_{b1}+(T_a+T_b+T_c)/2$	$T_a+T_b/2$	$S_{b1}+T_b+(T_a+T_c)/2$	$S_{b1}+T_b+(T_c/2)$
	S_{c1}	$T_b/4$	0	0	0
	S_{c2}	$S_{c1}+(T_a+T_b+T_c)/2$	$T_a/2$	$(T_a+T_c)/2$	$T_c/2$
B	S_{a1}	$T_b/4+T_c/2$	0	$T_c/2$	0
	S_{a2}	$S_{b1}+(T_a+T_b+T_c)/2$	$T_a+T_c/2$	$S_{a1}+T_b+(T_a+T_c)/2$	$T_b+(T_a/2)$
	S_{b1}	$(T_a+T_c)/2+T_b/4$	$T_a+T_b+T_c/2$	$T_b+(T_a+T_c)/2$	$T_c+T_b+T_a/2$
	S_{b2}	$S_{b1}+(T_a+T_b+T_c)/2$	$S_{a1}+T_c/2$	$S_{b1}+(T_a+T_c)/2$	$S_{b1}+T_a/2$
	S_{c1}	$T_b/4$	0	0	0
	S_{c2}	$S_{c1}+(T_a+T_b+T_c)/2$	$T_c/2$	$(T_a+T_c)/2$	$T_c/2$
C	S_{a1}	$T_b/4$	0	0	0
	S_{a2}	$S_{a1}+(T_a+T_b+T_c)/2$	$T_a/2$	$(T_a+T_c)/2$	$T_c/2$
	S_{b1}	$(T_a+T_c)/2+T_b/4$	$T_a+T_b+T_c/2$	$T_b+(T_a+T_c)/2$	$T_a+T_b+T_c/2$
	S_{b2}	$S_{b1}+(T_a+T_b+T_c)/2$	$S_{a1}+T_a/2$	$S_{b1}+(T_a+T_c)/2$	$S_{b1}+T_c/2$
	S_{c1}	$T_b/4+T_c/2$	0	$T_c/2$	$(T_a+T_c)/2$
	S_{c2}	$S_{b1}+(T_a+T_b+T_c)/2$	$T_a+T_b/2$	$S_{c1}+T_b+(T_a+T_c)/2$	$S_{c1}+T_b+T_c/2$
D	S_{a1}	$T_b/4$	0	0	0
	S_{a2}	$S_{a1}+(T_a+T_b+T_c)/2$	$T_c/2$	$(T_a+T_c)/2$	$T_c/2$
	S_{b1}	$T_b/4+T_c/2$	0	$T_c/2$	0
	S_{b2}	$S_{b1}+(T_a+T_b+T_c)/2$	$T_a+T_c/2$	$S_{b1}+T_b+(T_a+T_c)/2$	$T_b+T_a/2$
	S_{c1}	$(T_a+T_c)/2+T_b/4$	$T_a+T_b+T_c/2$	$T_b+(T_a+T_c)/2$	$T_c+T_b+T_a/2$
	S_{c2}	$S_{c1}+(T_a+T_b+T_c)/2$	$S_{a1}+T_c/2$	$S_{c1}+(T_a+T_c)/2$	$S_{a1}+T_a/2$
E	S_{a1}	$T_b/4+T_c/2$	0	$T_c/2$	$(T_a+T_c)/2$
	S_{a2}	$S_{a1}+(T_a+T_b+T_c)/2$	$T_a+T_b/2$	$S_{a1}+T_b+(T_a+T_c)/2$	$S_{a1}+T_b+T_c/2$
	S_{b1}	$T_b/4$	0	0	0
	S_{b2}	$S_{b1}+(T_a+T_b+T_c)/2$	$T_a/2$	$(T_a+T_c)/2$	$T_c/2$
	S_{c1}	$(T_a+T_c)/2+T_b/4$	$T_a+T_b+T_c/2$	$T_b+(T_a+T_c)/2$	$T_a+T_b+T_c/2$
	S_{c2}	$S_{c1}+(T_a+T_b+T_c)/2$	$S_{a1}+T_a/2$	$S_{c1}+(T_a+T_c)/2$	$S_{c1}+T_c/2$
F	S_{a1}	$(T_a+T_c)/2+T_b/4$	$T_a+T_b+T_c/2$	$T_b+(T_a+T_c)/2$	$T_c+T_b+T_a/2$
	S_{a2}	$S_{a1}+(T_a+T_b+T_c)/2$	$S_{a1}+T_c/2$	$S_{a1}+(T_a+T_c)/2$	$S_{a1}+T_a/2$
	S_{b1}	$T_b/4$	0	0	0
	S_{b2}	$S_{b1}+(T_a+T_b+T_c)/2$	$T_c/2$	$(T_a+T_c)/2$	$T_c/2$
	S_{c1}	$T_b/4+T_c/2$	0	$T_c/2$	0
	S_{c2}	$S_{c1}+(T_a+T_b+T_c)/2$	$T_a+T_c/2$	$S_{c1}+T_b+(T_a+T_c)/2$	$T_b+T_a/2$

III.8 Model predictive current control

After having presented the space vector PWM strategy usually used to control multi-level converters, this part of this chapter will be devoted to the presentation of the predictive control strategy. This type of control strategy is more and more used for the control of static converters due to its ease of implementation, its good dynamic performances, the possibility to take into account the non-linearity of a system and the evolutions of numerical control platforms.

The predictive control uses the discrete predictive model of the system to be driven associated with a selection criterion to choose, at each calculation step, the best control to apply to the process.

This control strategy is well suited to the control of multi-level inverters.

Indeed, the latter have a structural redundancy allowing the same output voltage level to be obtained from several different states of the inverter switches, which makes predictive control particularly suitable for their regulation.

A selection criterion «cost function» can guarantee the desired output voltage by keeping the input variables (currents and voltages) around the desired values.

III.8.1 Predictive control strategy

Different strategies, based on predictive control, have been proposed for the control of static converters.

All these strategies use the often simplified mathematical model of the converter to predict the evolution of the state variables at each sampling time. A classification of these strategies is shown in the figure III.25 [57].

Among these strategies are the deadbeat control [59] [60] [61], the hysteresis-based control [57], trajectory-based predictive control and the model predictive control [57] [58].

The strategies using a modulator make it possible to set the switching frequency of the converter, whereas those that generate the control commands directly have variable but controlled switching frequencies.

Apart from the use or not of a modulator, other criteria such as the implementation of some constraints on the cost function or the ease of its implementation generate an important differences between these strategies.

The predictive strategy contains elements that are significantly advantageous compared to other strategies. It can indeed be easily implemented even if there are others that are even easier to implement, such as the hysteresis strategy.

This strategy also uses a modulator for the management of the converter states and a selection criterion that can include constraints and linarites or non-linarites of the system.

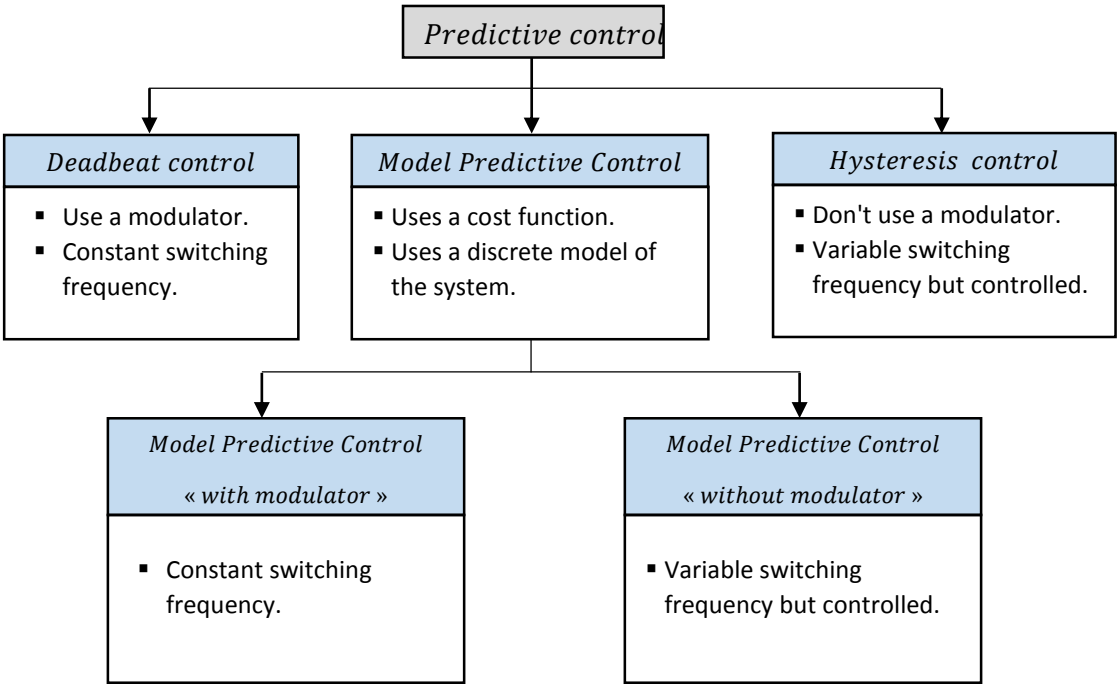

Figure III.25 Classification of control strategies based on predictive control.

in this thesis we will mainly study the case of a predictive strategy with modulator. Figure III.26 shows the basic diagram of the predictive strategy. The first block uses the converter model and the measurements of the variables $x(t)$ at time $t = kT_s$ to predict the evolution of these variables at the following calculation step $t = (k+1)T_s$. This prediction is made for all converter states using, if possible, the first-order approximation presented in the following equation (III.73).

$$\frac{dx(t)}{dt} \approx \frac{x(k+1)-x(k)}{T_s} = f(x(k), u(k) \dots) \qquad \text{(III.73)}$$

where T_s is the sampling period used, $x(k)$ is the value of the variable $x(t)$ at time $t = kT_s$ and $x(k+1)$ is the predicted value at time $t = (k+1)T_s$.

The second part of this strategy uses the predictions of the state variables $x(k+1)$ and the reference $x^*(k+1)$ to evaluate a cost function for all the states of the converter.

After choosing the optimal state, the signal x becomes T_s. This signal T_s corresponds to the commands of all switching cells associated with the state that will be applied to the inverter.

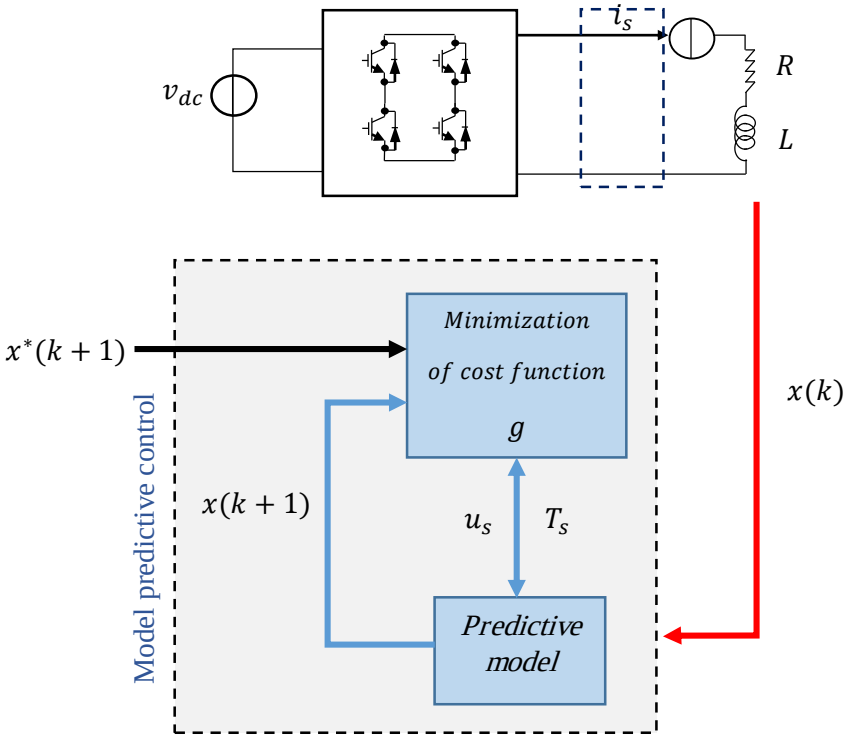

Figure III.26 Control principle of the MPC strategy.

Figure III.27 shows the functioning of this strategy over a finite horizon. At the beginning of each calculation period, all the steps of measuring, predicting, evaluating the cost function and selecting the optimal inverter configuration are carried out. The time used to perform these steps is defined as the sampling time T_s.

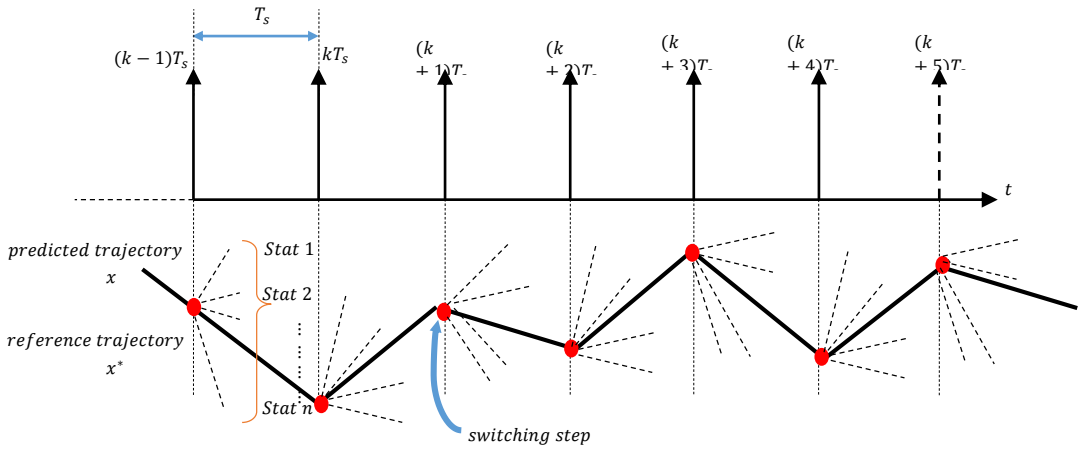

Figure III.27 Principle of predictive strategy over a finite horizon.

After this sampling time, the inverter switches takes the optimum configuration.

This procedure will be repeated regularly at etch calculation period T_s.

In this figure III.27, it can be noticed that there are not forcefully switches in all the modulation periods T_s. This strategy will therefore have a variable switching frequency, but as a general rule, the switching frequency will always be less than half the sampling frequency.

If we want to fix this frequency, we can use a term that is able to compel the inverter switching in each calculation period.

III.8.2 Discrete time model

A discrete-time model of the system (figure III.11) for a sampling period T_s , is used to obtain predictions for the future value of load current $i(k+1)$,with voltage vector $v(k)$ generated by the inverter and measured current at the k^{th} sampling interval, considering the possible output voltage vectors and measured currents at a sampling instant.

The derivation of load current form $di(t)/dt$ can be simplified by using the following approximation can be made equation as:

$$\frac{di(t)}{dt} \approx \frac{i(k+1)-i(k)}{T_s} \qquad \text{(III.74)}$$

Where ,

T_s is the sampling time and k is the current sampling instant.

The future load current vector can be determined by:

$$\mathbf{i}(k+1) = \left(1 - \frac{RT_s}{L}\right) \cdot i(k) + \frac{T_s}{L} \cdot v(k) + \frac{T_s}{L} \cdot e(k) \qquad \text{(III.75)}$$

Where,

$i\ (k+1)$ is the predictive load current value at the time $k+1$.

$i\ (k)$ is the measured load current value at time k .

$v(k)$ is the selected voltage vector during sampling time interval of k.

$e(k)$ is electromotive force of the load.

The value of the reference current $i^*(k)$ is obtained from the outer controller loop.

The corresponding load voltage vector is calculated for every valid switching state, using:

$$e(k-1) = e(k) \qquad \text{(III.76)}$$

The present value of load electromotive force $e(k)$ can be estimated from the load equation (III.75) by extrapolation from present and past values and measurements of the load voltage and current, the following approximation in equation (III.74) is used, resulting in the following expression:

$$\hat{e}(k) = v(k) + \left(\frac{L}{T_s} - R\right) i(k) - \frac{L}{T_s} i^*(k+1) \quad \text{(III.77)}$$

Where,

$\hat{e}(k)$ is the estimated back electromotive force value of $e(k)$.

$i(k+1)$ is the future reference current value, predicted from the present and previous values of the reference current.

III.8.3 The predictive model

Figure III.28 shows a block diagram of the three-phase h-bridge inverter under the model predictive control, where S_k is the switching function.

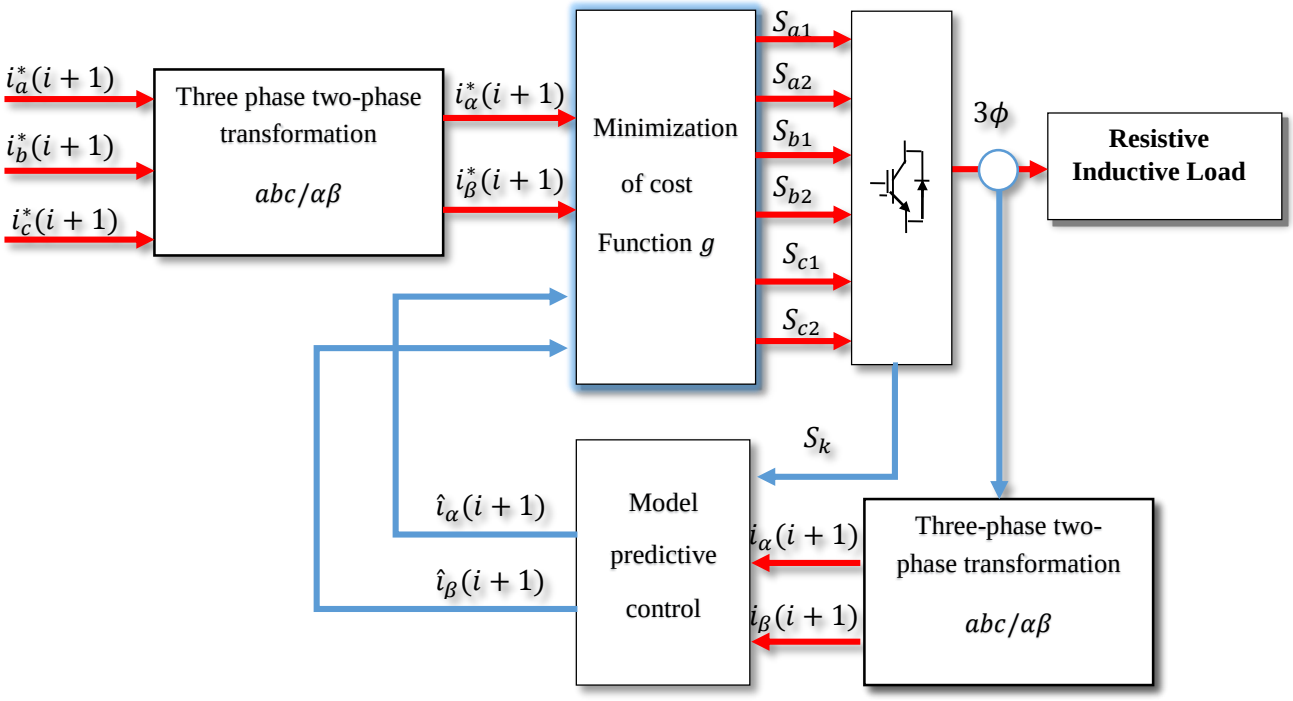

Figure III.28 Predictive control diagram of three phase three level h-bridge inverter.

The predictive controller predicts the behaviour of the converter for finite possible voltage vectors on each sampling interval.

The whole converter presents twenty-seven output voltage vectors, which mean that there are twenty seven possible load current vectors for future as the measured load current value $i(k)$ at time k.
It can be choose one possible of selected voltage vector to estimate the future behaviour of the system.
Based on the measured value $i(k)$, a prediction of next value $i(k+1)$ is made.
This value is compared to the reference value by minimizing the cost function, then the optimal switching state, S, is found. For every new sampling time, the calculations is repeated again
Where,
$i_\alpha^*(k+1)$ and $i_\beta^*(k+1)$ represent the reference current values for the predictive current control.
$i(k)$ is the m measurements taken at time k.
$i_\alpha(k+1)$ and $i_\beta(k+1)$ are the predicted values of the m states for n possible switching states at time $(k+1)$.
The time between k and $(k+1)$ is the prediction horizon, Δk.

$$\Delta k = [k\ , k+1] \tag{III.78}$$

III.8.4 The cost function

III.8.4.1 Choice of the cost function

The choice of the cost function depends mainly on the application envisaged and a study presented in [58] clearly establishes different criteria for the selection of this function. Among these criteria, we can cite the number of variables that the cost function possesses.
Thus, for a cost function which has only one variable, the determination of the optimal state can be made directly from the absolute value of the error between the prediction and the reference of this variable.
On the other hand, when several variables are included in this cost function, the square of the errors between the references and the predictions seems to be the best option.
Equation (III.79) presents an example of a cost function g including n variables to be controlled.

$$g = \alpha_1(i_1^*(k+1) - i_1(k+1))^2 + \alpha_2(i_2^*(k+1) - i_2(k+1))^2 + .. + \alpha_n(i_n^*(k+1) - i_n(k+1))^2 \tag{III.79}$$

With, $\alpha_1, \alpha_2, \dots \alpha_n > 0$
The coefficients α_1, α_2 and α_n are weighting factors that make it possible to set the priority of some variables over others or simply to compensate for differences in size and nature between variables. Other terms including non-linearities or constraints imposed for the proper operation of the converter (limitation of the switching frequency, restriction of some states, ...) can be included in this cost function g.

The choice of appropriate weighting factors α_1, α_2 and α_n is a current research topic and many solutions can be used depending on the intended application[58].

III.8.4.2 Minimization of the cost function

The cost function represent the desired behaviour of the system that should be defined according to the control requirements of the system by control the output current and keep it close to the reference value.

The current error (ε) between the reference current values and the predicted current values in the next sampling instant is obtained to minimize the cost function and the switching state signals, S.

The voltage that minimizes the current error is applied to the converter at the next sampling time [62].

The absolute error is used for computation simplicity in this thesis, it can be expressed as follows:

$$g = |i^*(k+1) - i(k+1)| \qquad \text{(III.80)}$$

Where,

$i^*(k+1)$ is the future reference current vector.

$i(k+1)$ is the predictive load current vector.

Furthermore, (III.81) can be derived in orthogonal coordinates as follow:

$$g = |i_\alpha^*(k+1) - i_\alpha(k+1)| + \left|i_\beta^*(k+1) - i_\beta(k+1)\right| \qquad \text{(III.81)}$$

Where,

$i_\alpha(k+1)$ and $i_\beta(k+1)$ are the real and imaginary parts of the predicted load current vector, respectively.

$i_\alpha^*(k+1)$ and $i_\beta^*(k+1)$ are the real and imaginary parts of the reference current vector, respectively.

III.8.5 Model predictive current control algorithm

The flow diagram of the predictive current control algorithm is shown in figure III.29.

The Predictive current control algorithm can be demonstrate in the following steps [63]:

1. Measure of the output load currents at a sampling time T_s.
2. The currents i_{abc} in stationary reference abc frame are transformed into $i_{\alpha\beta}$ in the orthogonal reference frame $\alpha\beta$ by using the Clarke transformation.
3. Predict the future load currents which is determined by measured load current for every possible voltage vectors using discrete time model in the next sampling time for all the possible switching states.

4. Minimizing the cost function for each prediction horizon Δk by calculating the error between reference current and load current values.

5. Optimal switching state is selected which minimizes the cost function g.

6. Apply the new switching state to the selected voltage vector is set to the gating signals.

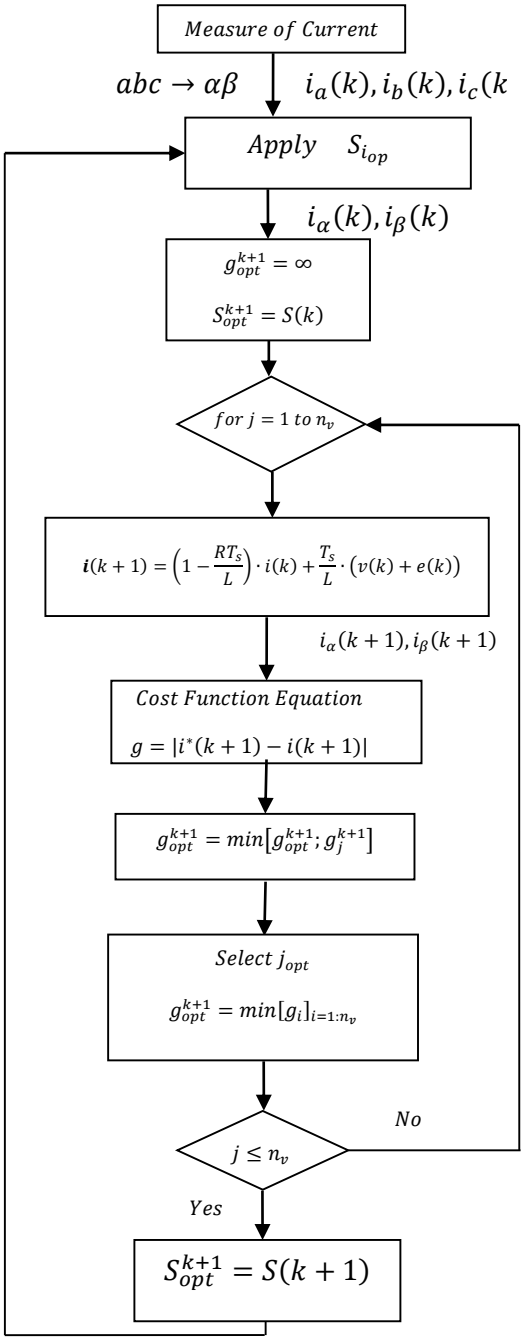

Figure III.29 Flow diagram of the predictive control algorithm

III.9 Conclusion

In this chapter two controls strategies are presented, in the first time we studied the dynamic of the space vector pulse width modulation then the model predictive control and applied them to the tow topologies of inverters, we beginning of three phase two level voltage source inverter then three phase three level h-bridge inverter.

There are a relationship between space vector pulse width modulation control and model predictive current control represented in the evaluation of the voltage vectors generated by using the model of the system (inverter load and dc-link voltage/switching states) based on space vector control transformation (Clarke transformation or Concordia transformation) means transform three phase system into biphase system in $\alpha\beta$ frame, these decompositions considerably reduce the complexity of the algorithm and the calculation time. Model predictive control compare between these voltage vectors and the reference state vectors by using an objective function(cost function) and the parameters of the model (the resistor and inductor) to obtain the discrete time model then choosing the optimal state vector near the reference and applied them to the inverter.

.

Chapter IV

Predictive Control Strategy for Three Phase VSI and Multilevel H-Bridge Inverter

IV.1 Introduction

In order to validate the effectiveness of the proposed predictive current control strategy (MPC) was cited in the last chapter for two topologies of inverters: three phase two level voltage source inverter and three phase multilevel h-bridge inverter and to evaluate the performance and to check the performance and robustness . The model predictive control strategy (MPC) was simulated using MATLAB software/Simulink with a comparison between this strategy and space vector modulation strategy.

IV.2 Presentation of Matlab environment

Matlab is a software mainly designed for scientific computing, modeling and simulation. The calculation core is associated with the Simulink environment, allowing modeling based on block diagrams. Special libraries are available the "Toolboxes" for most scientific fields requiring significant computing resources: automation, signal processing, applied mathematics, telecommunications…e.g.

IV.3 Simulation results

IV.3.1 The predictive control strategy for three-phase two-level voltage source inverter

The predictive control for a three phase two-level voltage source inverter was simulated using Matlab/Simulink software to evaluate its performance and to check the performance and robustness of the proposed predictive control technique. A sinusoidal reference current was applied to the system, and the amplitude of the reference current was set to $5\,A$ with a frequency of $50\,Hz$ per phase. A Resistive inductive load was then connected to the output of the inverter as shown in the figure IV.1.

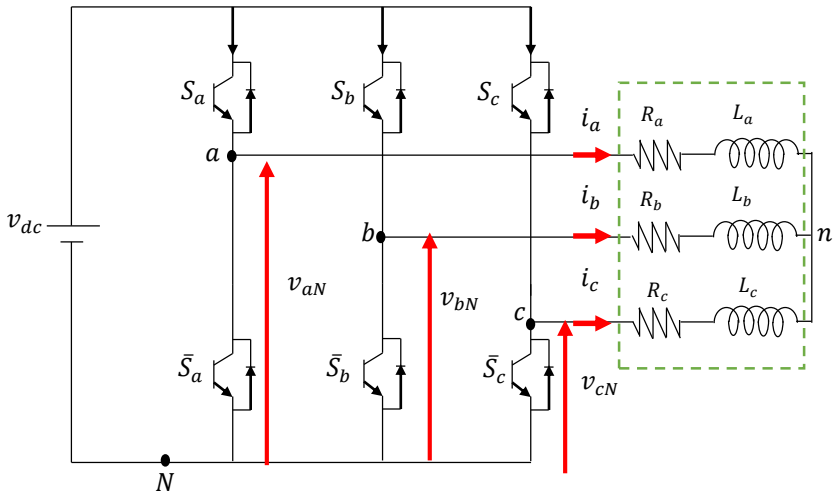

Figure IV.1 Three-phase two level voltage source inverter topology.

Table IV.1 shows the parameters used for the simulation.

Table IV.1 three phase voltage source inverter parameters

Parameter	Value
DC link voltage, v_{dc}	520 V
Inductance, L	20 mH
Resistance, R	10 Ω
Sampling time, T_s	25 μs
frequency, f	50 Hz
Reference current amplitude,i_{ref}	5 A

IV.3.1.1 Sinusoidal reference

The figure IV.2 shows the load currents i_a, i_b, i_c and the reference currents i_a^*, i_b^*, i_c^* with the amplitude of $5A$.

The system performance with a prediction horizon of one sample time illustrates how the output currents track their references, indicating that the control method shows excellent tracking behavior. Once more it can be seen that the ripples are very limited(figure IV.3).

The figure IV.4 show the load voltage v_{an} for the proposed predictive control, where the high switching behavior can be recognized clearly. During the simulation time of the current i_a, the load voltage, v_{an}, is kept at its maximum value until the reference current, i_a, is achieved (figure IV.4).

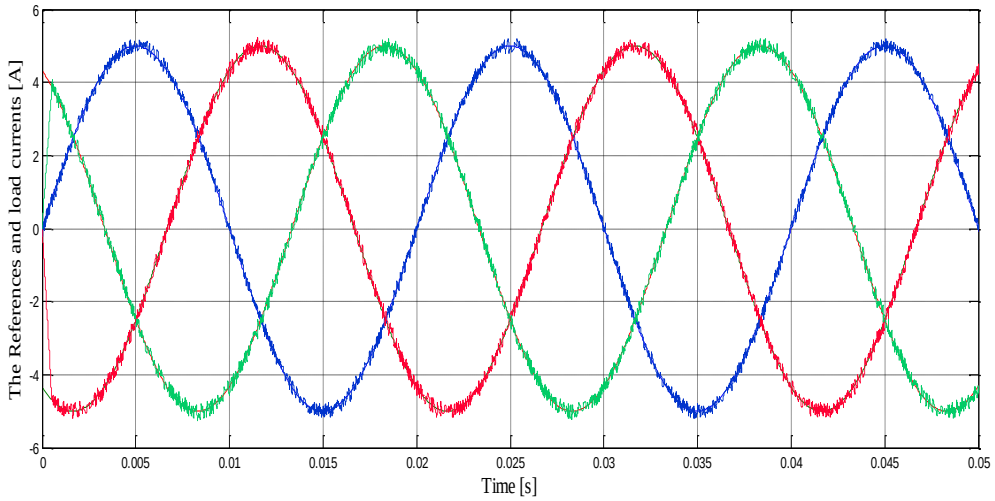

Figure IV.2 The load currents i_a, i_b, i_c and the reference currents i_a^*, i_b^*, i_c^* with the amplitude of $5A$

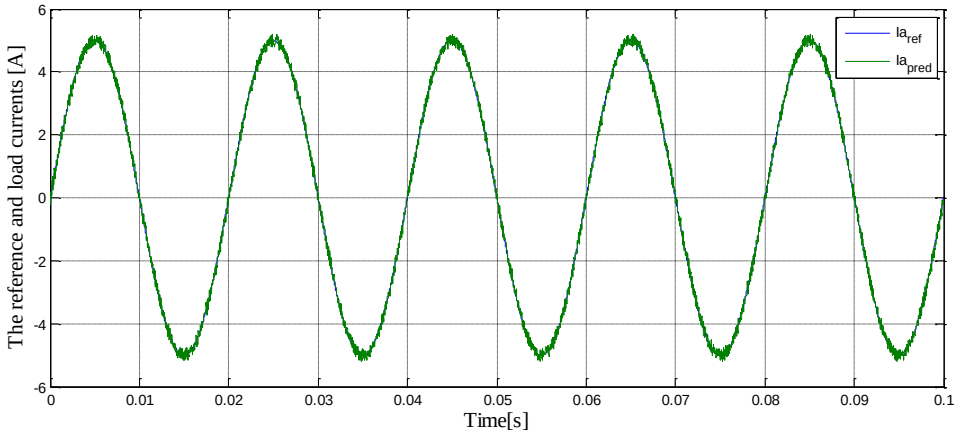

Figure IV.3 The reference currents i_a^*, i_b^*, i_c^* and load currents i_a, i_b, i_c in the steady state.

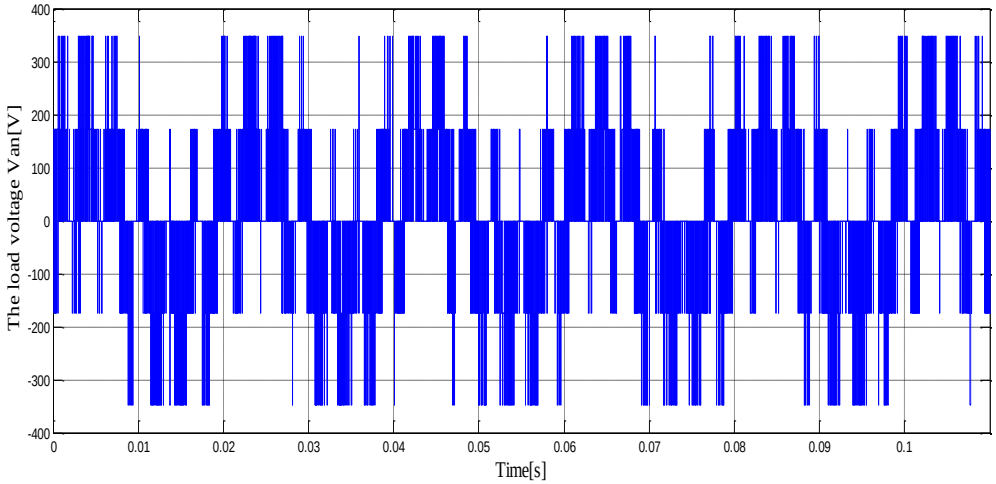

Figure IV.4 The load voltage v_{an} in the steady state.

The error between the reference and load current has been evaluated, and the error has been found to be small, as indicated in figure IV.5.

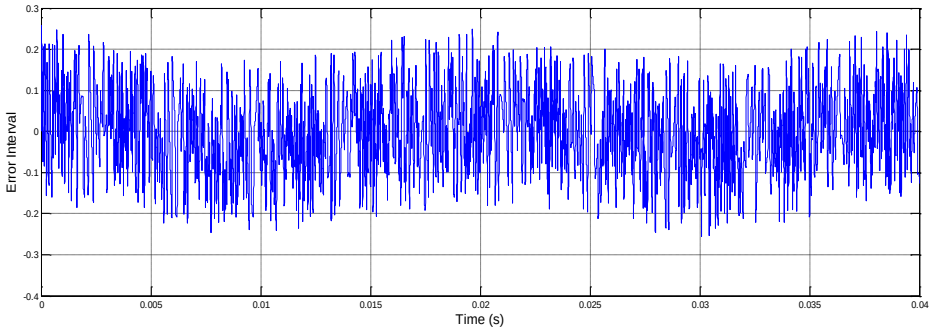

Figure IV.5 The error between reference currents i_a^*, i_b^*, i_c^* load currents i_a, i_b, i_c for the phase 'a'

IV.3.1.2 Reference tracking

The simulation was to assess the system performance when a step change in the amplitude of the reference tracking occurs for $T_s = 25\ \mu s$ for two tests:

The first test for one step change from 5A to 10A at the instant $0.05s$.

The second test for two steps change from 5A to 2A at the instant $0.05s$ than from 2A to 10A at the instant $0.1s$.

IV.3.1.2.1 The first test for one step change from $5A$ to $10A$ at time $0.05s$.

The model predictive control is not based only on the output voltage, but also based on the control of the load currents. To achieve this, the dynamic of the similar reference currents will be taken from the obtained currents. Figure IV.6 shows the reference currents i_a^*, i_b^*, i_c^* and the load currents i_a, i_b, i_c of the three phases a, b and c. It is evident that the dynamics of the application of the predictive model is appropriate, when the response to the decreasing and increasing of the current change does not affect its performance.

The amplitude of the references currents i_a was changed from $5A$ to $10A$ at $0.05\ s$.

It can be seen in Figure IV.7 that the current of the load of the phase 'a' follows the dynamics of the reference current, it is clear that the pursuit during the transient regime or change of the load is very fast, this dynamic is incomparable with conventional controls.

It is also possible to deduce the same statement for biphasic currents i_α, i_α^* and i_β, i_β^* according to the two dimensional axes $\alpha\beta$ (IV.8).

It can be explained by the sampling time of this controller, if this time is increased, better results can be obtained.

On the other hand, it is noted that the number of switching operations, which is a characteristic of the predictive algorithm, limits the switching losses in the power switches.

Figures IV.9, IV.10, IV.11 and IV.12 show the load voltage v_{an}, the phase voltage v_{aN}, the common-mode voltage v_{nN}, and the line voltage v_{ab} between phases respectively.

The common-mode voltage v_{nN}, can have a reduced RMS value, which is an added advantage, especially in electrical machine applications where the presence of this voltage can cause the rapid deterioration of the bearings. The load voltage v_{an} and the composed voltage v_{ab} are quite symmetrical where the harmonics of the third range and its multiples are almost equal to zero.

It can be concluded that the quality of the current are acceptable, however more ripples can be observed but within acceptable levels, furthermore the dynamics of the current indicates the validity

of the predictive control strategy in controlling the three-phase two level voltage source inverter with any difficulties.

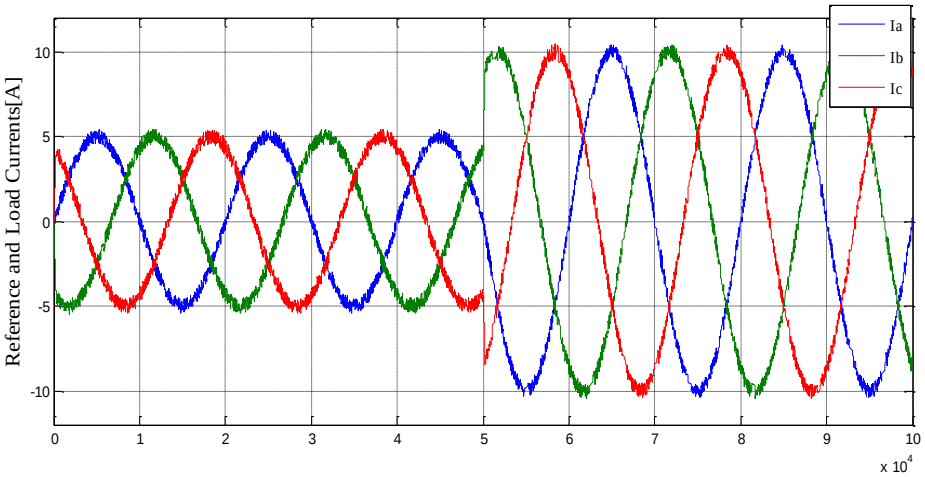

Figure IV.6 The reference currents i_a^*, i_b^*, i_c^* and load currents i_a, i_b, i_c

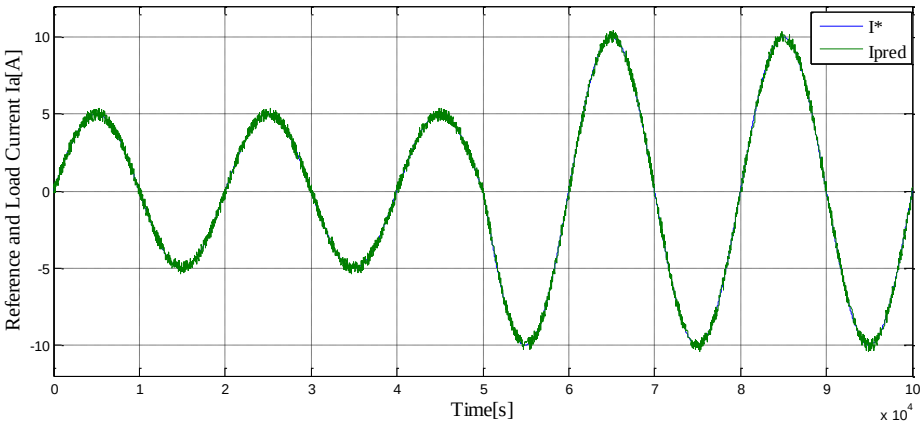

Figure IV.7 The load currents i_a and the reference current i_a^*

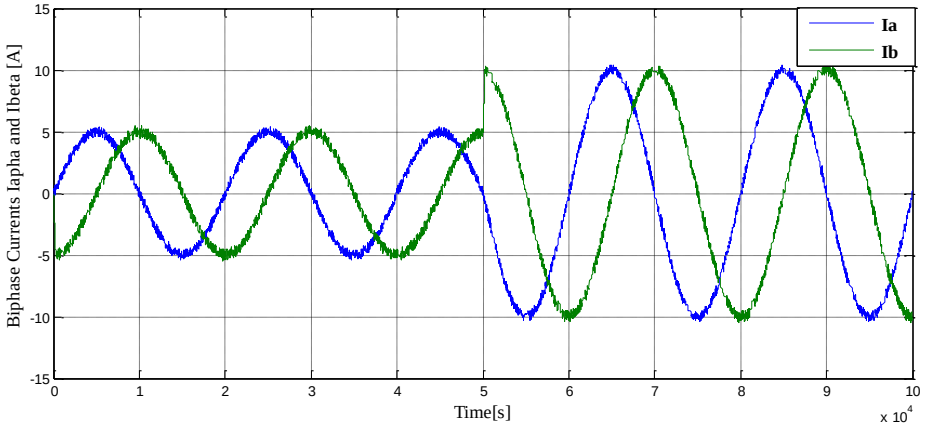

Figure IV.8 The diphase currents i_α, i_β

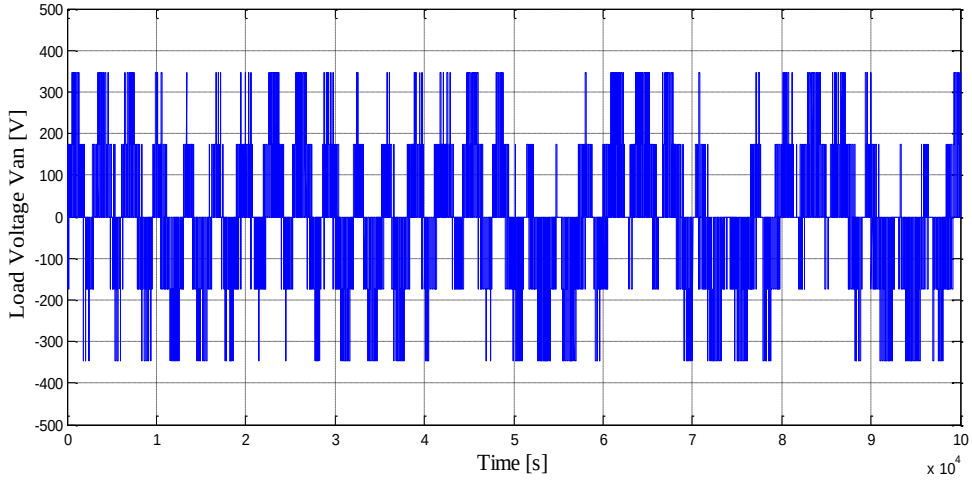

Figure IV.9 The load voltage v_{an}

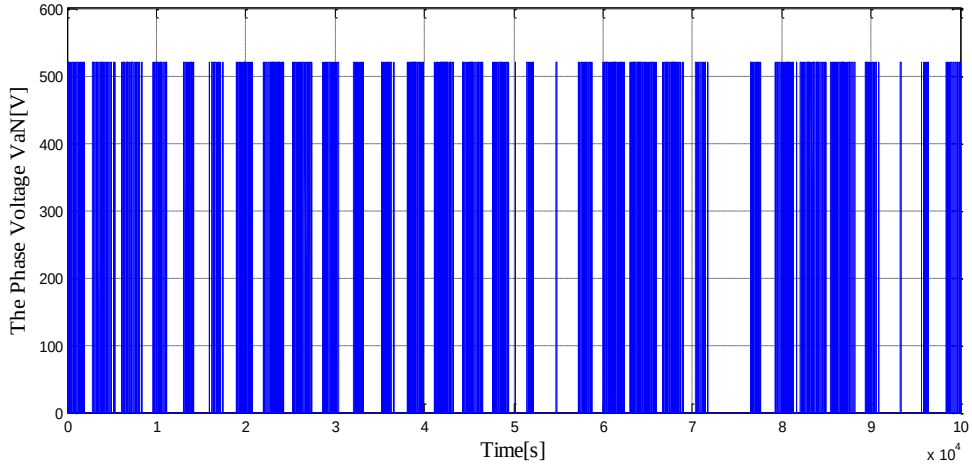

Figure IV.10 The phase voltage v_{aN}

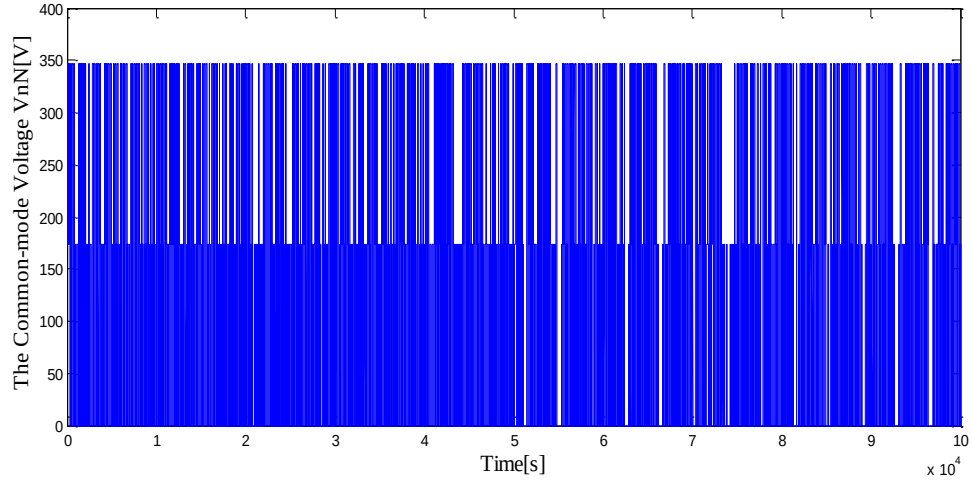

Figure IV.11 The common-mode voltage v_{nN}

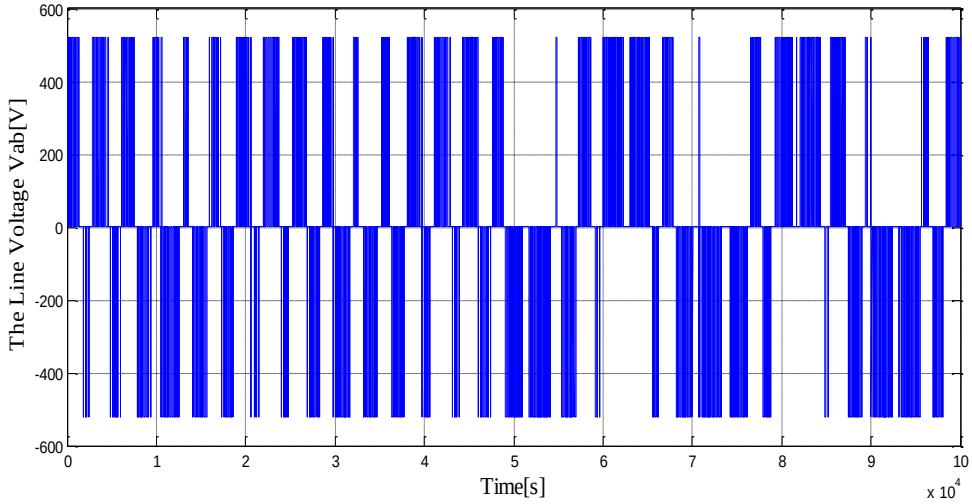

Figure IV.12 The line voltage v_{ab}

IV.3.1.2.2 The second test for two step changes from $5A$ to $2A$ at $0.05s$ than from $2A$ to $10A$ at $0.1s$.

In this simulation, the reference currents has two changes :

The first at the instant $0.05s$ with decreasing currents amplitude, the second at the instant $0.1s$ with increasing currents amplitude , the load current waveforms in the three phases are presented in figure IV.13.

It can be seen clearly that the dynamics of the application of the predictive algorithm is adequate, where the response to the decrease and the increase of the current change does not affect its quality.

To clarify the quality of tracking the reference current, the reference current and the obtained load currents of phase« a » are shown in figure IV.14.

The result of the step changes in the amplitude of the reference i_a was changed from $5A$ to $2A$ at $0.05\ s$ and from $2\ A$ to $10\ A$ at $0.1\ s$ respectively.

It is clear that the predictive control allows ensuring the accurate tracking of the references current, once more it can be seen that the ripples are very limited as well as the very short transition time.

Figure IV.15 shows the load voltage v_{an}, where the high switching behavior can be recognized clearly. Despite the step change of the current i_a, the load voltage, v_{an}, is kept at its maximum value until the reference current, i_a, is achieved (figure IV.15).

On the other side, the common mode voltage v_{nN}, based on the average values among the measured voltages in the three phases of the load between the star connection point « n » of the load and the fictive point « N » of the VSI inverter phases/legs .

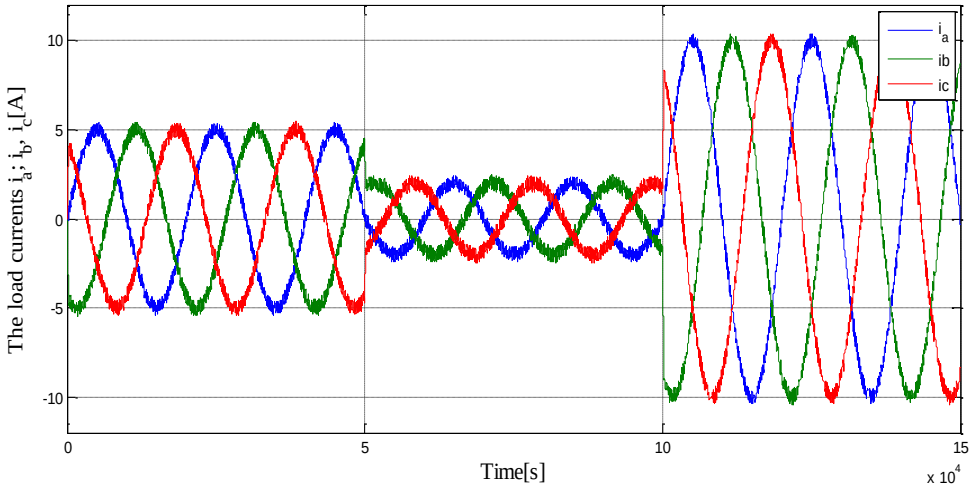

Figure IV.13 The sinusoidal reference steps for load currents i_a, i_b , i_c

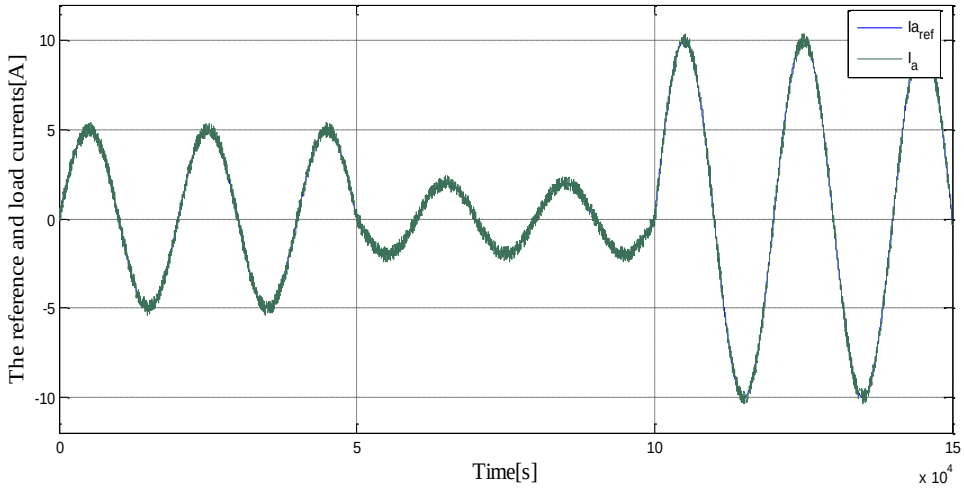

Figure IV.14 The sinusoidal reference steps for load current i_a

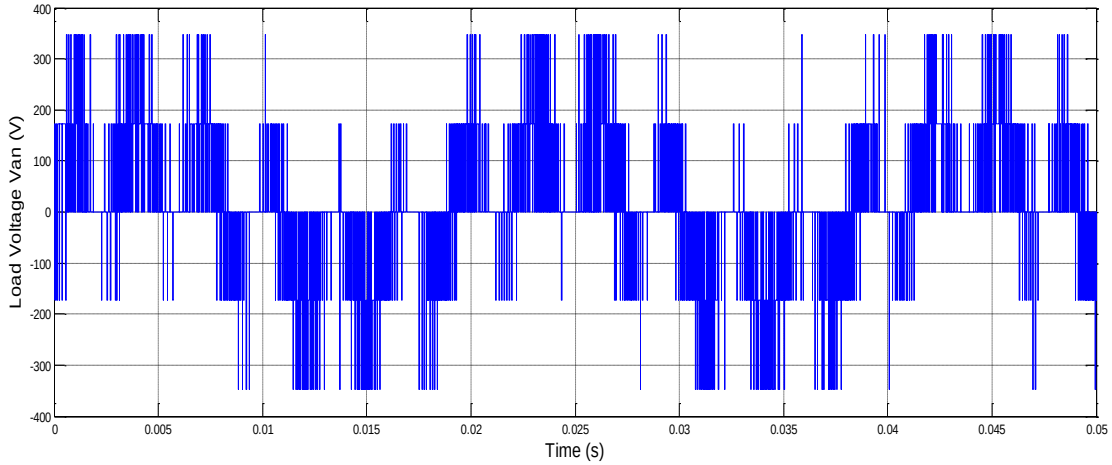

Figure IV.15 The sinusoidal reference steps for load voltage v_{an}

This simulation clearly demonstrated the ability of the proposed control algorithm to track sinusoidal reference currents.

From this simulation, it was noted that the predictive control method has a fast, dynamic response, and showed excellent tracking behavior.

Remark:

The change in the load inductance 'L' have a major importance for the load current prediction, and hence, in the behavior of the current control (figure IV.16 and figure IV.17).

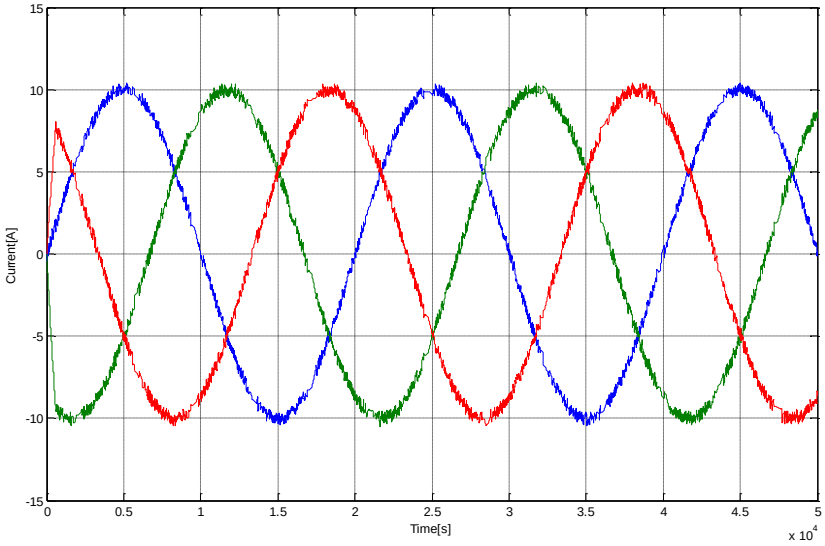

Figure IV.16 The load inductance for value $L = 10mH$

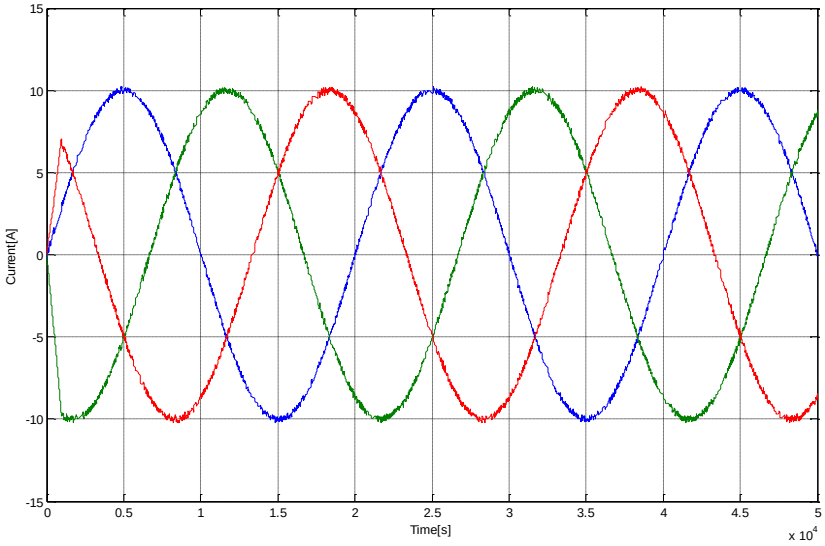

Figure IV.17 The load inductance for value $L = 20mH$

IV.3.1.3 Stability of control strategy of three phase inverter subject to a variable DC-link voltage v_{dc}, input

The robustness of the proposed control technique of the inverter subject to variable DC-link voltages was investigated in this section; more specifically, when the DC-link voltage was changed for different values of the DC-link voltage $400V$ and $500V$ for sampling time $T_s = 25\ \mu s$.

Figure IV.18(a and b) shows the output currents for different values of the DC-link voltage.

(a)

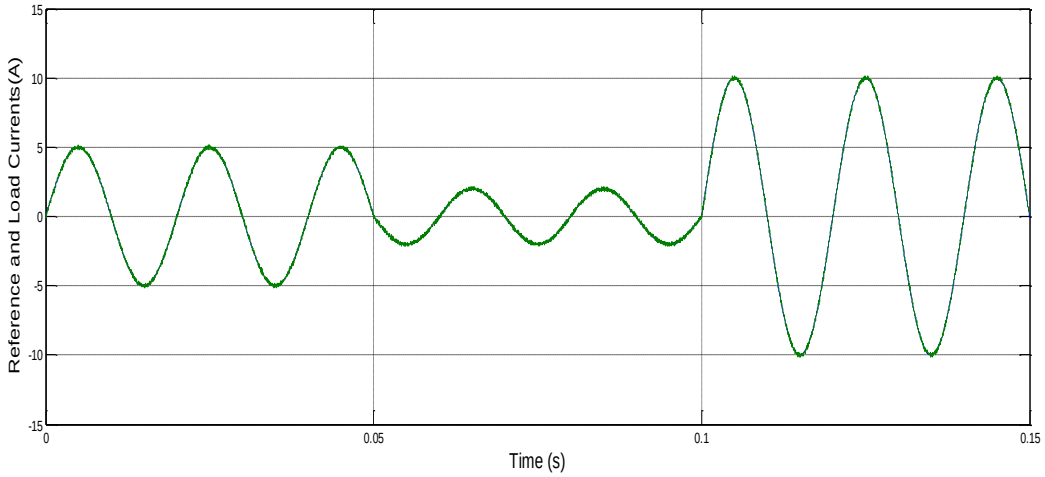

(b)

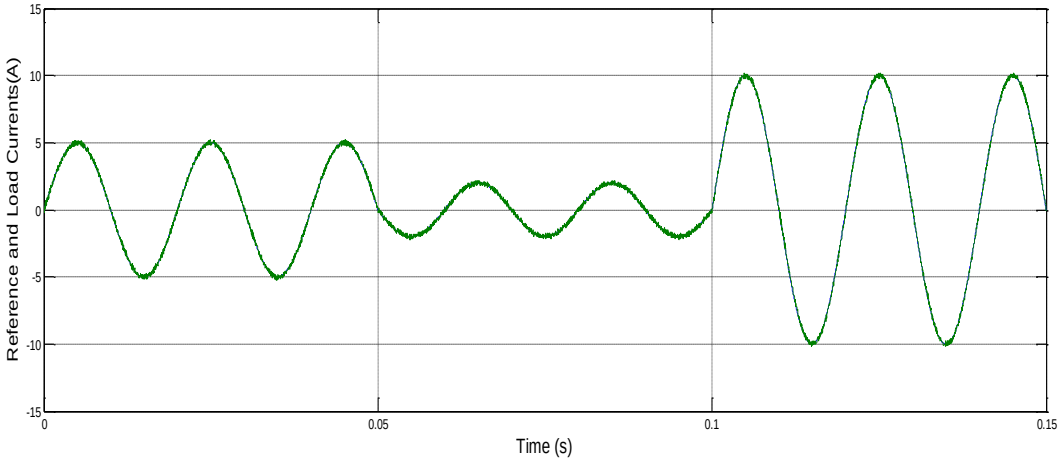

Figure IV.18: The output currents for different values of the DC-link voltage, v_{dc}

(a) For $v_{dc} = 400V$

(b) For $v_{dc} = 500V$

Observe that the proposed control algorithm has the ability to track sinusoidal reference currents irrespective of the DC link voltage variations around the desired voltage (figure IV.18).

It was noted that voltages lower than the designed DC-link voltage value of $500\ V$ produced a lower total harmonic distortion, which tracked the reference current with a very small error.

On the other hand, DC-link values greater than the designed value, produced higher total harmonic distortion but with a relatively small amplitude error.

This simulation confirms that the predictive control method has the ability, even with marginal differences in DC-link values, to track sinusoidal reference currents while showing excellent tracking behavior with all DC-link voltage values.

IV.3.1.4 Comparison of the model and actual system parameters

In the last evaluation, a mismatch between selected model parameters and the corresponding system parameters was considered. Different values were used for the load resistor and inductor.

These values were estimated in order to evaluate the parameter sensitivity of the proposed control algorithm and to determine how stably the system could track the reference signal and the variation of the total harmonic distortion.

The investigation in this section focused on the effect of parameter uncertainty in the system model under consideration.

The actual inductance was estimated to be 50% higher and lower than the parameter used in the model for sampling times $T_s = 25\ \mu s$ and $T_s = 100\ \mu s$.

In the other case, the inductance was increased to 100% for $T_s = 25\ \mu s$ and $T_s = 100\ \mu s$.

The actual resistance was estimated to be 40% higher and lower than the parameter used in the model for $T_s = 25\ \mu s$.

It was noted in Figure IV.19(a) and (c) that when the load inductance was estimated to be $+50\%$ ($THD = 1.02\%$) and $+100\%$ ($THD = 1.09\%$) respectively for $T_s = 25\ \mu s$, the control algorithm showed excellent reference tracking behavior. When the sampling time, T_s, was increased to $100\ \mu s$, the current ripple on the load current increased; this is shown in Figure IV.19(b) where $THD = 4.19\%$, and in Figure IV.19(d) where $THD = 3.16\%$.

(a)

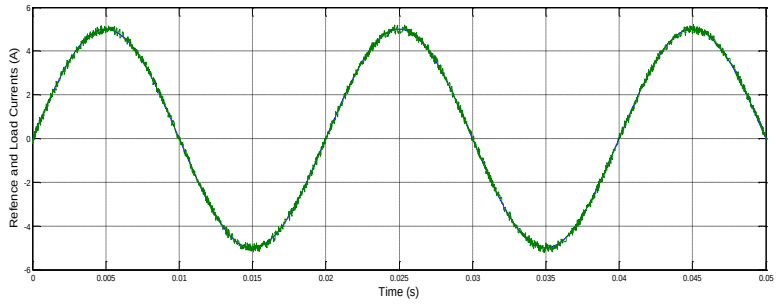

(b)

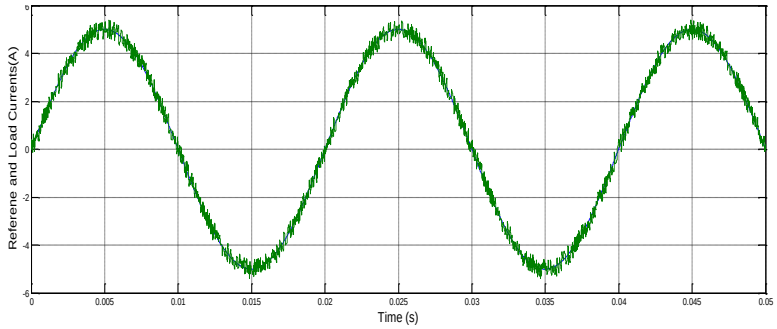

(c)

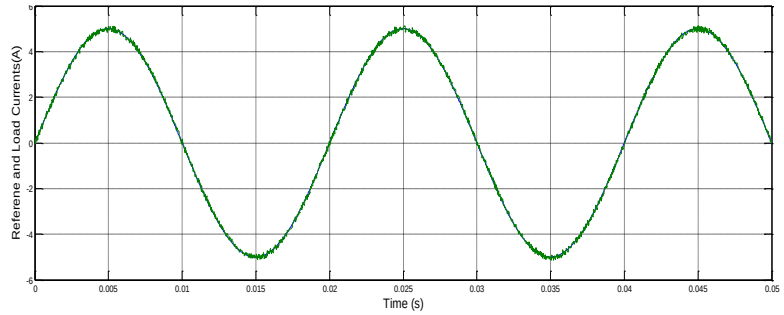

(d)

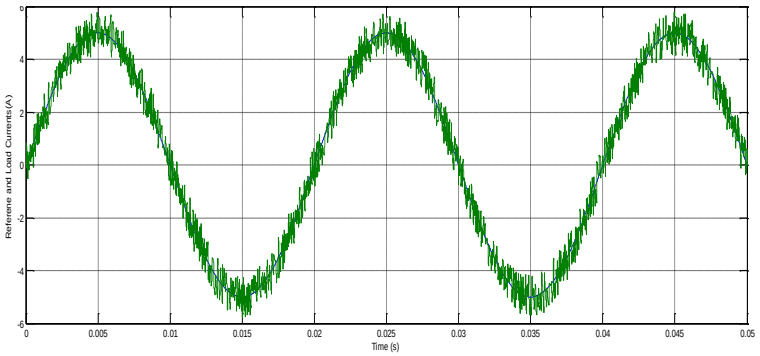

Figure IV.19 Inductance sensitivity for load current when estimated to be (a) $+50\%$ for $T_s = 25\ \mu s$, (b) $+50\%$ for $T_s = 100\ \mu s$, (c) $+100\%$ for $T_s = 25\ \mu s$ and (d) $+100\%$ for $T_s = 100\ \mu s$

If, however, the inductance was estimated to be 50% lower than the parameter used in the model for $T_s = 25\,\mu s$, the load current ripple increased a little, compared to the model inductance value ($THD = 3.44\%$); for $T_s = 100\,\mu s$, the current ripple increased ($THD = 14.28\%$).

IV.3.1.5 Comparison between space vector PWM control and predictive control :

In this section of chapter, we present a comparative assessment between predictive control strategy (MPC) and space vector modulation strategy (SVPWM).The two strategies presented above are based on the selection of the optimal state of the converter.

The predictive control strategy includes all variables in the cost function, whereas the vector control strategy includes only external (or output) variables.

In this sense, the predictive control strategy requires more work because the selection of weighting factors requires a large number of simulations around a given operating point.

The space vector control strategy uses fewer calculations due to the use of a simplified cost function. It does, however, require a state function that can control secondary variables and generate switch control commands.

One of the main advantages of the space vector control strategy compared to predictive control is that it uses fewer calculations.

IV.3.1.6 Evaluating system performance

the output reference signal of the two-level inverter is sinusoidal and independent of the parameters of the load; but, the output of the inverter is non-sinusoidal and has harmonics.

The performance of inverter is therefore evaluated in terms of total harmonic distortion (THD).

First, we will compare the two strategies for The operating point used for this comparison is:

- ✓ $v_{dc} = 10\,V$,
- ✓ $L = 6\,mH$,
- ✓ $R = 0.5\Omega$,
- ✓ $i^*(t) = 2sin(200\pi t)$A.

The sampling time, T_s, is set to $5\mu s$ for simulation.

The frequency of calculation used to evaluate the weighting factors of the classic strategy is $20kHz$Figure IV.20 shows the current output i_a of two level voltage source inverter (VSI) with space vector modulation strategy (SVPWM) .

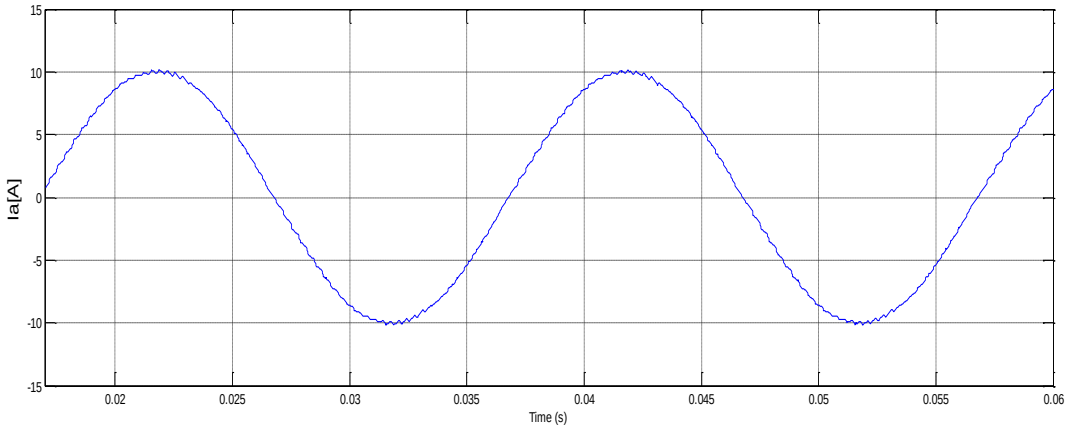

Figure IV.20 the output current i_a.

Figure IV.21 shows the THD of output current i_a. The current is not a pure sinusoidal wave and it has the harmonics. Fundamental component has a peak magnitude of 106.2 with THD =21.83 %.

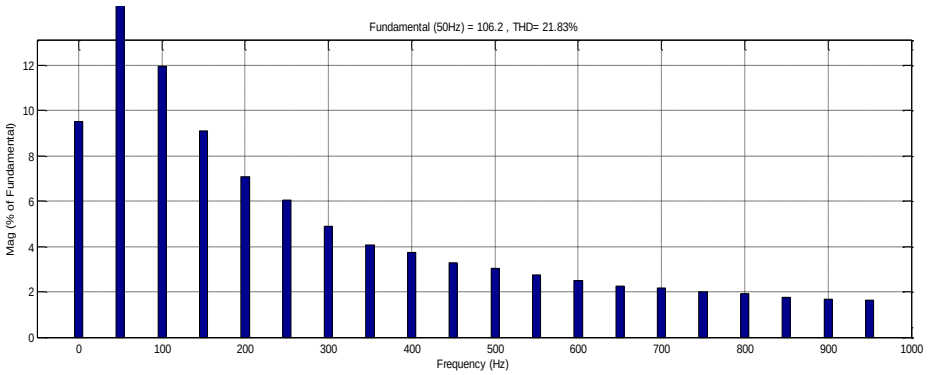

Figure IV.21 Current spectrum (THD) of the output current i_a

The figure V.22 and the figure IV.23 show load voltage v_{an} and line voltage v_{ab}, respectively.

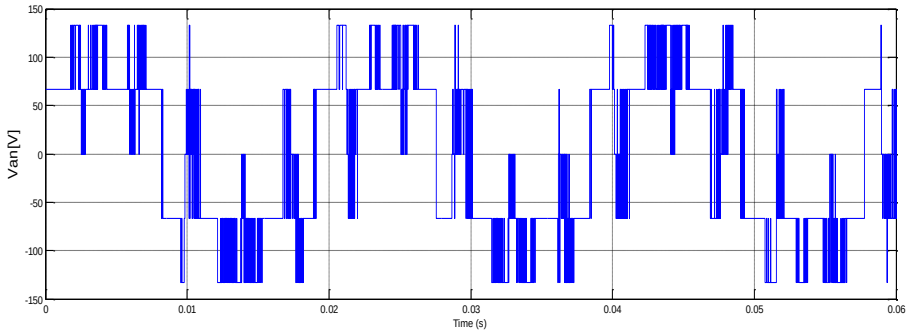

Figure IV.22 The load voltage v_{an}

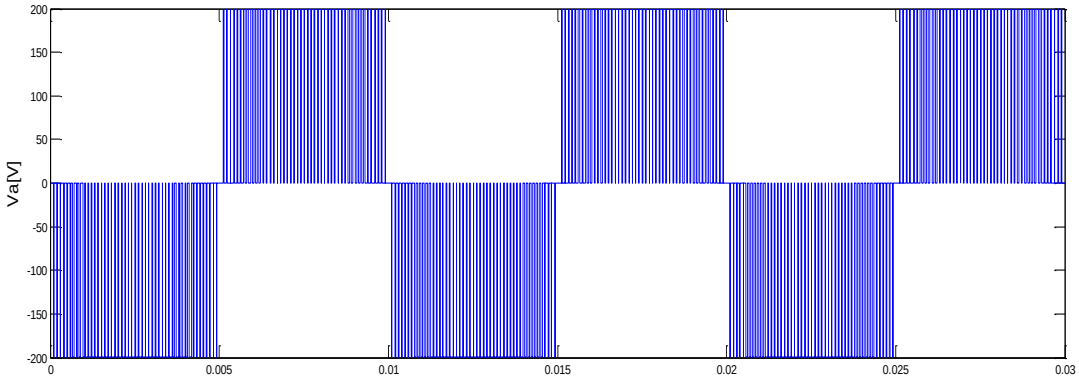

Figure IV.23 The line voltage v_{ab}

The current spectrum shows the values of the switching frequency of the space vector strategy, represented by the harmonics distributed over the whole frequency range.

Figure IV.24 presents the results of the same analysis for load voltage v_{an} and shows that v_{an} has fundamental component of 122.4 with a the THD equal to 25.67%.

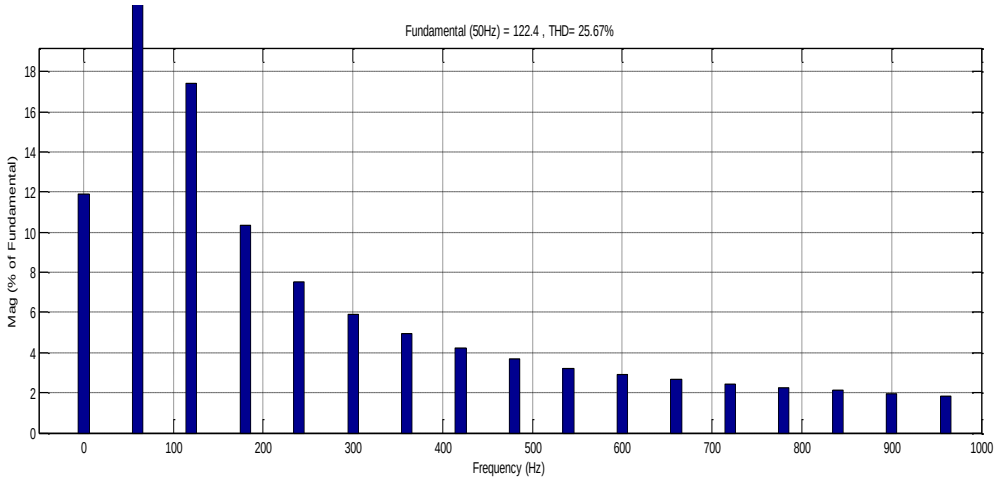

Figure IV.24 Current spectrum (THD) of the line voltage v_{ab}

Figure IV.25 shows the output of predictive control. Note that i_a is almost a pure sine wave.

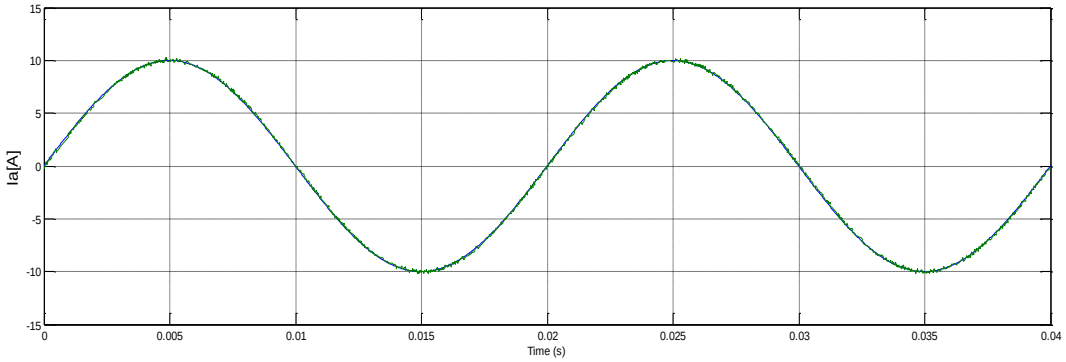

Figure IV.25 The output current i_a

Figure IV.26 and IV.27 show the current spectrum (THD) of i_a and v_{aN}.

The two figures indicate great improvement in THD analysis which is down from 21.83% to 1.25% for i_a and 25.67% to 1.35% for v_{aN}

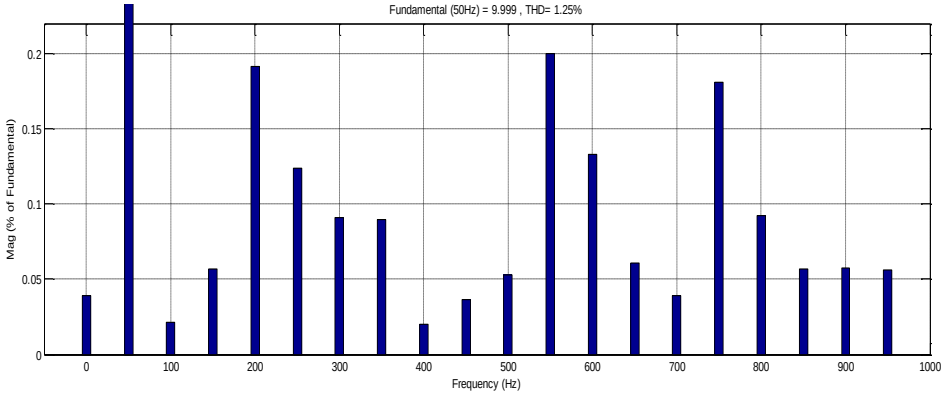

Figure IV.26 Current spectrum (THD) of the output current i_a

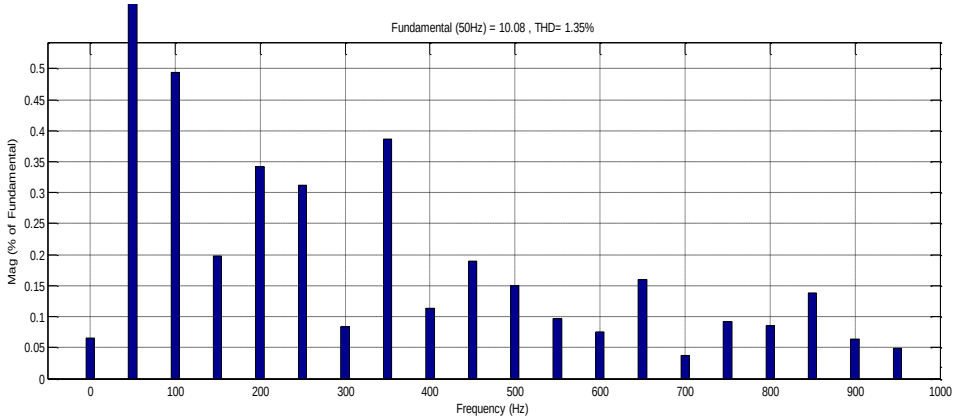

Figure IV.27 Current spectrum (THD) of the load voltage v_{an}

The Figure IV.28 and the figure IV.29 shows line voltage v_{ab} and the load voltage v_{an} respectively.

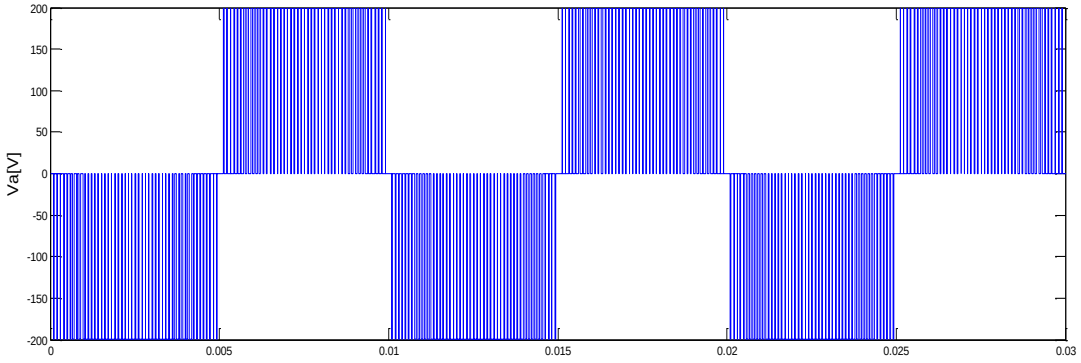

Figure IV.28 The line voltage v_{ab} (predictive control)

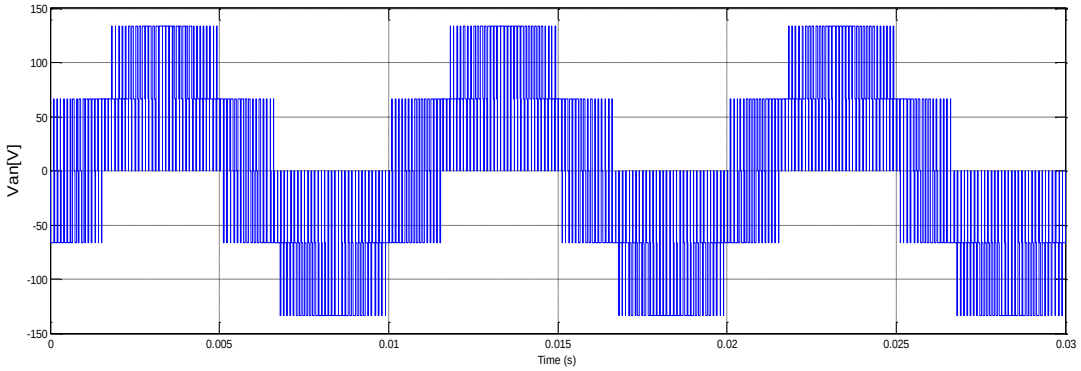

Figure IV.29 The load voltage v_{an} (predictive control)

From this comparison, we can draw the following conclusions:

1. The model predictive strategy can be easily adapted to different operating points without the need to calculate optimal relationships between several weighting factors.
2. The results obtained under steady state conditions are better for the predictive strategy. In addition to this, this strategy has the advantage of having good dynamic responses during the transitional regimes of the system.
3. The number of calculations carried out by the strategy proposed in each calculation step is 2 or 3 depending on the state of the converter.
4. The predictive strategy (MPC) applied on a multilevel inverter requires more calculations because the cost function would have to be evaluated for each inverter state.
5. Finally, this comparison show that predictive strategy (MPC) is superior to space vector modulation in terms of the total harmonic distortion (THD) and the implementation.

IV.3.2 Model predictive control strategy for a three-phase three level h-bridge inverter

A sinusoidal reference current was applied to the system, and the amplitude of the reference current was set to $10A$ at a frequency of $50Hz$ per phase.

resistive-inductive load is connected to the output of the three-phase three level h-bridge inverter as shown in figure IV.30

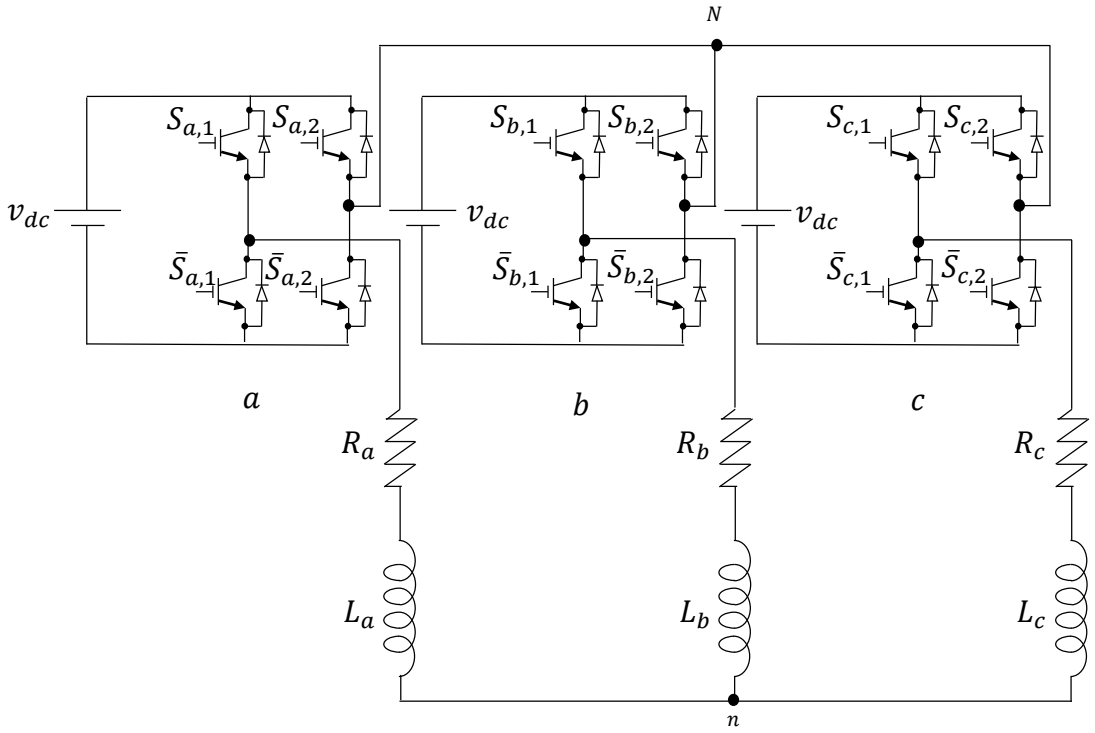

Figure IV.30 Three phase three level h-bridge inverter topology.

The predictive strategy where is presented in this thesis has been applied then to the three phase three level h-bridge inverter.

Simulation tests have been performed, in order to evaluate the performance and to check the robustness of used control technique in ensuring the control of the proposed topology of the inverter.

Two tests have been performed using two sampling times the basic sampling time :

- ✓ $T_s = 10\ \mu s$
- ✓ $T_s = 100\ \mu s$

A reference of a sinusoidal three-phase balanced currents have been used as the main input of the control block, where the magnitude has passed through three steps as shown in figure IV.31 :

- the first step from $0\ s$ to $0.06\ s$ with peak current of $12\ A$,

- the second step from $0.06\ s$ to $0.12\ s$ with peak current of $7\ A$
- the third step from $0.12\ s$ to $0.18\ s$ with peak current of $18\ A$

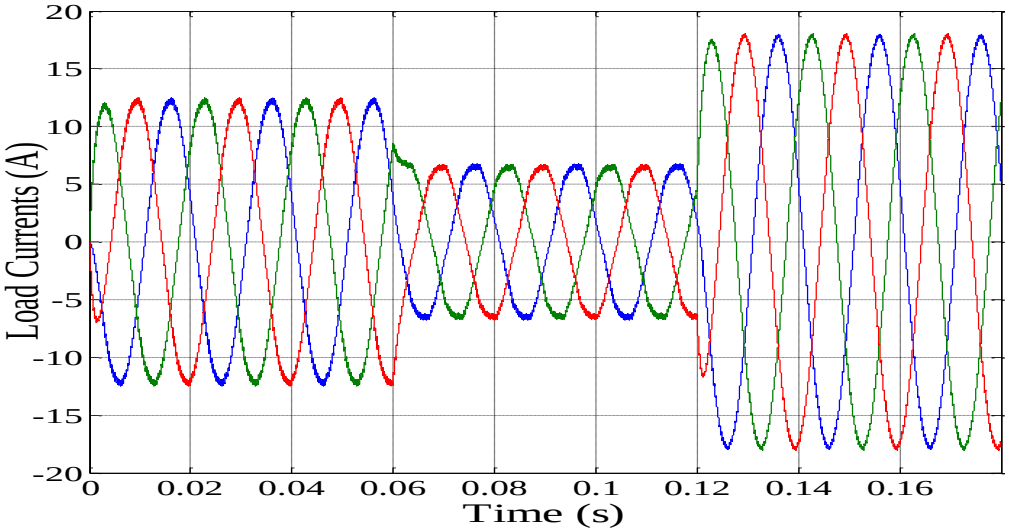

Figure IV.31 The load currents i_a, i_b, i_c of three phases a, b and c

Table IV.2 shows the parameters of the simulated system used for the simulation.

Table IV.2 Three phase h-bridge inverter parameters

Parameters	Value
DC link voltage, v_{dc}	370 V
Inductance, L	20 mH
Resistance, R	10 Ω
frequency, f	50 Hz
Reference current amplitude for the first step	12 A
Reference current amplitude for the second step	7 A
Reference current amplitude for the third step	18 A
The basic sampling time T_s	10 μs

IV.3.2.1 The first test with sampling time of $T_s = 10\ \mu s$.

For the first test, the load current waveforms in the three-phases are presented in figure IV.31.

It can be seen clearly that the dynamics of the application of the predictive algorithm is adequate, where the response to the decrease and the increase of the current change does not affect its quality.

Figure IV.32 shows the load current behavior in the $\alpha\beta$ frame.

Its circular form indicates that the three-phase currents of the load are balanced, while the width of the curve indicates that the ripples or the harmonics content are very less.

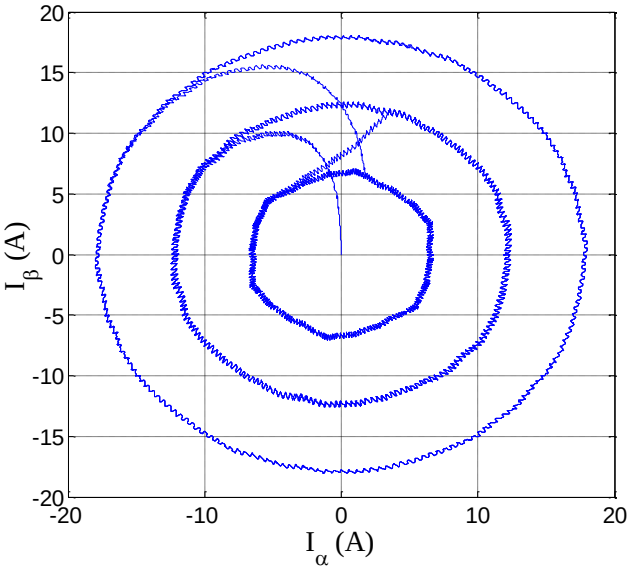

Figure IV.32 The load currents in the alpha beta frame

To clarify the quality of tracking the reference current, in figure IV.33 the reference current and the obtained load currents of phase « a » are shown:

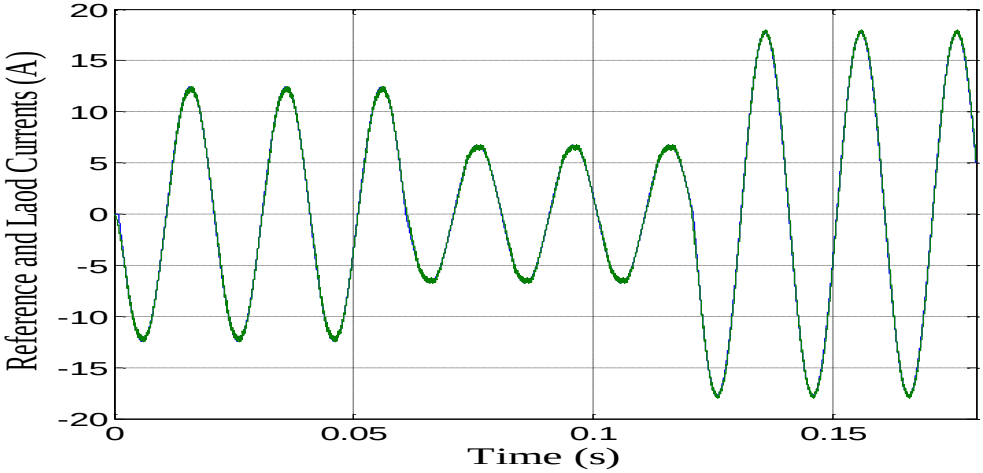

Figure IV.33 The load current i_a in the phase « a »

It is clear that the predictive control allows ensuring the accurate tracking of the references current, once more it can be seen that the ripples are very limited, to emphasize this issue a zoom is taken for each step of the load current as shown in figure IV.34.

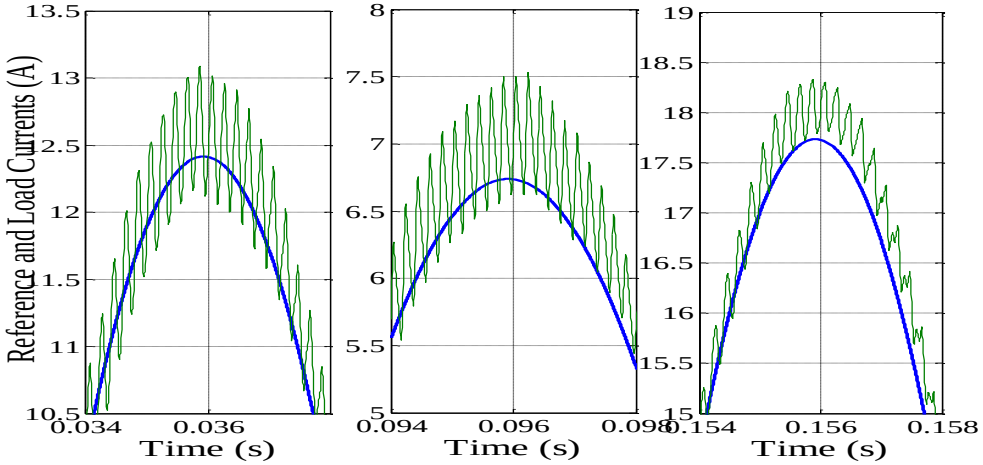

Figure IV.34 The load and reference current of phase « a » in each step of current change

The measured THD are : $1.63\ \%, 3.45\ \%$ and $0.80\ \%$ for each step respectively. All these values are very acceptable compared to the standard as they are below the value of 4%, it is worthy to notice that with high value of current, less harmonics are obtained and the value of the harmonic distortion is the best. Figure IV.35 shows the voltage v_{aN}, where the high switching behavior can be recognized clearly. On the other side, the common mode voltage v_{nN}, based on the average values among the measured voltages in the three phases of the load between the star connection point « n » of the load and the fictive point « N » of the h-bridge cells .

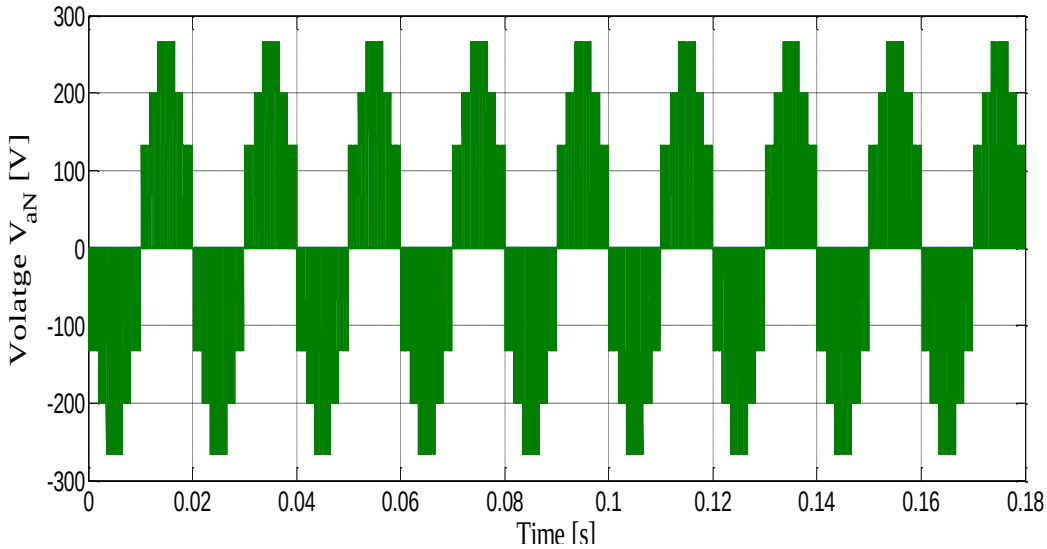

Figure IV.35 The voltage applied to the load in phase « a » between the star connection point of the load and the fictive point of among the h-bridge cells in the three phases

IV.3.2.2 The second test with sampling time of $T_s = 100\ \mu s$.

The second test has been performed with a sampling time of $T_s = 100\ \mu s$. As in the same test, the load currents in the three phase are shown in figure IV.36, on the other side the change in the current is the same as in the first test with the same peak value in each step. It can be concluded that the quality of the current are acceptable, however more ripples can be observed but within acceptable levels, furthermore the dynamics of the current indicates the validity of the predictive control strategy in controlling the three-phase h-bridge inverter with any difficulties.

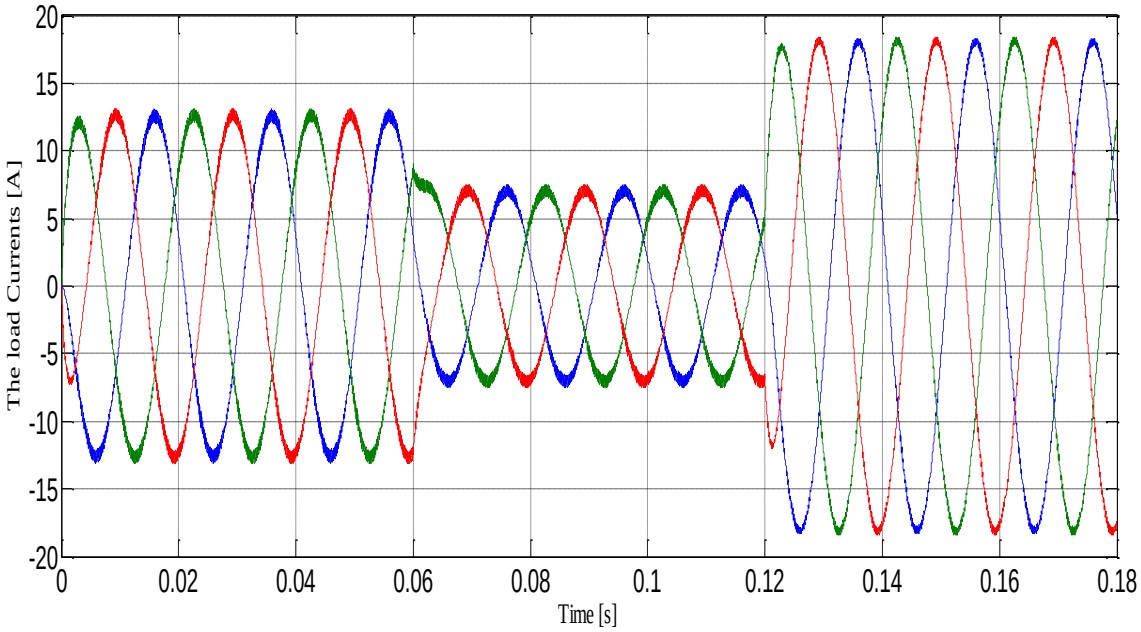

Figure IV.36 The load currents i_a, i_b, i_c of three phases a, b and c

The relationship of biphasic currents i_α , i_β in $\alpha\beta$ frame shown in figure IV.37 has a circular form which proves the quality of the balance of the three-phase load currents and give a clear image of the content of harmonics causing the neglected ripples presented in the load currents.

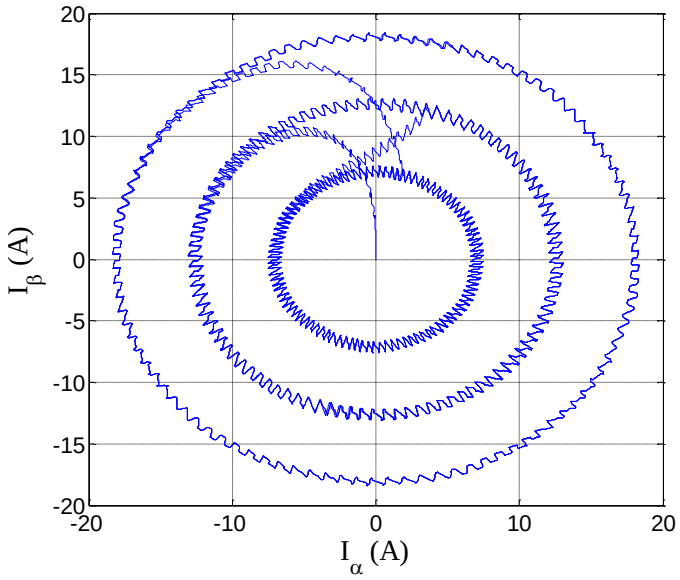

Figure IV.37 The load currents in alpha beta frame

Figure IV.38 shows the quality of tracking the reference current in phase «a» based on the predictive control strategy, where for each step as shown in figure IV.39.

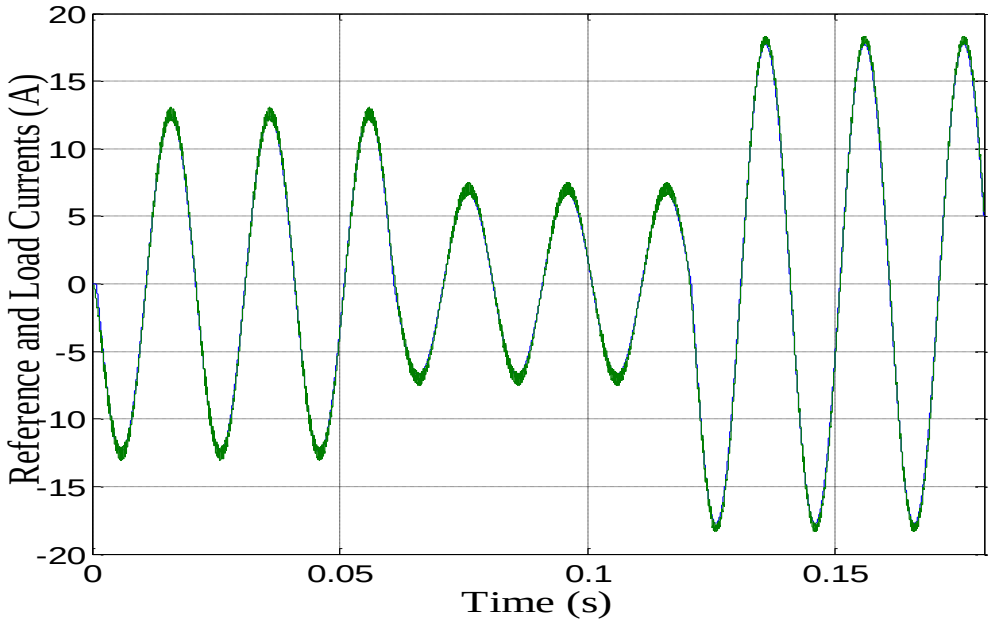

Figure IV.38 The load current in phase «a» and the corresponding reference current

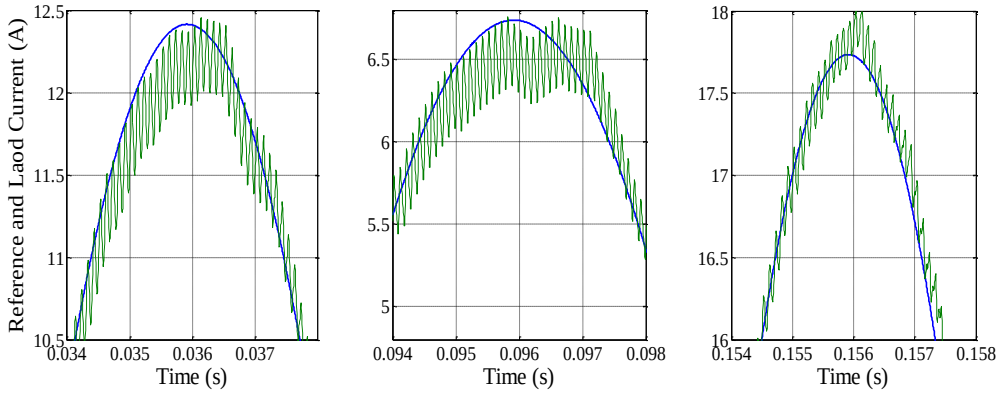

Figure IV.39 The load current i_a and the reference current i_a^* in each step of current change

The total harmonic distortion(THD) obtained are $2.65\ \%$, $4.24\ \%$ and $1.24\ \%$ for each step of current change respectively, these values of THD compared the ones obtained with the sampling time $T_s = 10\ \mu s$ have increased values, but they still within the acceptable norms.

Finally, in second test the voltage v_{aN} that is applied to the load in phase «a» has nearly the same characteristics as the one obtained in the first test (figure IV.34).

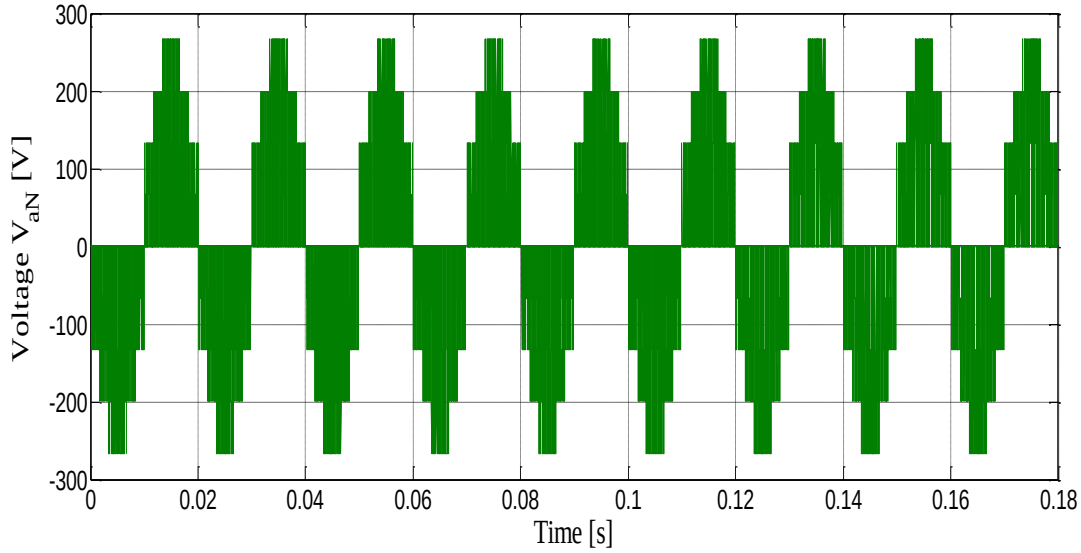

Figure IV.34 The voltage applied to the load in phase « a » between the star connection point of the load and the fictive point of among the h-bridge cells in the three phases

Based on the obtained results from the two simulation tests, it can be said that the model predictive control allows obtaining a precise current pursuit ability with a low total harmonic distortion.

Where easy implementation and less computation costs are required which can be considered as an advantage of this current control strategy.

On the other side, it is clear that the predictive current algorithm presents good dynamic response on reference tracking during transient response.

IV.6 Conclusion

This chapter presented the predictive current control strategy for two topologies of inverters :firstly the three phase two level voltage source inverter ,secondly the three phase three level h-bridge inverter. It can be conclude that the predictive control application with the more complicated inverters can be a more promising current control technique, especially with the actual advanced technologies of new fast microprocessors, which allow building the predictive control in a wide area of applications with very small sampling time or high sampling frequencies, especially for application where the problems of the transient behaviors should be overcome in tracking the references .

General Conclusion

This thesis work is part of the work carried out in the Applied Automation and Industrial Diagnostics laboratory, faculty sciences and technology of University ZIANE Achour of DJELFA on the subject of the H-Bridge Multi-level Inverter Model Predictive Control Based For Reliability Enhancement.

In the first chapter of this thesis, a general introduction about the state of the art of the predictive control strategies and general basic ideas shared between different important predictive control algorithms.

The principals points shared between different predictive control are the prediction of the future behavior of the system at the next time using the mathematical equations of the system and the using of the system limits such as: existence of the constraints or not, the waiting factors, the use of the objective function (the cost function)…e.g.

The second chapter was devoted to the discussion about the different multilevel inverters, especially the three most important inverters as follow:

- Neutral point clamped multilevel inverter
- Flying capacitor multilevel inverter
- Cascaded h-bridge multilevel inverter

Each one of the three topologies have a specification in term of its utilization, its characteristics, its advantages and disadvantages. Witch correspond to the characteristics; it means the schema structure of inverter like the numbers of levels and the position of its components such as the diodes, the IGBT's, the capacitors…e.g.

In the other side the quality of the signal, the harmonics in the spectrum of the output currents and voltages are other characteristics of multilevel inverters.

The chapter was conclude by the application of the inverters in the industry and other sectors like the electricity grids and a comparisons between the three topology of multilevel inverters.

The third chapter presented the application of two control technics the space vector pulse width modulation and model predictive current control the two kinds of inverters :

- Three phase two level voltage source inverter
- Three phase three level h-bridge inverter

The predictive control is based on the space vector voltages generated by the space vector modulation. The predictive current control uses the cost function. The cost function is to calculate the error between the reference current and load current and choice the best voltage vector near the reference then to applied to the inverter.

For the first topology of two level inverter there are eight voltage vectors, and for the second topology of three levels there are 27 different voltage vectors.

The minimization of the current and voltage in the cost function provide dynamic response of the load current control using the components of the system to investigate the system performance when power is supplied to a resistive inductive load.

In the last chapter a simulation results are presented to verify the theoretical study of the system model included in the last chapter. The proposed control strategy is applied to the two topologies of inverters: Three-phase two level voltage source inverter, three-phase three level h-bridge inverter. Finally, simulation results shown the advantages of the predictive control :

- ✓ Very powerful
- ✓ Very effectively,
- ✓ Satisfactory,
- ✓ Easy to implement,
- ✓ Good utilization of the DC link voltage and low current ripple.
- ✓ The load current having a good dynamic response,
- ✓ Good performance of the current tracking ability .

BIBLIOGRAPHICAL REFERENCES

[1] Camacho E. F., Bordons C. A., " Model predictive control in process industry ", Springer, London, United Kingdom. 1995.

[2] Richalet J., Rault A., Testud J. L. Papon J., " Algorithmic control of industrial processes ", Proc. 4th IFAC Symposium on identification and system parameter estimation, Tbilisi, USSR 1976.

[3] Rouhani R,. Mehra R.K., "Model algorithmic control (MAC); basic theoretical properties" Automatica , 1982, vol 18, no.4, pp.401-414.

[4] Cutler C. R., Ramaker B. C., " Dynamic matrix control - a computer control algorithm ", Proc. Automatic control conference, San Francisco, USA, 1980.

[5] Lee J. H., "Model Predictive Control: Review of the Three Decades of Development" International Journal of Control, Automation and Systems, 2011, vol. 9, no. 3, pp. 415-424.

[6] Morari M., Lee J. H., "Model predictive control: past, present and future," Computers and Chemical Engineering, 1999, vol. 23, pp. 667-682.

[7] Ydstie B. " Extended horizon adaptive control ", Proc. 9th IFAC world congress, Budapest, Hungary, 1984, vol. 07, pp. 133-137.

[8] Clarke D. W., Mohtadi C., Tuffs P. S., " Generalized predictive control ,Part I. The basic algorithm ", Automatica, 1987, vol. 23, pp. 137-148.

[9] Clarke D. W., Mohtadi C., " Properties of generalized predictive control ", Automatica, 1989, vol. 25, pp. 859-875.

[10] De Keyser R. M. C., " A Gentle Introduction to model based predictive control ", Proc. international conference on control engineering and signal processing, Piura, Peru, 1998.

[11] Greco C., Menga G., Mosca E., Zappa, G., " Performance improvement of self-tuning controllers by multistep horizons: the MUSMAR approach ", Automatica, 1984, vol. 20, pp. 681-700.

[12] Peterka V., "Predictor-based self-tuning control", Automatica, 1984, vol. 20, no. 1, pp. 39-50

[13] Qin S., Badgwell,T. "A survey of industrial model predictive control technology," Control Engineering Practice, 2003, vol. 11, no. 7, pp. 733-764,

[14] Richalet J., Abu el Ata-Doss S., Arber C., Kuntze H. B., Jacubash A. Schill W., " Predictive functional control. Application to fast and accurate robots ", Proc. 10th IFAC world congress, Munich, 1987.

[15] Camacho E. F., Bordons C. A., " Model predictive control in the process industry ", Springer, London, 1999.

[16] Morari M. " Model predictive control: Multivariable control technique of choice in the 1990s?, book chapter in advances in model-based predictive control ". Oxford University Press, Oxford, 1994.

[17] Bemporad A., Morari M., Dua V., Pistikopoulos, E. N. " The explicit linear quadratic regulator for constrained systems ". Automatica, 2002,vol. 38, pp. 3-20.

[18] Ramirez D. R., Camacho, E. F. " On the piecewise linear nature of min-max model predictive control with bounded uncertainties ", Proc. 40th conference on decision and control, Florida, USA, 2001.

[19] Richalet J., Rault A., Testud J. L. Papon J., " Model predictive heuristic control: Applications to industrial processes ", Automatica, 1978, vol. 14, pp. 413-428.

[20] Garcia C. E., Prett D. M., Morari M., " Model predictive control: Theory and practice - a Survey", Automatica, 1989, vol. 25, pp. 335-348.

[21] David E. G., " Genetic algorithms in search, optimization and machine learning ", Addison-Wesley, USA,1989.

[22] Fadi I,. " Commande prédictive non linéaire d'un lit mobile simulé ", Doctoral thesis, National Polytechnic Institute of Grenoble, French, 2006.

[23] Nabae A., Takahashi I., Akagi H., " A new neutral point clamped PWM inverter ", IEEE Transactions on Industrial Applications, 1981,vol.1, no.5, pp. 518-523.

[24] Kouro S., Malinowski M., Gopakumar K., Pou J., Franquelo L G., Wu B., Rodriguez J., Pèrez M. A., Leon J. I., " Recent advances and industrial applications of multilevel converters ", IEEE Transactions on Industrial Electronics, 2010, vol.57,no.8, pp.2553-2580.

[25] Baker R. H., Bannister L. H., " Electric Power Converter ", U.S. Patent, no.3 867 643, 1975.

[26] Bose B. K., “ Power electronics and motor drives recent progress and perspective ”, IEEE Transactions on Industrial Electronics,2009, vol. 56, no. 2, pp. 581-588.

[27] Baker R. H., “ Bridge converter circuit ”, U.S. Patent, no.4, 270, 163,1981.

[28] Rodriguez J., Lai J. S., Peng F. Z., “ Multilevel Inverters : A Survey of Topologies, Controls, and Applications ”, IEEE Transactions on Industrial Electronics, 2002, vol. 49, no. 4, pp. 724-738.

[29] Hammond P. W., “ Medium voltage PWM drive and method ”, U.S. Patent no.5 625 545, 1997.

[30] Malinowski M., Gopakumar K., Rodriguez J., Perez M., “ A survey on cascaded multilevel inverters ”, IEEE Transactions on Industrial Electronics, 2010, vol. 57, no. 7, pp. 2197-2206.

[31] Laali S., Abbaszadeh K., Lesani H., “A new algorithm to determine the magnitudes of dc voltage sources in asymmetric cascaded multilevel converters capable of using charge balance control methods“, 2010 IEEE ,International Conference on Electrical Machines and Systems (ICEMS), 2010, pp. 56-61.

[32] Ajami A., Oskuee M.R.J., Khosroshahi M.T., Mokhberdoran A., “Cascaded multi cell multilevel converter with reduced number of switches”, IEEE Transactions on Power Electronics, 2014, vol.7, no.3, pp.552-558.

[33] Rashid M. H., “ Power electronics hanbook ”, Acadimic Press, San Diego, CA, 2001,pp.327-331.

[34] Lai J. S., Peng F. Z., “ Multilevel converters - A new bread of power converters ”, IEEE Transactions on Industrial Applications, 1996, vol.32, no.3, pp.509-517.

[35] Yuan X., Barbi I., “ Fundamentals of a new diode clamping multilevel inverter ”, IEEE Transactions on Power Electronics, 2000, vol.15, no.4, pp.711-718.

[36] Khomfoi S., Tolbert L. M., “ Multilevel Power Converters ”, Power Electronics Handbook, 2nd edition, Elsevier, 2007, pp. 451-482.

[37] Lu S., Mariethoz S., Corzine K.A., “Asymmetrical cascade multilevel converters with non-integer or dynamically changing dc voltage ratios: Concepts and modulation techniques”, IEEE Transactions on Industrial Electronics, 2010, vol. 57, no. 7, pp.2411-2418.

[38] Xu, L. Agelidis, V., “Flying capacitor multilevel pwm converter based upfc” IEEE Proceedings Electric Power Applications, 2002, vol.149, no.4, pp.304-310.

[39] Peng F. Z., Lai J. S., " Multilevel cascade voltage source inverter with separate DC sources ", U.S. Patent , no.5, 642 275,1997.

[40] Ray R., Chatterjee D., Goswami S., "Harmonics elimination in a multilevel inverter using the particle swarm optimisation technique," IEEE Transactions on Power Electronics, 2009, vol.2, no. 6, pp. 646-652.

[41] Tolbert L. M., Peng F. Z., Habetler T. G., " Multilevel inverters for electric vehicle applications ", Proc. Power electronics in transportations , Dearborn, Michigan, 1998, pp.79-84.

[42] Teodorescu R., Blaabjerg F., Pedersen J. K., Cengelci E., Enjeti P. N., " Multilevel inverter by cascading industrial VSI ", IEEE Transactions on Industrial Electronics, 2002, vol.49, no.4, pp.832-838.

[43] Du Z.,Ozpineci B.,Tolbert L. M., Chiasson J. N., " DC-AC cascaded h-bridge multilevel boost inverter with no Inductors for electric-hybrid electric vehicle applications ", IEEE Transactions on Industrial Electronics, 2009, vol. 45, no.3, pp.963-970.

[44] Meynard T. A., Foch H., " Multilevel conversion : High-Voltage choppers and voltage source inverters ", PESC '92 Record, 23rd Annual IEEE power electronics specialists conference, 1992, vol.01, pp.398-403.

[45] Gritter D., Kalsi S. S., Henderson N., " Variable speed electric drive options for electric ships ", Proc. IEEE electric ship technologies symposium, Philadelphia, USA, 2005, pp.347-354.

[46] Shuai L., Keith C., " Multi-level multi-phase propulsion drives ", Proc. IEEE electric ship technologies symposium, 2005, pp.363-670.

[47] Oscar L. J., Alvarez J., Doval-Gandoy J.,Freijedo F. D., " Multi-level multi-phase space vector PWM algorithm with switching state redundancy ", IEEE Transactions on Industrial Electronics, 2009, vol.56, no.3, pp.792-804.

[48] Oscar L. J., Alvarez J., Doval-Gandoy J., Freijedo F. D., " Multilevel multiphase space vector PWM algorithm ", IEEE Transactions on Industrial Electronics, 2008, vol.55, no.5, pp.1933-1942.

[49] Calais M., Agelidis V. G., Meinhardt M., " Multilevel converters for single phase grid connected photovoltaic systems : an overview ", Elsevier Solar Energy, 1999, vol. 66, no. 5, pp. 325-335.

[50] Pena R., Cardenas R., Reyes C. E. J., Wheeler P., "A topology for multiple generation system with doubly fed induction machines and indirect matrix converter," IEEE Transactions on Industrial Electronics, 2009, vol.56, no.10, pp.4181-4193.

[51] Prasad M. V., Suresh K. S., "Control and performance of a cascade h-bridge MLI as STATCOM ", International journal of advances in engineering and technology, 2012, vol.2, no.1, pp.508-519.

[52] Cengelci E., Sulistijo S. U.,Woom B. O., Enjeti P.,Teodorescu R.,Blaabjerg F., " A New medium voltage PWM inverter topology for adjustable speed drives ", Regional Exchange Conference. IEEE-IAS, Annual Meeting, St. Louis, MO, 1998 pp. 1416-1423.

[53] Sepra L. A. , " Current control and strategies for multilevel grid connected inverters ", Doctoral Thesis, Swiss Federal Institute of Technology, FIT Zurich, 2007.

[54] Tolbert L. M., Peng F. Z., " Multilevel converters as utility interface for renewable energy systems ", IEEE power engineering society, summer meeting, 2000, pp.1271-1274.

[55] Ostojic D., " A multilevel converter structure for grid-connected PV plants ", Doctoral thesis, University of Bologna, 2010.

[56] Tahri A., Draou A., " A comparative modelling study of PWM control techniques for multilevel cascaded inverter ", Leonardo Journal of Sciences, 2005, no.6, pp.42-58.

[57] Cortes P., Kazmierkowski M., Kennel R., Quevedo D., Rodriguez J., " Predictive control in power electronics and drives ", IEEE Transactions on Industrial Electronics, 2008, vol.55, no.12, pp.4312-4324.

[58] Rodriguez J., Cortes P., " Predictive Control of Power Converters and Electrical Drives ". John Wiley & Sons, Chichester,UK,2012.

[59] Kukrer O., " Discrete-time current control of voltage-fed three-phase PWM inverters ", IEEE Transactions Power Electronics, 1996, vol.11, no.2, pp. 260-269.

[60] Zeng Q., Chang L., " An advanced SVPWM-Based predictive current controller for three-phase inverters in distributed generation systems ", IEEE Transactions on Industrial Electronics, 2008 vol.55, no.3, pp.1235-1246,.

[61] Saggini S., Stefanutti W., Tedeschi E., Mattavelli P. " Digital deadbeat control tuning for DC–DC converters using error correlation", IEEE Transactions Power Electronics, 2007,vol.22,pp.1566-1570.

[62] Perantzakis G.S., Xepaps F.H., Papathanassiou S. A., Manias S. N., " Predictive current control technique for three level NPC voltage source inverter ", PESC Record, IEEE 36th Annual power Electronics specialists Conference , 2005, pp.1241-1246.

[63] Cortes P., Rodriguez J., C. Silva, Flores A, " Delay compensation in model predictive current control of a three-phase inverter ",IEEE Transactions on Industrial Electronics, 2012, vol.59, no.2, pp.1323-1325.